Alma Mater Studiorum – Università di Bologna

DOTTORATO DI RICERCA IN

Scienze Biomediche e Neuromotorie

Ciclo XXXV

Settore Concorsuale: 05/H1

Settore Scientifico Disciplinare: BIO/16

NUCLEAR SHAPE INSTABILITY CAUSED BY LAMIN A DEREGULATION PROMOTES INVASIVENESS IN PEDIATRIC BONE SARCOMAS: FROM NUCLEO-CYTOSKELETON DYNAMICS TO NOVEL THERAPEUTIC OPPORTUNITIES

Presentata da: Francesca Paganelli

Coordinatore Dottorato
Chiar.ma Prof.ssa Matilde Y. Follo

Supervisore
Chiar.ma Prof.ssa Matilde Y. Follo

Co-Supervisore
Dott.ssa Francesca Chiarini

Esame finale anno 2022

INDEX

ABSTRACT

Osteosarcoma (OS) and Ewing sarcoma (EWS) are the two most frequent primary bone tumors, in which metastases remain the most relevant adverse prognostic factor. Lamin A is the main constituent of the nuclear lamina, with a fundamental role in maintaining the connection between nucleus and cytoskeleton (through LINC complex proteins interactions), and its alterations can be implicated in tumor progression.

We investigated how nucleo-cytoskeleton dynamics is influenced by lamin A modulation in OS and EWS, demonstrating that both these cancer models had low levels of lamin A, which are linked to a significantly more marked nuclear misshaping. In our *in vitro* studies, reduced levels of lamin A promoted migratory abilities in these tumors. Moreover, these findings were corroborated by gene expression analyses on EWS patient samples, showing that *LMNA* levels were significantly lower in metastatic lesions compared to primary tumors and that patients with low *LMNA* had a significant worse overall survival. We also found that *LMNA* expression significantly impaired EWS metastases formation *in vivo*.

We demonstrated that low lamin A expression was linked to a severe mislocalization of LINC complex proteins, thus disrupting nucleo-cytoskeleton interactions, with a corresponding gain in malignant properties, which resulted in increased invasiveness. Lamin A overexpression or its accumulation by a statin-based pharmacological treatment allowed us to reconstitute a functional nucleo-cytoskeleton interplay, which resulted in significant downmodulation of ROCK2 and YAP, two crucial drivers of EWS aggressiveness.

Our study demonstrated that lamin A is a favorable mediator of nuclear shape stability in bone sarcomas, and its modulation rescues LINC complex protein localization and regulates mechano-signaling pathways, thus promoting a less aggressive cancer phenotype. We also identified statins, already employed in clinical practice, as a tool capable to increase lamin A levels, and to reconstitute functional nucleo-cytoskeletal dynamics, resulting in reduced cellular migration.

PART I-BIBLIOGRAPHICAL OVERVIEW

CHAPTER I-BIOLOGY OF BONE SARCOMAS

1. Bone sarcomas

Primary bone sarcomas are defined as rare malignant tumors, representing less than 2% of all human neoplasms (1). They originate in bone tissues and constitute a highly heterogeneous tumor group, with osteosarcoma (OS), chondrosarcoma, and Ewing sarcoma (EWS), the most common types (1, 2).

Bone sarcomas also belong to mesenchymal tumor family, deriving from a mesenchymal stem cell (MSC) (3). The MSC is able to differentiate in different tissues, including cartilage and bone (4). When an oncogenic event occurs during MSC differentiation, the risk of their malignant transformation is very high and can result in osteoblastic or chondroblastic cancerous cells (3). While the perturbation of MSC differentiation process is a well identified and characterized event, which sustains osteosarcoma and chondrosarcoma genesis, the origin of EWS remains elusive and controversial. This tumor is characterized by the expression of a fusion protein deriving from chromosomal translocation between *EWSR1* (EWS breakpoint region 1) gene on chromosome 22 and a gene of *ETS* (E-twenty-six) family (most commonly *FLI1*, Friend leukemia virus integration1) (5). Different studies showed that ectopic expression of *EWS-FLI1* in bone marrow-derived human MSC initiates transition to an EWS-like cellular phenotype (6) (7). However, the immature phenotype of EWS, along with its gene expression signatures and its predisposition to neural differentiation also suggest a possible origin from neural crest (8). Neural crest stem cells, like EWS cells, are highly invasive and during embryogenesis migrate to various tissues throughout the body (9). von Levetzow et al. showed that neural crest-derived stem cells are permissive for *EWS-FLI1* expression and susceptible to EWS oncogenic transformation. Moreover, they demonstrated that EWS cells are genetically highly related to neural crest stem cells (8). Thus, EWS origin remains unclear with MSC and neural crest cells as the two major candidates.

Bone sarcomas can also be divided in two major categories based on genetic characteristics. The first includes sarcomas with near-diploid karyotypes and simple genetic alterations, while the second comprises sarcomas with complex and unbalanced karyotypes, characterized by multiple genomic aberrations (1). For example, in OS more than 80 mutations in several genes have been identified (10), conversely in EWS cells, the presence of the same chromosomal translocation is the main driver alteration (5).

Although bone sarcomas often share the same localization, they represent a molecularly, genetically and histologically heterogeneous group of tumors.

2. Osteosarcoma

Osteosarcoma is the earliest identified cancer. It was found in a 77-million-year-old dinosaur specie and identified also in 1.7-million-year-old hominin fossil rediscovered in South Africa (11) (12). Despite osteosarcoma can be defined "a very ancient cancer", the genetic alterations, oncogenic events and its evolutionary history, are poorly understood, thus limiting further improvements in genome-informed targeted therapy for this disease.

2.1 Epidemiology and pathology

Osteosarcoma is the most frequent bone cancer in children and adolescents, but it is classified as rare tumor as 800-900 new cases are diagnosed per year in the USA (12). OS is characterized by a bimodal age distribution, presenting the first peak of incidence during adolescence and the second peak in older adulthood. Most cases occur between 10 to 30 years of age, with a peak in the 10-14-year-old age group, coinciding with the pubertal growth spurt. The second peak of incidence is in adults older than 65 years of age, often manifesting OS as secondary cancer or related to Paget's disease (13). Generally, OS occurs in the metaphysis of long bones near the growth plates. The distal femur represents the most frequent site, followed by the proximal tibia and the proximal humerus (shoulder) (Figure 1) (14).

The majority of patients present a localized disease, while about 20% of patients develop metastases. Metastases arise preferentially in lungs (74% of patients) but can occur also in bones. A small percentage of patients, about 8%, present both bone and lung metastases (15).

Being OS a malignant neoplasm of the skeleton, patients present bone pain and localized swelling which lead to radiographic exams followed by biopsy to confirm the diagnosis (12).

Depending on the extent of tumor invasion, OS can be subdivided into three categories: high-grade, intermediate-grade, and low-grade. The latest is limited to the bone surface, the intermediate-grade involves the periosteum, while the high-grade OS represents the fastest-growing and the most aggressive group characterized by the presence of metastases (16).

Figure 1: Radiographic image of OS lesion in the proximal tibia (12)

Conventionally the term OS is used to refer to the high-grade tumor, the most frequent type, representing the 85% of all OS cases in childhood and adolescence (17).

2.2 Heterogeneous genetic landscape

OS is described as a very genomically complex disease and very few genetic alterations are common among OS cases (14). Currently, several syndromes, such as Li–Fraumeni, inherited retinoblastoma, RAPADILINO syndrome or Diamond–Blackfan anemia are considered as predisposing for OS development (18).

Identifying common genetic characteristic in OS is complicated by the presence of two phenomena in this type of cancer: chromothripsis and kataegis (14). The term chromothripsis indicates a complex pattern of alternating genes copy number changes (normal, gain or loss) along the length of a chromosome or chromosome segment (19). It has been demonstrated that chromothripsis is a common oncogenic event in OS and involves several chromosomes, thus complicating the identification of common genetic abnormalities among OS cases (20). This phenomenon, which results in a new chromosome setting, is present in about 77% of OS cases (21). In addition, the presence of kataegis (hypermutation in localized genomic regions) adds a further variable element in the identification of common genetic characteristics underlying OS development (22). However, several studies have identified some commonly altered genes during OS progression. Indeed, the

most frequent mutated genes in sporadic pediatric OS are *TP* (tumor protein) *53*, *RB* (retinoblastoma) gene, *MYC*, and *CDK* (cyclin-dependent kinases) (23).

OS patients present a gain of function mutation (R175H) in *TP53* gene which results in centrosome amplification, aberrant mitosis, and reduced apoptosis pathway activation (24) (25). About 70% of OS cases present *RB* mutation, and it has been demonstrated that *TP53* and *RB* mutations are sufficient to induce metastatic OS development in a murine model (26). These mutations also provide a fertile soil to DNA damage accumulation. *MYC* oncogene amplification, present in 10% of OS cases, contributes to metastases formation through the activation of MEK (mitogen-activated protein kinase kinase)-ERK (extracellular signal-regulated kinase) pathway and it is significantly upregulated in metastatic patients compared to primary samples, correlating with poor prognosis (27) (28) (29). *CDK4* is another gene generally overexpressed in OS and linked to metastatic capacity and poor prognosis. Indeed, its inhibition results in decreased cell proliferation and migration abilities in OS cell lines (30).

Regarding specific signaling pathways, OS do not present the frequent activating mutations in signaling genes normally observed in other cancers. Indeed, whole-genome sequencing, whole-exome sequencing and RNA sequencing analyses demonstrated heterogeneous aberrations in OS samples (14). These data showed a convergence of unique alteration in the activation of PI3K (phosphoinositide 3-kinases)-AKT-mTOR (mechanistic target of rapamycin) pathway, mainly due to PTEN (phosphatase and tensin homolog) inactivation (31).

Moreover, epigenetic mechanisms play a role in promoting cancer development. Analyses of OS samples have demonstrated a significant gene hypermethylation compared to normal tissues. In particular, the hypermethylation of specific genes promotes apoptosis resistance and tumor progression (1). For example, the promoter hypermethylation of *CDKN2A* gene, which acts as tumor suppressor by regulating cell cycle, is linked to metastasis formation in OS (32).

2.3 Prognosis and therapeutic approaches

Newly diagnosed OS patients present metastatic disease in about 10-15% of cases. The 5-year survival rate is only 20% for patients with metastases or recurrent disease, while it is approximately 60% among patients with localized tumor (33). Unfortunately, survival rate has not been improved during the last years and patients who develop osteosarcoma today receive treatment that is essentially unchanged since the 1970s (34). Indeed, the absence of common activating kinase

mutations present in other cancers, and the genome complexity make the development of new OS therapies really challenging.

Standard therapies consist of surgical removal of tumor mass. Nearly 85% of patients undergoing resection have been able to keep their limbs since the year 2000 (35). The most common chemotherapy regimen consists of the use of the three specific agents: methotrexate, doxorubicin, and cisplatin (MAP protocol), administrated both before and after surgical resection. For older patients, the use of methotrexate is often omitted to avoid the higher rate of toxic effects. Combinations with other drugs, such as ifosfamide and etoposide, have been tested but adding more agents does not improve patient's outcome (14). Several clinical trials have also demonstrated that the employment of ifosfamide and etoposide or gemcitabine and docetaxel can be effective in patients with unresectable or relapsed disease (36) (37) (38).

As described above, sequencing analyses failed in selecting potential targets for anticancer targeted therapy (39). Being p53 the most frequently mutated protein in OS, several compounds have been tested in preclinical studies, but no drugs have been able to restore the function of mutated p53 (40). The use of Cabozantinib, a vascular endothelial growth factor receptor (VEGFR) tyrosine kinase inhibitor that also possesses specific MET (mesenchymal-epithelial transition factor) receptor inhibitory activity, demonstrated cell growth inhibition in OS cell lines (41). The efficacy and safety of Cabozantinib have also been tested in a multicenter, single-arm phase 2 trial demonstrating anti-tumor activity and well tolerability in patients (42).

OS is defined as a sarcoma subtype that can potentially respond to immunotherapy, but data obtained with the use of this approach are not encouraging.

The use of interferon alfa is being tested in OS patients who receive standard chemotherapy, but the 3-year event-free survival do not shown significant differences compared to control group (patients treated with only standard therapies) (43). However, long-term follow up is still in progress. Also, the addition of mifamurtide, an immune stimulant, to therapeutic protocol has not shown significant efficacy in ameliorating the overall survival rate and its use has not been approved by FDA (Food and Drug Administration) (44). Engineered antibodies have been also tested in OS. Being HER2 (human epidermal growth factor receptor) receptor overexpressed in some OS patients, an HER2 monoclonal antibody, combined with chemotherapy was tested in patients with metastatic disease but the use of trastuzumab (directed against HER2) did not show advantages compared to chemotherapy alone (45). The use of CAR (Chimeric Antigen Receptor)-T cells specific for molecules overexpressed in OS are currently under investigation (12).

The properties of OS microenvironment may be the cause of the failure of immune-based therapies in this type of cancer. Indeed, vascular abnormalities and alterations in tumor-associated macrophages constitute an unfavorable environment for T-cells infiltration (46) (47).

To conclude, finding new therapeutic opportunities for OS patients still remains an open research field.

3. Ewing sarcoma

In 1920, James Ewing was the first to describe an unusual cancer in an adolescent as a "diffuse endothelioma of bone" during a meeting of the New York pathological society (48).

For more than 70 years the diagnosis of this type of tumor remained difficult and often it had initially been diagnosed as an osteosarcoma.

Only when the chromosomal translocation that drives the malignant transformation was identified, this type of tumor was unequivocally diagnosed as Ewing sarcoma (49).

3.1 General features

Ewing sarcoma is an aggressive bone (affecting predominantly femur, tibia, pelvis and ribs) and soft-tissue (thoracic wall, pleural cavities, gluteal and cervical muscles) cancer (50). It represents the second most frequent bone cancer in childhood. Indeed, EWS affects mainly children and young adults with an incidence of 1 case per 1.5 million population that reaches the peak at 15 years of age, and a slight predilection for males (50).

Histologically, EWS is characterized by a proliferation of uniform undifferentiated and monomorphic round cells with prominent nuclei and minimal cytoplasm (Figure 2). Cells present chromatin finely stippled, nucleoli are not observable, and usually deposits of glycogen are well visible in the cytoplasm (50).

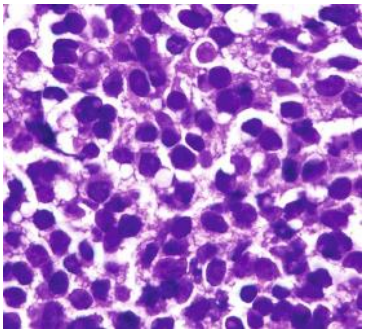

Figure 2: Histomorphology of Ewing sarcoma (50)

EWS patients present nonspecific symptoms such as localized intermittent mild pain which increases at night or after exercise. Pain sometimes can be also accompanied by swelling (51) . In a substantial number of patients, pain is followed by the appearance of a palpable soft-tissue mass. Moreover, 10-15% of cases present a pathological fracture, and patients with advanced disease also manifest fever, weight loss, night sweats, and fatigue (51). Due to the presence of nonspecific clinical features, the diagnosis of EWS can be delayed, with the median time to diagnosis of 3–9 months (50). Diagnosis consists of histological, immunochemical and molecular analysis of biopsy sample or surgically resected tumor tissue (5). Immunochemistry evidences a strong and diffuse expression of CD99 in about 95% of EWS cases (50). CD99 is cell-surface glycoprotein with a central role in EWS mediating tumor differentiation, migration, invasion, and malignancy (52). Indeed, the absence of CD99 expression virtually excludes EWS diagnosis. Definitive diagnosis is performed by *in situ* hybridization or quantitative polymerase chain reaction analysis that identifie the presence of specific chromosomal translocation (*EWS-FLI1*) (5).

3.2 Genetic alterations

EWS is genetically well-characterized. This tumor presents the lowest mutational rates of all cancers, carrying a very low mutational load, with 0.15 mutations per megabase (53) (54). The main driver alteration is one of different possible chromosomal translocation that leads to the fusion between *EWSR1* and a gene encoding a member of *ETS* family (5). *EWSR1* belongs to FET family RNA-binding proteins (encoded by *FUS*, *EWSR1* and *TAF15*) involved in splicing and transcription processes (50). *In vivo* studies demonstrated that *EWSR1* is implicated in meiosis, B-cells maturation, DNA repair, and hematopoietic stem-cell maturation (55). It has been also described the role of *EWSR1* in maintaining neuronal structure and dopaminergic signaling (56). Instead, ETS family is a group of transcription factors which mediates cell proliferation and differentiation, cell-cycle regulation, angiogenesis and apoptosis (50). All members of this family present a DNA-binding domain, defined as ETS binding motif, which recognizes the consensus sequence 5'-GGAA/T-3' DNA motif (5). In about the 85% of EWS cases the chromosomal translocation t(11;22)(q24;q12) is present, resulting in the fusion of *EWSR1* to *FLI1* and generating *EWS-FLI1* fusion gene (49).

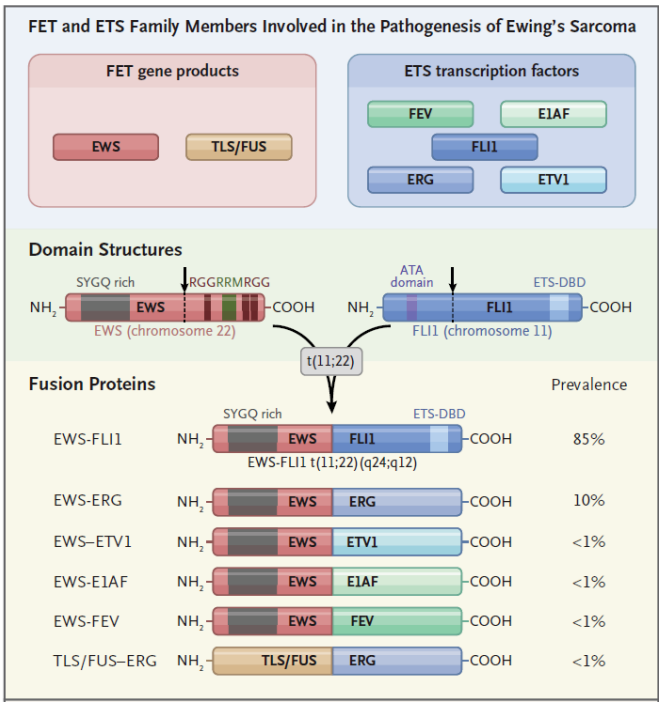

Figure 3: FET and ETS members involved in Ewing sarcoma pathogenesis (5)

After chromosomal translocation, the portion of the 3' ETS-binding domain of *FLI1* that becomes fused to *EWSR1* undergoes a conformational change, which allows it to activate a wider range of genes than wild-type *FLI1* does (57) (58). Although most cases bear *EWS-FLI1* chromosomal translocation, in about 1% of cases *EWSR1* is substituted by *FUS* with the same effects on EWS phenotype and behavior (59) (60). Similarly, *FLI1* can also be replaced by other ETS factors, such as *FEV*, *ETV1*, *ERG*, and *E1AF* (Figure 3) (5).

Whatever it is the chromosomal translocation, the *FET-ETS* fusion gene always results in a chimeric peptide which acts as an aberrant transcription factor, promoting the expression of oncogenic factors and inhibiting several other genes (61). However, the majority of functional studies have been focused on the most representative chromosomal translocation, *EWS-FLI1*. The fusion gene is present at the beginning of the disease, and it is retained along the tumor evolution. It is fundamental for malignant transformation and its silencing leads to EWS cell lines growth arrest and tumor formation inability in mice (62) (63). On the contrary, when *EWS-FLI1* is expressed in fibroblasts, it results in a EWS phenotype (64). *EWS-FLI1* orchestrates multiple oncogenic hits and is defined the crucial driver of this pathology. It mediates epigenetic mechanisms, and promotes chromatin-remodeling, thus setting a new paradigm for oncogene-mediated epigenetic instruction of cell transformation. Indeed, *EWS-FLI1* establishes new enhancer regions which causes the malignant transformation of permissive cells. The enhancer genome-wide signature observed in

EWS is unique and enriched in GGAA microsatellites (65) (66) (67). *EWS–FLI1* can overcome the closed chromatin conformation of these GGAA microsatellites, allowing greater DNA accessibility to other transcription factors, chromatin modifiers and remodeling complexes (65) (67). In particular, a domain of *EWSR1* fused to *FLI1* can interact with BRG1–BRM-associated factor (BAF) chromatin-remodeling complexes, recruiting BAF complexes at GGAA microsatellites. This recruitment regulates genomic architecture and DNA accessibility, establishing *de novo* enhancer elements that activate EWS transcriptional program (66) (67).

Moreover, *EWS-FLI1* mediates chromatin remodeling through the recruitment of specific enzymes which act on methylation and acetylation of specific lysine residues on histone 3, thus resulting in chromatin relaxation (65).

The presence of the fusion gene is a necessary condition for EWS development, but other mutations can be identified in some EWS cases. They may include mutations of *STAG2* (Cohesin subunit SA2) in 15–21% of cases and *TP53* (detected in 5–7% of cases) genes, as well as a deletion of *CDKN2A*, a cyclin-dependent kinase that regulates cell proliferation, in 10–22% of cases (54).

3.3 Metastasis

The presence of metastases at diagnosis, in about 20-25% of patients, is the most adverse prognostic factor in EWS (68) (69). Metastatic sites are generally lungs, bones, and bone marrow. However, metastasis can also occur in liver, lymph nodes, and brain (68) (70). Several studies are now focusing on clarify the dynamics of metastatic processes, identifying molecular pathways related to EWS metastatic phenotype. Molecules, which are differently expressed in metastatic patients compared to patients with localized pathology, have been found. For example, high SIRT1 (NAD-dependent protein deacetylase sirtuin 1) expression was associated with EWS metastasis and poor prognosis (71). Transcriptomic analyses between primary tumors and metastatic ones have demonstrated that tyrosine-protein kinase transmembrane receptor ROR1 is a regulator of EWS metastatic potential, and its inactivation contributes in decreasing cell migration *in vitro* (72). ERBB4 (Erb-B2 Receptor Tyrosine Kinase 4) is also significantly more expressed in metastatic EWS samples compared to primary tumors and mediates the metastatic process regulating the activation of the phosphoinositide 3-kinase (PI3K)–AKT and FAK (focal adhesion kinase) pathways (73). Sechler et al. demonstrated that the overexpression of histone demethylase KDM3A (lysine demethylase 3A), and its downstream target MCAM (melanoma cell adhesion molecule), promotes EWS cell migration and metastasis in both *in vitro* and *in vivo* models (74). Moreover, EWS cells also overexpress proteins

such as MMP (matrix metalloproteinase)-2, MT1-MMP, and MMP-9, which are critical for tumor dissemination and metastasis (75). ROCK2, is another factor, whose high expression has been associated with *in vitro* EWS cell migration and anchorage-independent growth capabilities (76). The zyxin-related protein thyroid receptor interacting protein 6 (TRIP6) is also overexpressed in EWS and has been identified as an oncogene that partially accounts for the autonomous migratory, invasive and proliferative properties of this tumor (77). Balestra et al. described the role of CD99 in repressing zyxin protein expression. This protein is a negative regulator of cell migration, survival and growth in anchorage-independent conditions and its inhibition, by high expression of CD99 in EWS, contributes to tumor cell growth and migration (78).

The microenvironment also plays a role in metastatic processes. Indeed, MSCs can migrate to the lungs and differentiate into endothelial cells and pericytes, promoting tumor blood vessel formation to support metastasis (79). Additionally, cell stresses, such as hypoxia or growth factors privation can promote CXCR4 (chemokine receptor type 4) chemokine receptor upregulation, resulting in increased migration and invasion of EWS cells (80).

Other studies explored whether the presence of *EWS-FLI1*, directly modulates tumor cell features that supporting metastasis, such as cell adhesion and cell migration. Chaturvedi et al. proposed a 'passive/stochastic metastasis model' in which the loss of cell adhesion needed to promote tumor cell dissemination might be induced by the *EWS-FLI* oncogene itself. The authors show that *EWS-FLI1* expression loosens cell adhesion, and they therefore propose that poorly attached EWS cells passively disseminate in the circulation (81). *EWS-FLI1* can also directly mediate the autophosphorylation of FAK, resulting in enhanced focal adhesion formation and Rho-dependent cell migration *in vitro* (82).

However, the role of *EWS-FLI1* in metastatic processes is complicated by the fact the EWS cells present variable expression levels of this fusion gene. In this model, cells with high expression of *EWS1–FLI1* (EWSR–FLI1^{high}) are the major population; they are responsible for its proliferation behavior, and display high cell–cell adhesion tendency. A small number of EWS cells present low expression of *EWS-FLI1* (EWS1–FLI1^{low}) and can acquire a mesenchymal-like phenotype, interact with matrix molecules and metastasize. Hence EWS-FLI1^{high} cells proliferate, EWS-FLI1^{low} cells are migratory and invasive (83). Cells variation due to the expression level of *EWS-FLI1* may constitute a critical component of the metastatic process. Katschnig et al. provided a mechanistic basis for spontaneous fluctuations in *EWS-FLI1* levels and the linked EWS-FLI1-dependent reversible cytoskeletal reprogramming of EWS cells. They demonstrated that *EWS-FLI1* suppresses the Rho-

actin pathway by perturbation of a MRTFB (Myocardin Related Transcription Factor B)/YAP (Yes Associated Protein)-1/TEAD (TEA domain family member 1) transcriptional module, which directly affects the actin-autoregulatory feedback loop, thus orchestrating key steps of the EWS migratory gene expression program (84). A recent study also showed that expression levels of TAZ, a co-activator of TEAD, are upregulated in the migratory EWS-FLI1^{low} state (migratory state) and associated with adverse prognosis in EWS patients (85).

3.4 Prognosis, conventional and experimental therapeutic strategies

The presence of metastasis at the diagnosis remains the worst prognosis factor. Indeed, the current therapeutic strategies allowed to obtain a 5-year overall survival of ~70-80% in patients with localized disease, while the 5-year overall survival for patients with metastasis is significantly lower (< 30%) (69) (50). In absence of metastasis, other factors contribute to prognosis. For example, the tumor site is the major prognostic factor in patients with localized tumor. Patients with primary tumors in the pelvis and sacrum have worse clinical evolution than patients with tumors in distal sites (68) (86). Other clinical factors linked to unfavorable outcome are a large primary lesion, older age at diagnosis, and increased levels of LDH (lactate serum dehydrogenase) (87) (68).

Current management consists of local approach (surgery and radiotherapy) and intensive induction chemotherapy, which includes doxorubicin, vincristine, etoposide, cyclophosphamide, and ifosfamide (at interval of 21-28 days) to target primary tumors (88) (89). Therapeutic protocol's variations have been also evaluated. The US Children's Oncology Group demonstrated that shortening intervals between doses is more effective and it is associated with fewer collateral effects (90) (91). European centers have also developed a protocol which adds a consolidation treatment with high-dose of busulfan or melphalan plus autologous stem cell rescue and total-lung irradiation. This intensive approach is feasible and long-term survival is achievable in ~50% of patients (89).

EWS metastatic patients are treated with the same clinical approach used for the care of patients with primary tumor, but several preclinical and clinical studies are currently investigating new approaches to meliorate their outcomes.

A randomized phase III clinical trial is evaluating how the combination of chemotherapy with or without ganitumab, that block the IGF (insulin growth factor)-1R pathway, works in treating patients with newly diagnosed metastatic EWS (NCT02306161, ClicalTrials.gov). Treatment with drugs, such as ganitumab, may interfere with the ability of tumor cells to grow and spread. Moreover, a phase

2 study is now recruiting EWS metastatic patients to test the effects of BIO-11006 (a ten-amino acid peptide aerosolized dual inhibitor of mucus hypersecretion and pulmonary inflammation) in combination with gemcitabine and docetaxel for the treatment of lung metastases in pediatric patients (NCT04183062, ClicalTrials.gov).

Targeted therapy can be also considered to tune more effective therapeutic strategies. Although the obvious approach could be the direct targeting of EWS-FLI1 fusion protein, the absence of its any enzymatic activity makes very difficult this strategy. However, the use of YK-4-279 was able to reduce EWS cell proliferation *in vitro* and in xenografts (92). This molecule is a small inhibitor that prevents the binding of EWS-FLI1 to RNA helicase A, a crucial component of transcriptional program (50). Preclinical studies with PARP (poly (ADP-ribose) polymerase) inhibitors had showed promising results in EWS models, but the results of clinical trials were disappointing (93) (94).

Targeting CD99 is an attractive strategy in EWS, due to its very high expression in this tumor. CD99 stimulation by monoclonal antibodies activates a non-canonical apoptosis pathway, leading to hyperstimulation of macropinocytosis and selective death of EWS cells (95). Celik et al. demonstrated that the use of clofarabine, which directly binds CD99 molecule, is effective in inhibiting growth of three different EWS xenografts (96). Moreover, a recent study showed that the use of the YAP/TAZ/TEAD complex inhibitor verteporfin results in decreased EWS cell migration *in vitro* and reduction of metastasis formation *in vivo* (97).

Although several therapeutic approaches are now under investigation, the cure of metastatic disease still remains a challenge.

CHAPTER II-CELL NUCLEUS

1. Cell nucleus organization and dynamic

The cell nucleus was described as a central “clear area” in salmon blood cells by Antonie van Leeuwenhoek, for the first time in the seventeenth century. A more detailed description was then provided by the botanist Robert Brown, who first introduced the concept of nucleated cells as the structural unit in plants. Today, this organelle is recognized as fundamental for several cellular functions and it is identified as a crucial player in cancer initiation and progression (98).

1.1 Structural features of nuclear membrane

The cell nucleus is highly organized and compartmentalized organelle. It is surrounded by a double membrane which constitutes the nuclear envelope (NE) and physically separates the nuclear interior from the cytoplasm. The nuclear interior contains chromatin, the nucleolus, subnuclear structures such as nuclear speckles and Cajal bodies (99-101).

The NE protects the genome and controls the gene expression, regulating the import of transcription factors to the nucleus and the RNA release from it (102).

It is composed of two phospholipids bilayers, the inner nuclear membrane (INM) and the outer nuclear membrane (ONM), that are divided by an intermembrane space (~30-50 nm) and are fused at hundreds of specific sites linked to the multiprotein nuclear pore complexes, controlling the nuclear transport of high molecular weight macromolecules (103).

More than 250 proteins are identified as constitutive of the nuclear membrane (104). At least 70-100 specific proteins are located at the INM, such as emerin, LAP2, the lamin B receptor (LBR), MAN1 (LEM) family proteins, and the Sad1p/UNC-84 (SUN) proteins (105) (106). SUN protein can interact with nucleoplasmic protein (e.g. lamins in the nuclear lamina) on one side and with ONM proteins on the other side, thus linking nucleoskeleton and cytoskeleton (107).

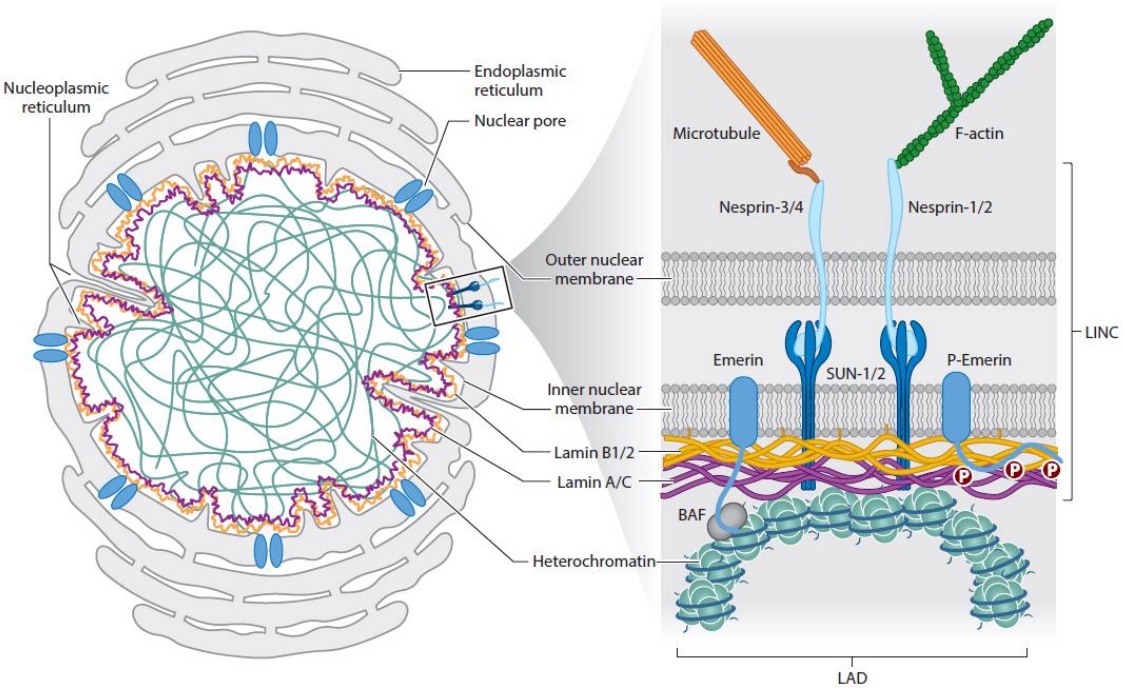

Figure 4: Nuclear membrane composition (106)

The ONM is continuous with the endoplasmic reticulum and its surface is scattered with ribosomes, and it is composed of specific nuclear proteins. In mammals, the most important ONM family proteins is represented by the KASH (Klarsicht/ANC-1/Syne homologue)-domain-containing nesprins, which are directly or indirectly connected to cytoskeletal components (98). Moreover, beneath the INM, a dense network of proteins constitutes the nuclear lamina mainly formed by lamins.

1.2 Structure and functions of nuclear lamins

In mammals, nuclear lamins exist in different isoforms. They are subdivided in A-type lamins and B-type lamins, that are the product of two different genes. *LMNA* gene encodes, via alternative splicing, the predominant isoforms lamin A and lamin C, a minor isoform lamin A Δ10, and a germ-cell specific isoform (lamin C2). Instead, B-type lamins include the lamin B1 and B2, encoded by *LMNB1* and *LMNB2* genes, respectively (108).

Both A- and B-type lamins are mainly localized at the nuclear lamina (underlying the INM) of which they represent the most abundant component (109). However, they are also found in the nucleoplasm where they have a role in spatial chromatin organization through the dynamic binding

to specific genomic regions and promoter subdomains, thereby affecting epigenetic pathways and chromatin accessibility (110).

Moreover, lamin isoforms present a cell type-specific expression. Indeed, although most cells express A- and B-type lamins, there are some exceptions, such as blood cells (B ad T cells) which express only B-type lamins. Several studies have also demonstrated that the adult brain preferentially expresses lamin C rather than lamin A (111).

All nuclear lamins belong to class V of intermediate filaments with which share the structural organization (112).

Like all intermediate filaments proteins, lamins are composed of a central coiled coil (rod) domain which consists of four α-helical subdomains (1A, 1B, 2A, 2B) connected by flexible regions (113). The N-terminal domain (head) and the C-terminal domain (tail) contain lamin-specific motifs. The tail includes a nuclear localization signal (NLS), an immunoglobulin (Ig) fold domain, and a C-terminal CaaX (C:cysteine; a: aliphatic amino acid; X: any amino acid) specific sequence. CaaX motif is present in A and B-type lamins but it is absent in lamin C isoform (114).

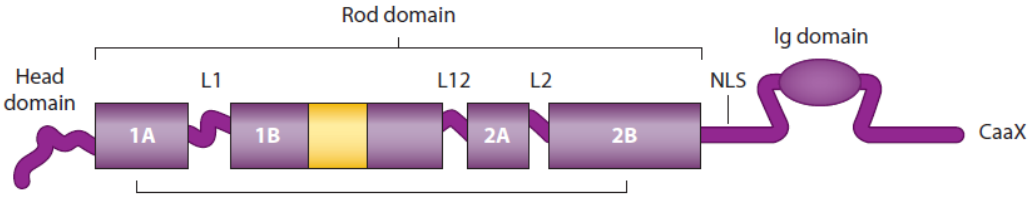

Figure 5: Organization of lamin domains (114)

To obtain the mature form of lamin A protein, the precursor undergoes to specific posttranslational modifications which mainly involve the C-terminal CaaX motif. Firstly, the cysteine residue is farnesylated, and then the –aaX residues are proteolytically removed from lamin A precursor (prelamin A) by the zinc metalloprotease ZMPSTE24 and from prelamin B1 and prelamin B2 by the endopeptidase Rce1. The CaaX motif processing is completed by the isoprenyl carboxymethyltransferase which methylates the farnesylated cysteine residue (109) (115). While the B-type lamins remain permanently farnesylated, the protease ZMPSTE24/FACE1 removes the terminal 15 amino acids (including the farnesyl-cysteine residue) from prelamin A to release the mature and shorter lamin A protein (116). A recent study demonstrated how lamin proteins are structured in their native microenvironment. Cryo-electron tomography analysis in mouse embryonic fibroblasts showed that A- and B-type lamins assemble into tetrameric filaments of

3.5 nm thickness with a length of 380 nm. Thus, lamins exhibit a structure that is remarkably different from the other canonical cytoskeletal elements (117). These filaments are located immediately beneath the INM and their basic building blocks are coiled-coil dimers disposed in parallel and in register (118).

Lamins functions comprise defining nuclear shape, mechano-signaling, participating in stress responses, organizing spatial disposition within the nucleus, controlling gene expression, regulating DNA replication and repair, contributing to cell cycle progression, and tethering chromatin (119). In particular, the heterochromatin localized adjacent to the nuclear lamina contains lamina associated domain (LAD) that interacts with nuclear lamins and other proteins of NE. LADs are enriched in low gene density and activity, and histone marks characteristics of heterochromatin, such as histone 3 lysine (H3K)9 methylation(me)2, H3K9me3, and H3K27me3 (120) (121).

Lamins present two domains that interact with chromatin, one is located in the tail region between the rod domain and the Ig domain, and the other is inside the rod domain (122) (123). Lamin expression levels perturbations often result in heterochromatic changes, like decreased levels of the heterochromatin histone markers H3K9me3 and H3K27me3, and increased levels of H4K20me3 (124).

How each lamin isoform contributes to LAD organization and regulation is still under debate. Chromatin immunoprecipitation and sequencing analysis in HeLa cells revealed particular LAD regions that are specific to lamin A or lamin B (125). Moreover, studies in mammalian cells demonstrated that the depletion of A-type lamins in differentiated cells is able to perturb LAD organization despite the presence of B-type lamins (126) (109).

However, the most known role of nuclear lamins is to provide shape and mechanical stability to the nucleus and the cell itself. The stoichiometric ratio of A- to B-type lamins is fundamental to regulate nuclear stiffness. It is proposed that lamin A acts as a highly viscous fluid that prevents nuclear deformation, while lamin B behaves as an elastic wall which tries to reestablish the original profile of nuclear shape following deformation stimuli (127). Stiffened nuclei, due to high levels of lamin proteins, are able to impair cell migration of hematopoietic cells and cancer cells (128) (129); on the contrary, depleted or low levels of lamin A can cause frequent nuclei ruptures and subsequent genomic instability (130).

The role of lamins, in particular lamin A, in maintaining nuclear shape is well established. Indeed, fibroblasts without A-type lamins show severe nuclear irregularities and a loss of nuclear circularity

(131). *LMNA* mutations result in nuclear shape anomalies, such as invagination of NE and nuclear blebs formation in human cells (132).

Also, B-type lamins play a role in the maintaining of nuclear structure stability. If they are silenced, the develop of small fragile nuclei, having functional nuclear pore complexes, takes place but these cells are not able to replicate their DNA, resulting in cell death (133).

Lamins can also indirectly influence nuclear stiffness through their downstream effects on chromatin, whose distribution can influence nuclear stiffness. The binding of heterochromatin to the nuclear lamina is known to contribute to nuclear stiffness, and the loss of lamins results in the detachment of this heterochromatin to the nuclear lamina. This is demonstrated in Hutchinson-Gilford Progeria syndrome where the presence of a mutant lamin A results in aberrant connection between peripheral heterochromatin and the nuclear lamina, leading to heterochromatin disposition throughout all the nucleus and softer chromatin which impair nuclear stiffness (134) (135) (136).

Moreover, lamin A also influences the perinuclear cytoskeletal distribution and stability. For example, the loss of A-type lamins prevents the formation of F-actin caps, making the cell nuclei much more sensitive to stretch induced by deformation (137).

1.3 Nucleo-cytoskeletal coupling

Lamins also play a fundamental role in mechano-transduction physically interacting with LINC (linker of nucleoskeleton and cytoskeleton) complex components (109). Conserved interactions between the SUN and KASH protein families (the main constituents of LINC complex), one anchored to the inner and the other to the outer NM, revealed that the nuclear membranes are physically coupled (138).

SUN proteins exist in five isoforms, with SUN1 and SUN2 that have partial functional redundancy in several cellular processes, assembling in oligomers to perform their functions in the NE (139). SUN1 and SUN2 are the most widely expressed mammalian SUN proteins, while SUN3, SUN4 and SUN5 are expressed only in testis-specific cells. However, all SUN isoforms are extended in the space between the INM and the ONM (i.e. the perinuclear space), where they interact with the KASH domain (140). A large SUN coiled-coil region spans the NE and reaches the INM where these proteins are anchored. Indeed, their N-terminal domain resides within the nucleoplasm, where interacts with A-type lamins, chromatin, and other INM proteins (141).

KASH proteins include nesprins, a protein family composed of four members (nesprins 1-4) (142). Giant nesprins (nesprin-1 and nesprin-2) are the largest isoforms, having a size of ~ 976 kDa and ~ 764 kDa, respectively, and contain the N-terminal calponin homology (CH) domain responsible for F-actin binding (143). They are composed of a spectrin-repeat-containing N-terminal domain that protrudes from the ONM to the cytoplasm, where interacts with cytoskeleton elements, such as F-actin, microtubule and intermediate filaments (144). Within the perinuclear space of the NE, nesprins interact with SUN proteins through their KASH domain, stabilizing their interaction with the INM (145).

The LINC complex contributes in regulating nuclear shape and positioning, and meiotic chromosome movements (146). Arsenovic et al. demonstrated that nesprin-2 giant (nesprin-2G) can sense myosin-dependent cellular tension to alter the nuclear shape, and it has been shown that the NE-actin binding can affect centrosome and meiotic chromosome positioning to control cell division and replication (147). LINC complex seems to be also involved in DNA repair mechanisms as demonstrated in mouse embryonic fibroblasts. *SUN1/2* genes knockdown leads to accumulation of DNA damage with consequent increased genome instability, and compromised DNA repair mechanisms (148).

Moreover, LINC complex is implicated in mechano-transduction. Through its interaction with cytoskeletal components, it can mediate the transmission of mechanical stimuli from the extracellular matrix to the nucleus, resulting in chromatin reorganization and gene expression regulation (149) (150). This reorganization can also modulate epigenetic mechanisms which controls cell differentiation. For example, several evidence identified the LINC complex as a crucial factor involved in MSC fate decision and phenotypic commitment (149). Indeed, nesprin-1 is required for a correct nucleus positioning and myotube formation, playing a role in MSC myogenic differentiation (151). The interactions between LINC complex and cytoskeletal elements are also central in cell migration. It has been demonstrated that the connection with the contractile actin cap plays a central role in fibroblasts 3D cell migration by promoting the formation of protrusions and by actively compressing the nucleus (152).

1.4 Alteration of nuclear composition and cancer progression

Historically, lamins have been described exclusively as structural proteins implicated in rare genetic disorders called laminopathies. More than 450 mutations have been identified in the *LMNA* gene associated with more than 15 syndromes (153) (154). Due to their phenotypic characteristics,

laminopathies are classified in five groups including muscular dystrophies, neuropathies, cardiomyopathies, lipodystrophies, and progeroid syndromes (155). However, several studies in the last two decades demonstrated the role of lamin proteins in influencing chromatin organization and gene expression, and their involvement in specific cellular signaling, as mechano-transduction events (156) (157). These evidences have allowed to highlight the possible role of lamins in the oncogenic processes.

Indeed, malignant cells often present specific differences in nuclear architecture, compared with normal cells. Tumor cells have misshaped and increased size of cell nucleus, and present alterations in NE composition and in the spatial arrangement of both chromosomes and chromatin (158) (159). It has been demonstrated that variations in the expression levels of structural proteins of the nuclear lamina are responsible for the acquisition of different and pathological nuclear characteristics by cancer cells. Alterations of lamin A expression levels have been detected in various cancer types, but there is not a general pattern to describe these changes during malignant transformation. For example, lamin A/C is downregulated in lymphoma, leukemia, breast and endometrial cancer samples (160) (161) (162), while an increase in lamin A/C protein expression levels has been observed in prostate cancer, ovarian and squamous cell carcinoma (163) (164). Moreover, the expression of lamin A can be considered as a prognostic factor in some cancers. Indeed, the absence of lamin A correlates with increased risk of recurrence in patients with stage II and III colon cancer and is associated to a worse prognosis in the early stages of breast carcinoma (165) (166). On the contrary, the overexpression of lamin A is correlated with a reduced overall survival in patients affected by glioblastoma multiforme (167). The expression levels of lamin A/C can also be different within tumor subtypes and associated to specific phenotypic characteristics. For example, small cell lung carcinomas present a strong expression of lamin A/C, while this protein is low/absent in non-small cell lung carcinomas (162).

The importance of lamin A levels in *in vivo* cell migration is further exemplified in neutrophils that downregulate lamin A expression during their differentiation processes to acquire nuclear deformability which is critical for the passage through narrow capillaries less than one-fifth of the cell diameter (168). In particular, the decrease of lamin A in the nuclear lamina results in more deformable and plastic nuclei that undergo to remarkable deformation, promoting the passage of cells through the basement membrane or 3D interstitial tissue, leading to the propagation of cancer cells and consequent metastases formation (169) (170). Indeed, during metastatic process, cancer cells have to squeeze through the constriction formed by the extracellular matrix and to pass tight

interstitial spaces (2 µm in diameter), which are substantially smaller than the size of the nucleus, and then disseminate in the vascular or lymphatic systems (171) (172). The main obstacle to cell deformation is represented by the nuclear stiffness, and the absence of lamin A can confer an advantage to cancer cells (173). Indeed, several studies demonstrated that highly metastatic cells have more deformable nuclei due to the absence of lamin A. Bell et al. demonstrated that the low levels of lamin A/C lead to increased nuclear deformability enhancing cell migration in breast cancer cells (174). The downregulation of lamin A has also a crucial role in metastases formation in the pulmonary adenocarcinoma cells and in the metastatization of osteosarcoma cells (175) (176).

As described above, lamin A can also modulate cytoplasmic stiffness and whole-cell mechanics through its interaction with LINC complex (177). It has been demonstrated that the expression of *LMNA* scales with tissue stiffness and cancer cell sensitivity to mechanical stress is related to *LMNA* levels (178) (127).

Lamins and associated LINC complex proteins play crucial roles in organizing cytoskeletal components, dynamics, and polarity, which are fundamental for cell migration. Damage of nucleo-cytoskeletal coupling by the absence of lamin A or altered composition/localization of NE proteins results in altered organization of cytoskeletal networks and impaired cell polarization and 2D cell migration, although effects on migration are various in different cellular models (reviewed in (178)). A global loss of NE proteins has been described in breast cancer cells and identified as a fundamental pathological player in breast cancer progression (179). Moreover, the loss of emerin, a ubiquitously expressed integral INM protein which interacts with lamins and LINC complex, is responsible for nuclear structural defects required for increased cell migration of breast cancer cells (180). The mislocalization of emerin, caused by lamin A downregulation, also discriminates cancer from benign tissue and correlates with disease progression in a prostate cancer cohort (181).

Moreover, the NE plays a fundamental role in protecting the genome, and the loss of its integrity could cause DNA damage. NE ruptures can allow uncontrolled content exchange between nucleus and cytoplasm, thus promoting DNA damage which results in genomic instability of cancer cells (182) (183) (184). In particular, lamin A influences the ability of cells to repair DNA damage, regulating p53-binding protein-1 (53BP1), a DNA repair protein and potential tumor suppressor (185). It has been demonstrated that both mouse and human fibroblasts show reduced 53BP1 stability upon lamin A loss, resulting in impaired DNA reparation (186) (187).

Finally, current data demonstrate that lamins and NE proteins can fill a very crucial role in malignant cell transformation, regulating cellular processes fundamental for cancer progression.

PhD THESIS'S AIM

A-type lamins are the main constituent of the nuclear lamina and are emerging as signaling hub able to biochemically transduce a physical stimulus from the extracellular matrix into the nucleus, affecting chromatin organization and controlling downstream effectors (188). Through their interactions with LINC complex components, they physically couple cytoskeleton and nucleoskeleton, maintain nuclear architecture, and are crucial in cell mechano-sensitivity, regulating nucleo-cytoskeletal dynamics (109). Changes in lamin A/C levels are often associated with poor prognosis in multiple human cancers (160). Indeed, the nuclear envelope, including A type lamins, influences cellular migratory capacities of cells, regulating the interplay between cytoskeletal signaling and chromatin remodeling.

The aim of this PhD project was to evaluate lamin A role in osteosarcoma and Ewing sarcoma, the two most common primary bone tumors. They are developmental, very aggressive tumors with an urgent need of novel therapeutic strategies to counteract metastases (1). Indeed, presence of metastases is the major criticism in the treatment of OS and EWS. Being the prognosis of patients with metastatic disease still dismal, novel strategies are required against these very complex diseases to control migration and dissemination of tumor cells. We identified the modulation of lamin A and the reconstitution of the functional nucleo-cytoskeletal dynamics such as one of these possible strategies. In particular, lamin A is required to maintain a correct nuclear envelope composition and high lamin A levels contribute to maintain the rigidity of nuclear envelope, thus limiting cell migration (189). Moreover, changes in the shape of cell nuclei are a frequent consequence of malignant transformation (158). Based on these findings, we wanted to evaluate lamin A expression levels in OS and EWS settings, analyzing its downstream effectors modulation, mechano-signaling events, and their impact on cellular differentiation, malignancy and migration capacity both in *in vitro* and *in vivo* models. Our hypothesis is that low levels of lamin A mediate nuclear envelope instability, altering the nucleo-cytoskeletal dynamics, and thus enhancing cancer cells growth and metastasis dissemination. We propose that drugs able to modulate prelamin A and lamin A levels, such as statins, may reverse this condition and may reprogram gene expression towards a more differentiated and less invasive and aggressive phenotype.

PART II-MATERIALS AND METHODS

1. Cell cultures

Human osteosarcoma cell lines HOS, 143B, MG63, SaOS2, U2OS were obtained from Deutsche Sammlung von Mikroorganismen und Zellkulturen GmbH (DSMZ, Braunschweig, Germany).

Adipose-derived Stem Cells (ADSCs) were acquired from Thermo Fisher Scientific and cultured in Complete MesenPro RS medium (Gibco, Thermo Fisher Scientific).

We also employed EWS cell lines (i.e. A-673, LAP-35, TC-71). LAP-35 cells were immortalized in the Experimental Oncology Laboratory, Rizzoli Orthopedic Institute of Bologna (190).

OS cell lines were cultured in DMEM (1 mg/mL glucose, Gibco, Thermo Fisher Scientific) while for EWS cell line we used IMDM (Iscove' Modified Dulbecco's Medium), supplemented with 10% fetal bovine serum (FBS, Life Technologies), 2mM l-glutamine, 100 U/mL penicillin and 100 µg/mL streptomycin (Sigma-Aldrich). All cell lines were incubated at 37 °C in a humidified atmosphere of 5% CO_2.

2. Chemicals

We employed Mevinolin (Sigma Aldrich), an inhibitor of the hydroxymethyl-glutaryl-synthase, an enzyme essential for the farnesylation of prelamin A. OS and EWS cells were treated at 2.5, 5 10, 15 or 20 µM and cellular effects were evaluated at different time points.

3. Cell Proliferation

Cytotoxic effects and cell viability after mevinolin treatment in OS cell lines were determined using MTT cell (3-(4,5-Dimethylthythiazol-2-yl)-2,5-diphenyltetrazolium bromide) proliferation kit (Roche Diagnostics), following manufacturer's instructions.

4. Annexin V-FITC/PI Staining

We employed the Annexin V-FITC Apoptosis Detection kit (eBioscience, Thermo Fisher Scientific) to perform apoptosis analysis in OS cells according to manufacturer's instructions. Analyses were assessed using a FC500 flow cytometer (Beckman Coulter) equipped with the appropriate software (version 2.2, CXP, Beckman Coulter). At least 10.000 events for sample were acquired.

5. Cell differentiation

We performed several cell differentiation experiments. ADSCs were differentiated toward the osteogenic lineage by seeding cells at low density and changing the culture medium after 2 days with Complete STEMPRO Osteogenesis Differentiation Medium (Gibco, Thermo Fisher Scientific).

We also stimulated osteoblast's differentiation of primary osteoblasts from healthy donors by BioLaM biobank (IOR CE approval 0018259-01-13, issued on 05/09/2016). These cells were cultured with osteogenic medium containing 10% FBS, 1% penicillin and streptomycin, 50 µg/mL of ascorbic acid, and 10 mM β-glycerophosphate, changing the medium every 3 days. We confirmed osteogenic differentiation by Alizarin Red Staining assay. Cells were fixed with neutral buffered formalin (10%) for 10 min, then cells were rinsed with PBS and stained with 0.5% Alizarin Red staining solution (Sigma-Aldrich, St. Louis, MO, USA) (pH 4.2) for 10 min at room temperature. Finally, the mineralized nodules were imaged by a scanner.

We also differentiated TC-71 cells toward the neural lineage, by seeding cells at low density in IMDM with 1%FBS for 72 hours.

6. qRT-PCR

RNA extraction was performed using the RNeasy Mini Kit (Qiagen), following the manufacturer's instructions. High-Capacity cDNA Reverse Transcription Kit (Thermo Fisher Scientific) was employed to obtain the c-DNA. Quantitative gene expression was assessed employing the TaqMan® Gene Expression Master Mix, using the QuantStudio1 Real-Time PCR (Thermo Fisher Scientific). *GAPDH* or *RNA 18S* ribosomal 1 gene were used as internal control genes. To assess the amount of interest genes the following probes were employed: alkaline phosphatase (*ALPL*) probe (Hs.PT.56a.40555206) from Roche Diagnostics (Basel, Switzerland), *LMNA* probe (Hs.01108900_g1), *RUNX2* (Hs.00231692_m1), *nestin* (Hs.PT.58.1185097), *SOX2* (Hs.PT.58.237897.g), Connective Tissue Growth Factor (*CTGF*) (Hs00170014), Cysteine Rich Angiogenic Inducer 61 (*CYR61*) (Hs00155479), Neurofilament H (*NEF-H*) (Hs00606024) and *β3-tubulin* (Hs.PT.58.20385221). All of these were purchased from Thermo Fisher Scientific (Waltham, MA, USA).

Results were expressed as $2^{-\Delta Ct}$ (ΔCt = CT gene of interest − CT internal control) to compare the relative gene expression among samples, and as $2^{-\Delta\Delta Ct}$ (ΔΔCt = ((CT gene of interest − CT internal control) sample − (CT gene of interest − CT internal control) universal)) to compare gene expression of the treated (or silenced/overexpressed) cell lines with that of untreated (or empty) control.

7. Western blotting

Western blotting analyses were performed using a standard method. OS and EWS cells were lysed in RIPA lysis buffer (containing 20 mM Tris-HCl (pH 7.5), 150 mM NaCl, 1 mM Na2EDTA, 1 mM EGTA1, % NP-40, 1% sodium deoxycholate, 2.5 mM sodium pyrophosphate, 1 mM, b-glycerophosphate 1 mM, Na3VO4, 0.1% SDS) plus protease inhibitors, and then sonicated. We recovered protein fractions by centrifugation at 13,000× *g*, 4 °C, for 10 min. We loaded and resolved 20-30 µg of proteins by SDS– PAGE, employing Criterion TGX polyacrylamide gels (Bio-Rad).

For samples preparation, sample buffer with β-mercaptoethanol was added to the proteins, and the samples were then heated to 95°C for five minutes. Each sample was pipetted into its own pocket in the gel, which was previously immersed in running buffer (25mM Tris base, 190mM glycine, 0.1% SDS) in the electrophoresis apparatus. Proteins were separated applying to the electrophoretic apparatus a voltage of 100 V and 125 mA.

Proteins were transferred into a nitrocellulose membrane using Trans-blot Turbo apparatus (Bio-Rad, Hercules, CA, USA) and immunoblotted.

Antibody	Product code	Company	Application	Species
LAMIN A/C	#4777	CST	WB, ICC	Mouse
GAPDH	#5174	CST	WB	Rabbit
ROCK2	PA5-78290	Invitrogen	WB	Rabbit
β-ACTIN	#4970	CST	WB	Rabbit
SUN1	HPA008346	Sigma-Aldrich	WB, ICC	Rabbit
SUN2	HPA001209	Sigma-Aldrich	WB, ICC	Rabbit
EMERIN	#30853	CST	WB, ICC	Rabbit
NESPRIN2 G	#IQ562	IMMUQUEST	ICC	Mouse
PRELAMIN A	MABT858	Merck Millipore	WB	Mouse
YAP	#14074	CST	WB, ICC	Rabbit
Phospho-YAP	#13008	CST	WB	Rabbit
MYC	#18583	CST	WB	Rabbit
β3-TUBULIN	T5076	Sigma-Aldrich	ICC	Mouse
NEUROFILAMENT-H	#2836	CST	WB, ICC	Mouse

Table 1: List of antibodies employed

Membrane was washed with PBS/Tween-20 (PBS/T) 1X and saturated for 1 hour at room temperature with 5% non-fat milk diluted in PBS/T. After three washes with PBS-T, the membrane was incubated overnight with primary antibodies (listed in Table 1) diluted in 5% of BSA in PBS/T at 4 C°.

The next day the membrane was washed with PBS/T and incubated with the appropriate secondary antibodies diluted in PBS/T. Secondary antibodies were conjugated to horseradish peroxidase.

The detection of the bands of interest was carried out with the ChemiDoc-It®2Imager digital system (UVP), using the Cyanagen Westar ECL western blotting detection reagent. Densitometric analyses were performed with the appropriate software.

8. Immunofluorescence and confocal analyses

To determine the expression and subcellular localization of the proteins of interest, OS and EWS cells were seeded on coverslips in 12-well and then fixed with cold methanol (100%) or paraformaldehyde 4% (in this case a permeabilization step with methanol/triton X-100 was performed) in PBS for 8 minutes. TC-71 cells were seeded on fibronectin-coated coverslips.

Cells were blocked with 3% BSA in PBS solution for 1 h. The incubation with primary antibodies (see Table 1) diluted in 3% BSA-containing PBS were performed overnight at 4 °C and revealed by using secondary antibodies from Thermo Fisher after an incubation for 1 hour at room temperature. Samples were mounted with a DAPI-containing anti-fade reagent (Molecular Probes, Thermo Fisher) and observed with a Nikon Eclipse Ni epifluorescence microscope. The images were detected with NIS-Elements 4.3 AR software and processed using Photoshop CS6 (Adobe Systems, Inc., San Jose, CA, USA).

We also used a Leica TCS-SP8X laser-scanning confocal microscope (Leica Microsystems, Mannheim, Germany) equipped with tunable white light laser (WLL) source, 405 nm diode laser, 3 Internal Spectral Detector Channels (PMT), and 2 Internal Spectral Detector Channels (HyD) GaAsP. Sequential confocal images were acquired using an HCPLAPO 63x oil-immersion objective (1.40 numerical aperture, NA, Leica Microsystems).

9. Gene overexpression/silencing

OS transient transfections were performed according to manufacturer's protocol, using Lipofectamine 3000 (Thermo Fisher Scientific). We overexpressed lamin A-GFP plasmid, using a pEmpty-EGFP as control, in 143B and HOS cells.

We also employed Empty-GFP and Lamin A-GFP plasmids (Clontech) carrying the Enhanced Green Fluorescent (EGFP) gene and a neomycin resistance gene expression cassette to stably transfect TC-71 cells. We obtained three stably transfected clones: Empty-GFP vector #2, lamin A-GFP #30-40 and lamin A-GFP #84.

We also performed a loss of function approach, silencing *LMNA* gene. We employed siRNAs duplexes specific for human *LMNA* (siRNA *LMNA*) purchased from Thermo Fisher Scientific. Scrambled duplexes were used as control. Approximately at 50% of confluence, MG-63, A-673 and LAP-35 cells were transfected with the specific siRNA-*LMNA* and siRNA-scrambled using lipofectamine 3000 protocol.

We also overexpressed an unprocessable prelamin A isoform (LA-C661M), in both OS and EWS cell lines.

10. Wound healing

OS and EWS cells were seeded in multi-well plates and left to grow until they reached the confluence. Then, a reproducible longitudinal scratch was made in the confluent monolayer by the use of a sterile micropipette tip. The process of wound closure was monitored at 0 and 24 hours with inverted light microscopy (Olympus CKX41, Olympus Corp.) mounted with a digital camera (C-7070 Wide Zoom, Olympus) at 10X magnification. To standardize every time the illustrated field (our region of interest (ROI)), we traced a horizontal line under each plate passing through the center of all wells. We used a computerized image analysis system (Qwin, 3.0 software, Leica Microsystem Imaging Solution, Ltd., Wetzlar) to assess morphometric analysis of cell migration. The wound healing closure was determined as (1-Ax/A0) %, where A0 and Ax correspond to the empty scratch area at 0 and 24 h, respectively.

11. Migration and invasion assays

We employed CytoSelect Cell Migration Assay Kit and Invasion Assay Kit (Cell Biolabs.) to study the migration and invasion abilities of EWS cell lines. Kit is composed of transwells covered with 8 µm pore size polycarbonate membrane for migration assay, while the membrane contains a layer of matrigel in the invasion assay kit. To be considered invasive cells must before degrade the matrigel layer and then migrate through the pores of the membrane. Each experiment was performed in 24-well plates. We added 300 µl of serum-free medium to each transwells to rehydrate the membranes and incubated them at 37°C for one hour. Then, we removed the serum-free medium and added 500 µl of 20% fetal bovine below the transwell. An exact number of OS and EWS cells have been

resuspended with 1% serum-free medium and seeded in 300 µl for each transwell. We incubated the plates at 37°C, in 5% CO2 in a humidified atmosphere. At different time points (24 or 48 hours), the medium was removed from the transwell and the inserts have been stained with 400 µl of Cell Stain Solution and incubated for 15 minutes at room temperature. We then performed several washings and used cotton swabs to remove the excess of colorant. At the end, inserts were incubated with 200 µl and the solution read using an ELISA plate reader (absorbance at 570 nm). Finally, the data obtained were reported as percentages, considering the invasion of Empty vector or scramble cells as 100%.

12. Patients

Microarray data analyses were performed in EWS samples (GSE17679 in gene expression omnibus (GEO)) to assess *LMNA* gene expression (probe 203411_s_at) (191). We evaluated *LMNA* levels in 64 patients and these values were plotted for metastatic samples and primary samples. We also analyzed microarray data (GSE63157) of EWS patients (192). We considered EWS patient's clinical data and we created a Kaplan-Meier graph plotting 5 years overall survival rate in relation to *LMNA* values.

13. Immunohistochemistry

We assess lamin A immunostaining through avidin–biotin–peroxidase method. The nuclear shape in relation to *LMNA* expression was evaluated in four representative EWS samples (patients R72, R80 R48, R29) from GSE17679 (191). Prior to incubation with the anti-lamin A/C antibody (E-1, mouse, sc-376248 dilution 1:100; Santa Cruz Biotechnology), the antigen retrieval was performed using citrate buffer pH 6.0. Representative images were captured with a Nikon Microscope (100X). We used the contour ratio algorithm to measure nuclear circularity. The following formula, with the use of NIS-Elements 4.3 AR software were applied: Contour ratio=4π x nuclear area/nuclear perimeter^2**.**

14. *In vivo* studies

For the in vivo studies, immunodeficient double knockout BALB/c Rag2-/-;Il2rg-/- mice were kindly provided by the Central Institute for Experimental Animals (Kawasaki, Japan) (193) and bred in the Animal Care Facility of the Laboratory of Immunology and Biology of Metastasis (University of Bologna). To evaluate the metastatic potential of EWS cells, we injected intravenously (iv) 2× 10^6 cells/mouse of TC-71 parental cells and the stably transfected clones, Empty-GFP vector #2, lamin-

GFP #30-40 and lamin-GFP #84 in mice. Each group was composed of 7 male mice, 19-33-week-old**.** On the basis of age, the animals of each litter were randomly assigned to the different experimental groups. Mice were sacrificed after 4 weeks and the count of metastases was performed. We analyzed metastatic lesions at adrenal glands, interscapular brown fat, lymph nodes, kidneys, lungs (stained with black India ink), and livers (fixed in Fekete's solution). We measured the size of liver metastases macroscopically visible on the surface of liver lobes with calipers and individual metastasis volume was calculated as $\pi \cdot [\sqrt{(a \cdot b)}]3/6$ where a and b are the two maximal perpendicular diameters.

15. Statistical analysis

All *in vitro* experiments were repeated three times independently, and the mean/median values ± SD were plotted. Quantitative data were compared by two-tailed unpaired Student's t-test and ANOVA with Bonferroni's or Dunnet's post-test multiple comparisons test when appropriate.

LMNA gene expression values in primary versus metastatic tumors and individual liver metastasis volume analyses were expressed as mean ± SEM.

Spearman rank correlation analysis was performed to assess correlation analyses between lamin A protein expression levels and EWS migration capabilities. We estimated the survival probability of EWS patients according to their median value of *LMNA* using the Kaplan-Meier method and log-rank tests.

Differences in metastases number and volume in *in vivo* models were evaluated with the nonparametric Mann-Whitney test.

Variances with p values <0.05 were considered statistically significant (p values: $*p < 0.05$; $**p < 0.01$; $***p < 0.001$). Statistical analyses were performed using Graph Prism Software (version 5).

PART III-RESULTS AND DISCUSSION

MANUSCRIPT 1: LAMIN A AND PRELAMIN A COUNTERACT MIGRATION OF OSTEOSARCOMA CELLS

Camilla Evangelisti[1,2,†], **Francesca Paganelli**[3,†], Gaia Giuntini[4], Elisabetta Mattioli[1,2], Alessandra Cappellini [3], Giulia Ramazzotti [3], Irene Faenza[3], Maria Cristina Maltarello[5], Alberto M. Martelli[3], Katia Scotlandi[6], Francesca Chiarini[1,2,*] and Giovanna Lattanzi[1,2,*]

[1] CNR Institute of Molecular Genetics "Luigi Luca Cavalli-Sforza" Unit of Bologna, 40136 Bologna, Italy
[2] IRCCS Istituto Ortopedico Rizzoli, 40136 Bologna, Italy
[3] Department of Biomedical and Neuromotor Sciences, University of Bologna, 40126 Bologna, Italy
[4] Department of Molecular and Development Medicine, Cellular and Molecular Physiology Unit, University of Siena, 53100 Siena, Italy
[5] Laboratory of Musculoskeletal Cell Biology, IRCCS Istituto Ortopedico Rizzoli, 40136 Bologna, Italy
[6] Experimental Oncology Laboratory, IRCCS Istituto Ortopedico Rizzoli, 40136 Bologna, Italy

* Authors to whom correspondence should be addressed.
† These authors contributed equally to this work.

Published on *Cells* 2020, *9*(3), 774; **https://doi.org/10.3390/cells9030774**

Abstract: Lamin A/C is the main constituent of the nuclear lamina and changes in its expression levels correlate with malignant transformation in several tumors. However, the role of lamin A has not been explored in osteosarcoma (OS). Here, we assessed the role of lamin A in OS aggressiveness. Firstly, we evaluated lamin A/C expression in OS cells compared to osteobalsts (OBs) and the we studied the effects of lamin A overexpression in OS cell lines. We demonstrated that lamin A expression increases during OBs differentiation, while it is expressed at very low levels in OS cell lines. Low expression of lamin A promotes migratory abilities in OS cells; on the contrary, the OS migratory potential resulted attenuated after lamin A overexpression. Moreover, we overexpressed an unprocessable prelamin A, which also led to decreased OS cell migration. To accumulate prelamin A, we treated OS cells with mevinolin, a statin able to inhibit lamin A maturation and we obtained a significantly reduction in migration abilities. Mevinolin treatment also induced an apoptotic cell death in a RAS-independent, lamin A-dependent manner. Pro-apoptotic effects and cell migration inhibition obtained by mevinolin treatment are comparable to those obtained by prelamin A overexpression, suggesting that modulation of lamin A expression and its post-translational processing can be a novel strategy to reduce migratory capacities in OS.

1. Results

1.1 Lamin A levels increase during osteogenic differentiation

We cultured osteoblasts from healthy donors in differentiation medium for 21 days and we observed morphological changes and the formation of hydroxyapatite crystals in cell cultures after 7 days of culture (Figure 6a).

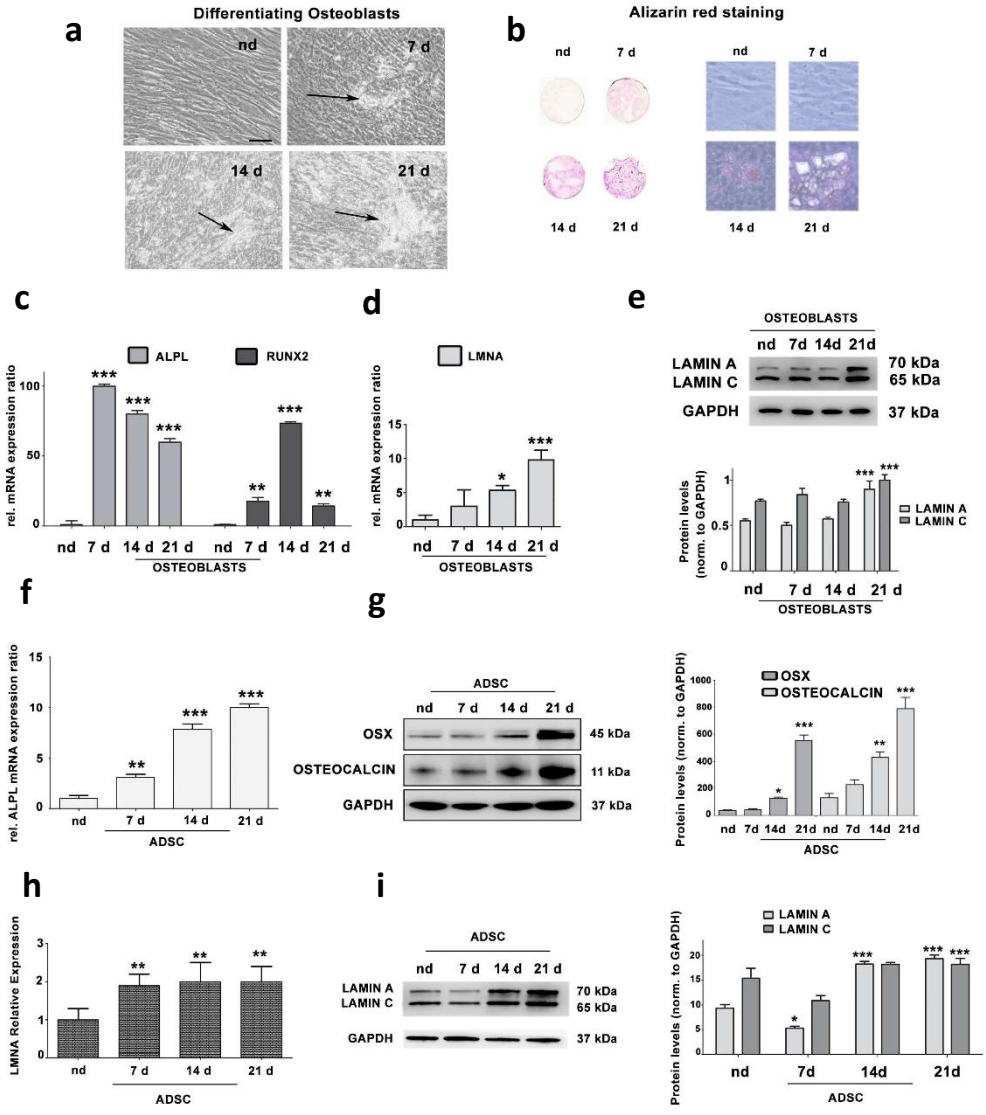

Figure 6: (**a**) Representative images of osteoblasts cultured for 7, 14, 21 days in differentiating medium. Arrows indicate hydroxyapatite crystals; (**b**) Alizarin Red staining of osteoblasts at 7, 14 or 21 days in differentiation medium; (**c**) *ALPL* and *RUNX2* gene expression by qRT-PCR analysis in nd versus differentiated osteoblasts (OBs); (**d**) *LMNA* gene expression analysis by qRT-PCR in nd versus differentiated osteoblasts (OBs); (**e**) Western blotting analysis of lamin A/C protein expression in nd and differentiated OBs. Densitometric analysis is shown as mean values ± SD of three different experiments; (**f**) *ALPL* gene expression by qRT-PCR analysis in nd versus differentiated osteoblasts; (**g**) Protein expression analysis of Osterix (OSX) and Osteocalcin by western blotting. Densitometric analyses are plotted on the right; (**h**) *LMNA* gene expression analysis by qRT-PCR in ADSCs versus differentiated OBs; (**i**) Western blotting analysis of lamin A/C protein expression in non-differentiated ADSCs (nd) and differentiated OBs. Densitometric analysis is reported as mean ± SD.

Alizarin red staining confirmed osteoblast differentiation (Figure 6b), and we found a strong upregulation of *ALPL* and *RUNX2* genes, well-established osteoblast differentiation markers (Figure 6c). Moreover, *LMNA* gene and lamin A/C protein levels were significantly upregulated during osteoblast differentiation, relative to undifferentiated cells (nd) (Figure 6d, 6e). We also employed adipose tissue-derived pluripotent stem cells (ADSCs), which can differentiate into different cell types, including osteoblasts (194) (195). After 21 days of cell culture in osteogenic differentiation medium, we demonstrated a significant increase in *ALPL* gene expression (Figure 6f). Moreover, protein levels of osteogenic differentiation markers Osteoblast-specific Transcription Factor Osterix (OSX) and Osteocalcin were significantly increased in ADSCs at 14 and 21 days in differentiating medium (Figure 6g). During ADSC osteogenic differentiation, also *LMNA* gene expression was significantly increased (Figure 6h), accompanied by a significant upregulation of lamin A/C protein at day 14 and 21 (Figure 6i).

1.2 Osteosarcoma cells express low levels of lamin A/C

Western blot analysis showed that OS cell lines expressed significantly lower lamin A expression levels relative to OBs from healthy donors differentiated for 21 days (Figure 7a, 7b).

However, as compared to other OS cell lines, MG63 showed higher amount of lamin A (Figure 7a, 7b), while the lowest lamin A/C levels were detected in HOS cells, and in the 143B Ras-mutated HOS-derived cell line (Figure 7a, 7b).

Immunofluorescence analyses demonstrated that lamin A/C was localized at the nuclear periphery in OS cells (Figure 7c, 7e). We observed morphological nuclear abnormalities both in osteoblasts and osteosarcoma cells. However, honeycomb structures, typical of some laminopathic cells, were only detected in OS nuclei (Figure 7d, 7f).

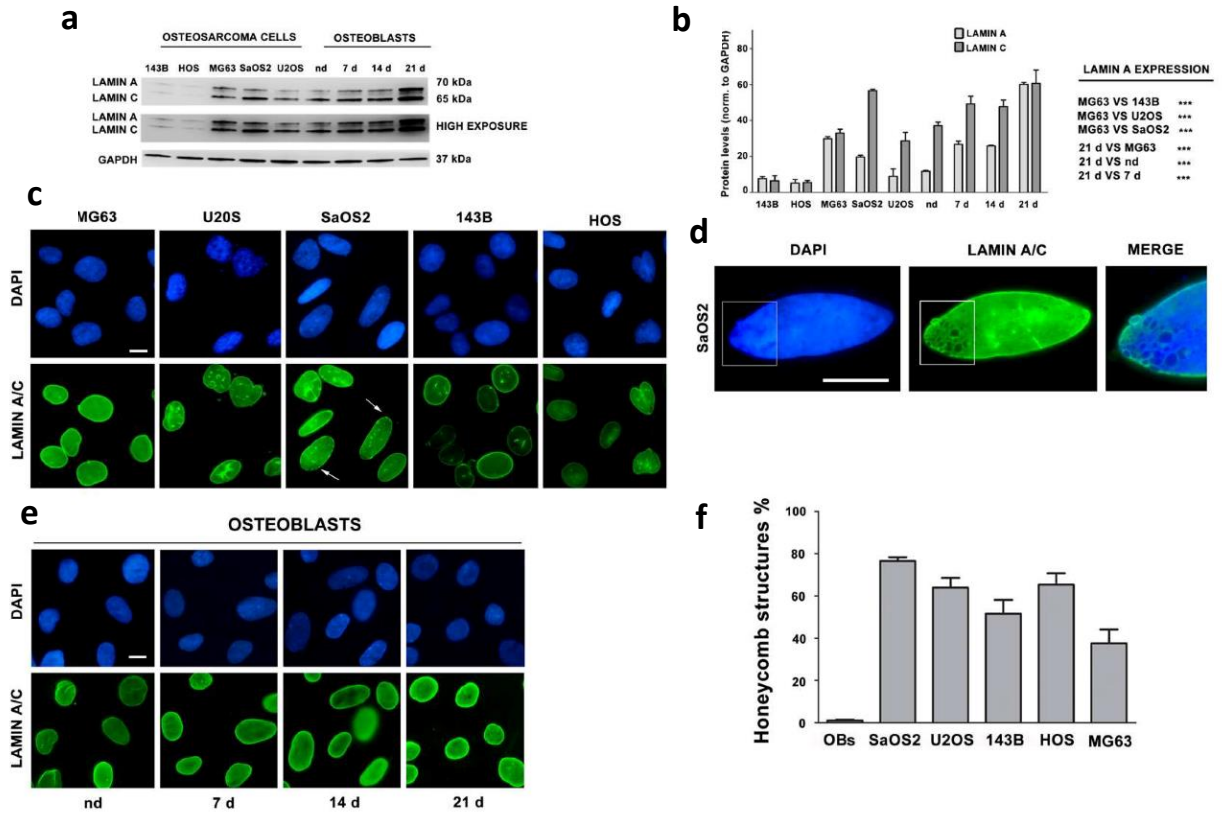

Figure 7: (**a**) Western blotting analysis of lamin A/C in osteosarcoma (OS) cell lines, and OBs from healthy donor differentiated for 7, 14, 21 days in osteogenic medium; (**b**) Densitometric analysis of lamin A/C as mean values ± SD of three different experiments; (**c**) Immunofluorescence staining of lamin A/C in OS cell lines. Arrows indicate honeycomb structures; (**d**) High magnification of a honeycomb structure in a SaOS2 nucleus. The area indicated in the rectangle is shown at higher magnification in the merged image (merge); (**e**) Immunofluorescence staining of lamin A/C in osteoblasts (OBs) from healthy donors differentiated for 7, 14 or 21 days in osteogenic medium; (**f**) Percentage of honeycomb structures detected in osteoblasts at all differentiation stages or in osteosarcoma cells. Mean of values ± SD are plotted.

1.3 Low *LMNA* expression confers migration and proliferation abilities to OS cells

We overexpressed lamin A/GFP fusion protein in 143B and HOS cell lines, which have the lowest lamin A/C levels. Western blotting analyses confirmed lamin A/C overexpression after 24 h of transfection in 143B and HOS cells (Figure 8a). Then, we wanted to analyze the effect of lamin A overexpression on cellular proliferation. Overexpression of lamin A also impacted on cell proliferation leading to decreased cell proliferation in 143B cells 24 and 48 h after transfection with lamin A/GFP vector (Figure 8b). Then, we tested migration abilities of lamin A transfected cells. Lamin A overexpressing cells displayed a significantly lower migration potential in wound healing assay compared to cells only expressing GFP (Figure 8c). We confirmed the involvement of lamin A in reducing cellular migration, silencing the *LMNA* gene in MG63 cells and demonstrating that the silenced cells migrated faster compared to scramble (Figure 8d, 8e).

Based on these results, we performed a wound healing assay on five OS cell lines. 143B and HOS, which express the lower amount of lamin A/C, completeley repaired the wound after 24 h. On the

contrary, MG63 cells, with the highest lamin A amount among OS cell lines, were not able to totally repair the wound in the same time (Figure 8f, 8g).

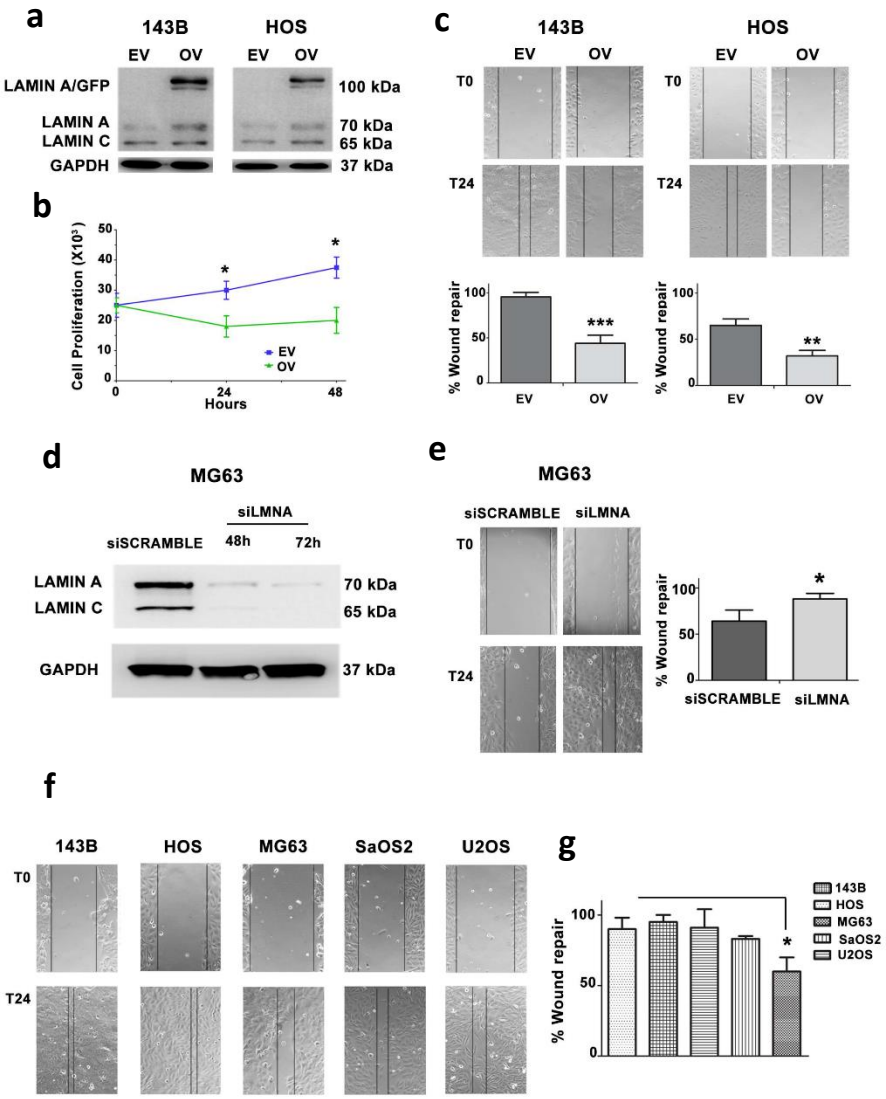

Figure 8: (**a**) Western blotting analysis of lamin A/C in 143B and HOS cells transfected with GFP and lamin A/GFP; (**b**) Cell count of 143-B viable transfected cells after 24 and 48 h after transfection; (**c**) Wound healing assay in 143B- and HOS-transfected cells. Representative pictures were taken at 0 and 24 h after scratching. Magnification 10×. Histograms of cell migration of 143B- and HOS-transfected cells are plotted; (**d**) Western blotting analysis of lamin A/C in siScramble- and siLMNA-transfected MG63 at 48 and 72 h of transfection; (**e**) Wound healing assay of siScramble- and siLMNA-transfected MG63. Representative pictures were taken at 0 and 24 h after scratching. Magnification 10×; (**f**) Wound healing assay of OS cell lines; (**g**) Histograms of OS cell migration in wound healing assay as mean ± SD.

1.4 Prelamin A accumulation decreases migration abilities of OS cells

We then tested if an unbalance in lamin A maturation could reduce migration potential of OS cells. To this aim, we expressed an unprocessable prelamin A sequence (LA-C661M), which causes accumulation of non-farnesylated prelamin A, in 143B and HOS cells. As expected, we obtained prelamin A accumulation in both cell lines (Figure 9a) which lead to a significant decrease in migration ability in 143B and HOS cells (Figure 9b).

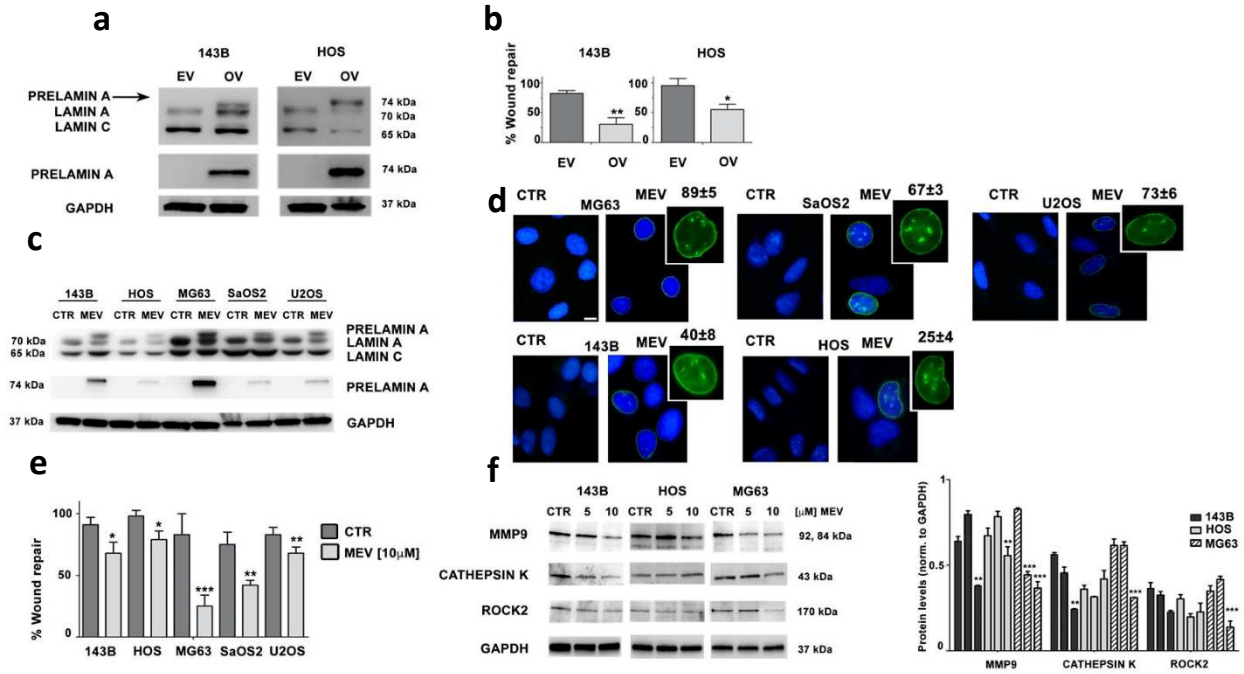

Figure 9: (**a**) Western blotting analysis of prelamin A and lamin A/C in 143B and HOS cells overexpressing prelamin A; (**b**) Wound healing assay performed in 143B and HOS cells overexpressing prelamin A; (**c**) Western blotting analysis of lamin A/C and prelamin A in OS cell lines treated with mevinolin (10 μM); (**d**) mmunofluorescence analysis of prelamin A in OS cells treated with mevinolin (10 μM) for 24 h; (**e**) Wound healing assay of OS cell lines treated with mevinolin (10 μM); (**f**) Western blotting analysis of MMP9, Cathepsin K, and ROCK2 proteins in 143B, HOS, and MG63 cells treated with mevinolin. Densitometric analyses are plotted on the right.

We then employed mevinolin, a drug known to reduce the production of farnesyl-pyrophosphate that is fundamental for prelamin A farnesylation and further lamin A maturation, causing accumulation of non-farnesylated prelamin A (196). We treated OS cell lines with mevinolin, obtaining accumulation of prelamin A (Figure 9c). Prelamin A accumulation was also confirmed in immunofluorescence analysis which also showed intranuclear clusters and invaginations, typical nuclear morphological changes associated with this phenomena (Figure 9d) (197). After mevinolin treatment, we also obtained a decrease in cell motility in all OS cells (Figure 9e).

Moreover, we evaluated signaling effectors of cellular migration and invasion, like MMP9 (matrix metallopeptidase 9) and Cathepsin K, showing a significant decrease in their protein expression levels in MG63 OS cells tratedi with statin and, to a lesser extent in the other OS cell lines (Figure 9f). Finally, ROCK2 (Rho-associated protein kinase 2) kinase, a crucial intracellular player regulating OS migration (198) (76), was significantly downregulated in MG63 OS cells (Figure 9f).

1.5 Effects induced by mevinolin are mediated by prelamin A accumulation in OS cells

We treated OS cells with increasing concentration of mevinolin and evaluated concentration-dependent viability. Only 143B and HOS cells showed a significant reduction in cell viability (around 25% when mevinolin was employed at 10 µM concentration) after 24 or 48 h of treatment (Figure 10a). However, the most significant effect of mevinolin was observed after 72 h of treatment in MG63 cells , expressing the highest prelamin A levels (Figure 10a). Consinstent with this, after long-term mevinolin treatment, MG63 cells show the highest percentage of apoptotic cells (Figure 10b).

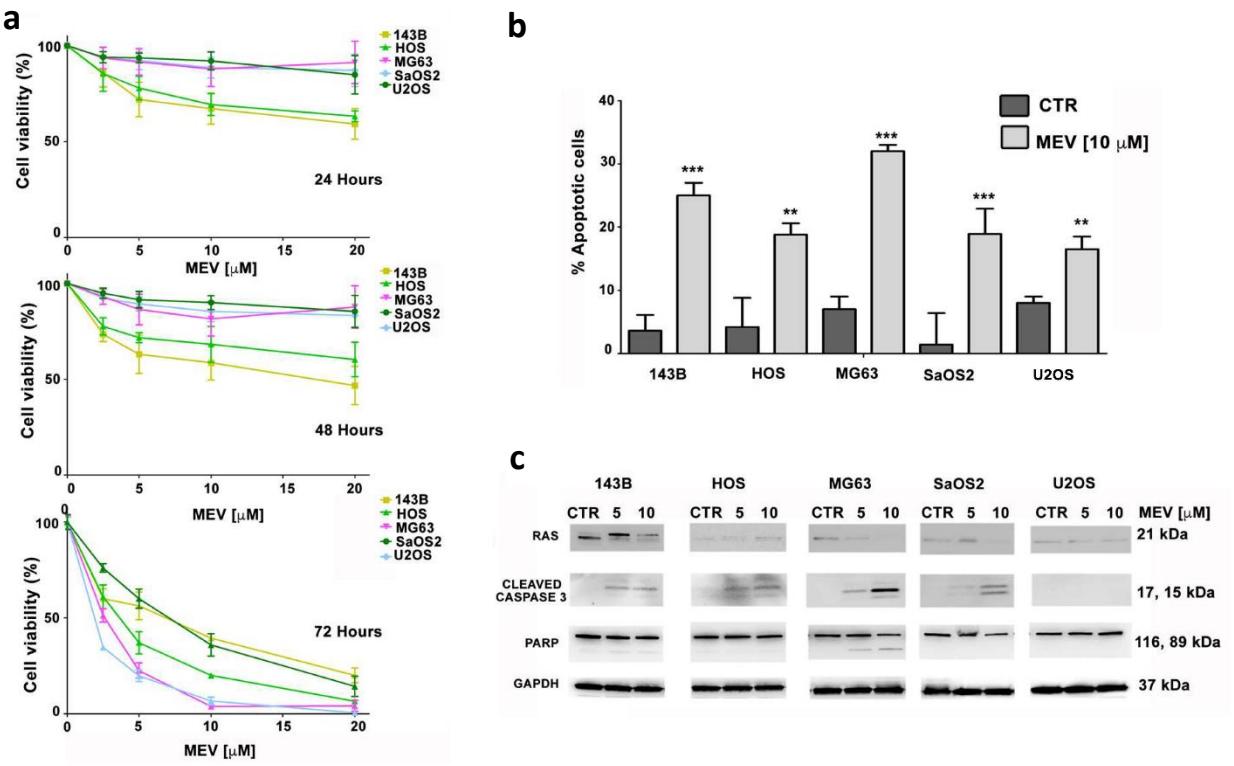

Figure 10: (**a**) MTT assays performed at 24, 48, and 72 h after treatment with increasing concentrations of mevinolin; (**b**) Percentage of apoptotic (Annexin V-FITC/PI staining) OS cells treated with mevinolin for 48 h; (**c**) Western blotting analysis of Ras, cleaved caspase 3 and PARP protein in OS cell lines treated with mevinolin.

Proliferation and cell survival, particularly in cancer cells, is also related to Ras, whose activity is dependent on farnesylation (199). Since 143B cells carry a Ras mutation (200), we reasoned that mevinolin-induced reduction of cellular viability could be also related to the effects on Ras de-farnesylation. Interestingly, while impairment of Ras farnesylation by mevinolin was evident in 143B cells, the highest activation of apoptotic markers, such as cleaved Caspase 3 and PARP (Poly (ADP-ribose) polymerase), was obtained in mevinolin-treated MG63 cells (Figure 10c). These results suggest that, although effects of mevinolin on apoptosis and cell viability are partly mediated by Ras inhibition, the most effect on cell survival is associated with prelamin A accumulation.

2. Discussion

Recently, an increasing number of studies has reported the implication of lamin proteins in human cancers (160). However, their role in OS, the most common primary malignant neoplasia of the skeletal system (14) , has not been investigated.

Lamin A seems to be involved in differentiation of human bone marrow stromal cells as its levels increase during osteogenesis (201). Here, we firstly evaluated lamin A physiological expression in ADSCs and in differentiated OBs derived from ADSC cells or from healthy donors, demonstrating that lamin A plays a role in differentiation process. Indeed, our results are consistent with prevoius reports that demonstrated the involvement of lamin A in differentiation of several cellular types (202). In particular, it has been demonstrated that lamin lamin A/C knockdown suppresses OB differentiation (201) (203). We observed lower lamin A expression levels relative to differentiated OBs in all OS cells here examined, suggesting that the loss of lamin A could play a role in OS tumorigenesis. Consistent with this hypothesis, we demonstrated that lamin A protein levels directly correlate with deceased migration and proliferation of OS cells and overexpression of lamin A in 143B OS cells, which express very low lamin A levels, is sufficient to significantly reduce cellular migration.

On the basis of these results, we tested the effects of mevinolin, a statin that interferes with processing of prelamin A, lamin A precursor protein, inhibiting the HMG-CoA (3-hydroxy-3-methylglutaryl-coenzyme A) reductase enzyme. This one is fundamental for farnesyl production which is required for prelamin A maturation, and its inhibition results in the block of isoprenoid lipids in the mevalonate pathway (197) (204). This condition reduces availability of the farnesyl amount to many cellular constituents, among which prelamin A and Ras are examples. Currently, statins are used in human to hypercholesterolemia treatment. Previous studies demonstrated that statins sensitize OS cells to chemotherpy, having a synergistic effect in reducing cell invasiveness of human and murine OS cells (205) (206). Here, we wanted to evaluated the role of prelamin A in statin-dependent effects. We confirm that mevinolin effects are related to Ras de-farnesylation and inhibition, but our data show that the highest efficacy of mevinolin treatment is obtained in OS cells that accumulate the highest prelamin A levels. This supports the observation previously proposed in a study performed in laminopathic mice (207), that prelamin A accumulation per se reduces tumor cell migration and metastatic potential. The role of prelamin A accumulation in reducing cell migration was also demonstrated in pancreatic cancer cells (208). In addition, our study demonstrated that the reduction of cellular migration is the first effect of statin in OS cells, while

effects on cellular viability are visible later on. The effects of statin tretatment on cell migration could be linked to lamin A and prelamin A accumulation at the nuclear lamina and changes in cytoskeleton-dependent dynamics, previously well documented (209) (129, 156).

What is the mechanism regulated by prelamina A and resulting in decreased OS cell migration remains to be investigated. A possible explanation could be that changhes in lamin A levels are reflected in LINC-dependent effects on mechanosignaling and cell migration. In fact, previous studies demonstrated that accumulation of prelamin A can increase SUN1 levels having effects on nucleo-cytoskeleton interplay (209, 210). Accordingly, a recently published paper shows that low levels of SUN1 increase migration of bone-marrow derived MSCs (211).

This study demonstrates for the first time a role of lamin A in the regulation of crucial tumor aspects, such as proliferation, differentiation and migration capabilities of OS cells. Although further studies are fundamental to validate the clinical relevance of our observations, these data support the possible use of statins as adjuvant agent in OS therapy.

MANUSCRIPT 2: LAMIN A AND THE LINC COMPLEX ACT AS POTENTIAL TUMOR SUPPRESSORS IN EWING SARCOMA

Francesca Chiarini[1,2,*,†], **Francesca Paganelli**[1,3,†], Tommaso Balestra[4,5], Cristina Capanni[1,2], Antonietta Fazio[3], Maria Cristina Manara[4], Lorena Landuzzi[4], Stefania Petrini[6], Camilla Evangelisti[3], Pier-Luigi Lollini[5], Alberto M. Martelli[3], Giovanna Lattanzi[1,2,*]and Katia Scotlandi[4,*]

[1]CNR Institute of Molecular Genetics "Luigi Luca Cavalli-Sforza", Unit of Bologna, 40136, Bologna, Italy
[2]IRCCS Istituto Ortopedico Rizzoli, 40136, Bologna, Italy
[3]CNR Institute of Molecular Genetics "Luigi Luca Cavalli-Sforza", Unit of Bologna, 40136, Bologna, Italy
[4]Alma Mater Studiorum, University of Bologna, Department of Biomedical and Neuromotor Sciences, 40136, Bologna, Italy
[5]IRCCS Istituto Ortopedico Rizzoli, Experimental Oncology Laboratory, 40136, Bologna, Italy
[6]Alma Mater Studiorum, University of Bologna, Department of Experimental, Diagnostic and Specialty Medicine, 40138, Bologna, Italy
[7]IRCCS Istituto Ortopedico Rizzoli, 40136, Bologna, Italy
[8]Confocal Microscopy Core Facility, Research Center, Bambino Gesu' Children's Hospital IRCCS, 00146, Rome, Italy
[9]CNR Institute of Molecular Genetics "Luigi Luca Cavalli-Sforza", Unit of Bologna, 40136, Bologna, Italy
[10]IRCCS Istituto Ortopedico Rizzoli, 40136, Bologna, Italy
[11]IRCCS Istituto Ortopedico Rizzoli, Experimental Oncology Laboratory, 40136, Bologna, Italy

* Authors to whom correspondence should be addressed.
† These authors contributed equally to this work

Published on *Cell Death and Disease* 2022 Apr 14;13(4):346; **doi: 10.1038/s41419-022-04729-5**

Abstract: Lamins are type V intermediate filaments which constitute the nuclear lamina and are involved in a wide range of nuclear functions, including higher order genome organization, transcriptional regulation, stress response and mechano-signaling. Lamin A interacts with LINC complex components, constituted by the nuclear envelope proteins SUN1, SUN2 and nesprins that connect the nucleoskeleton to the cytoskeleton, cooperating in mechano-transduction. Alterations in lamin A/C expression levels correlate with malignant transformation in several types of cancer. However, the role of lamin A/C has not been explored in Ewing sarcoma (EWS), an aggressive developmental bone tumor. Here, we investigated lamin A fate and biological role in EWS settings. We found a significant inverse correlation between lamin A expression and invasiveness, showing that low *LMNA* levels are an unfavorable prognostic marker in EWS patients. *In vitro* experiments demonstrated that low lamin A expression correlated with increased cell invasion, and with enhanced metastatic load *in vivo*.

We further observed that LINC proteins are mislocalized in EWS cells, while increase of lamin A or prelamin A levels rescue LINC complex mislocalization, thereby promoting a more differentiated phenotype and a significant decrease in invasiveness, also mediating a significant downregulation of YAP/TAZ signaling. Based on these findings, we tested statins, as a tool to promote accumulation of prelamin A. Interestingly, in EWS cells, mevinolin not only induced prelamin A accumulation, but also increased lamin A/C expression and rescued LINC complex proteins, an effect reflected on cytoskeleton reorganization and differentiation. As a consequence, mevinolin-treated EWS cells acquired a more differentiated phenotype and significantly reduced their migration and invasion abilities. These results demonstrate that acting on nuclear envelope remodeling could be a new strategy to be exploited to improve EWS outcome.

1.Results

1.1 Low *LMNA* levels correlate with aggressiveness and poor prognosis in EWS patients

To assess the role of lamin A/C in EWS, we firstly evaluated microarray datasets. We analyzed *LMNA* transcript expression in sixty-four samples (GSE 17679), divided in patients with primary tumors or with metastatic lesions (191), showing a significant lower *LMNA* gene expression in metastasis (Figure 11a). We then verified the status of cell nuclei's shape in relation to lamin A expression levels in four (2 primary local tumors vs 2 metastatic lesions) representative clinical samples from patient tissue samples of GSE17679. Immunohistochemistry analyses and contour ratio analyses of EWS cell nuclei demonstrated that cells with higher lamin A expression (primary lesions) and cells with lower levels of lamin A (metastatic lesions) had significant difference in the contour ratio values. In particular, cells with lower *LMNA* levels (from metastatic lesions) showed significant less nuclear circularity, compared to cells from primary patients with higher *LMNA* gene expression (Figure 11b). We then evaluated another dataset (GSE63157) which included clinical data from primary EWS tumors, founding a correlation between *LMNA* gene expression and five years overall survival of EWS patients (192). We classified patients as high- or low- *LMNA* expressors, according to the median value of *LMNA* gene expression, obtaining a Kaplan-Meier survival curve, which indicated that patients with higher expression of *LMNA* in their primary tumors had a significantly better overall survival ($p < 0.04$) (Figure 11c). Based on these findings, we performed deeper *in vitro* analysis using a panel of patient-derived EWS cell lines. We evaluated lamin A/C protein levels and we found that it is expressed at low levels in EWS cell lines, except for LAP-35, which derives from a PNET (Primitive Neuro-Ectodermal Tumors) tumor and showed a more differentiated phenotype (190) (Figure 11d).

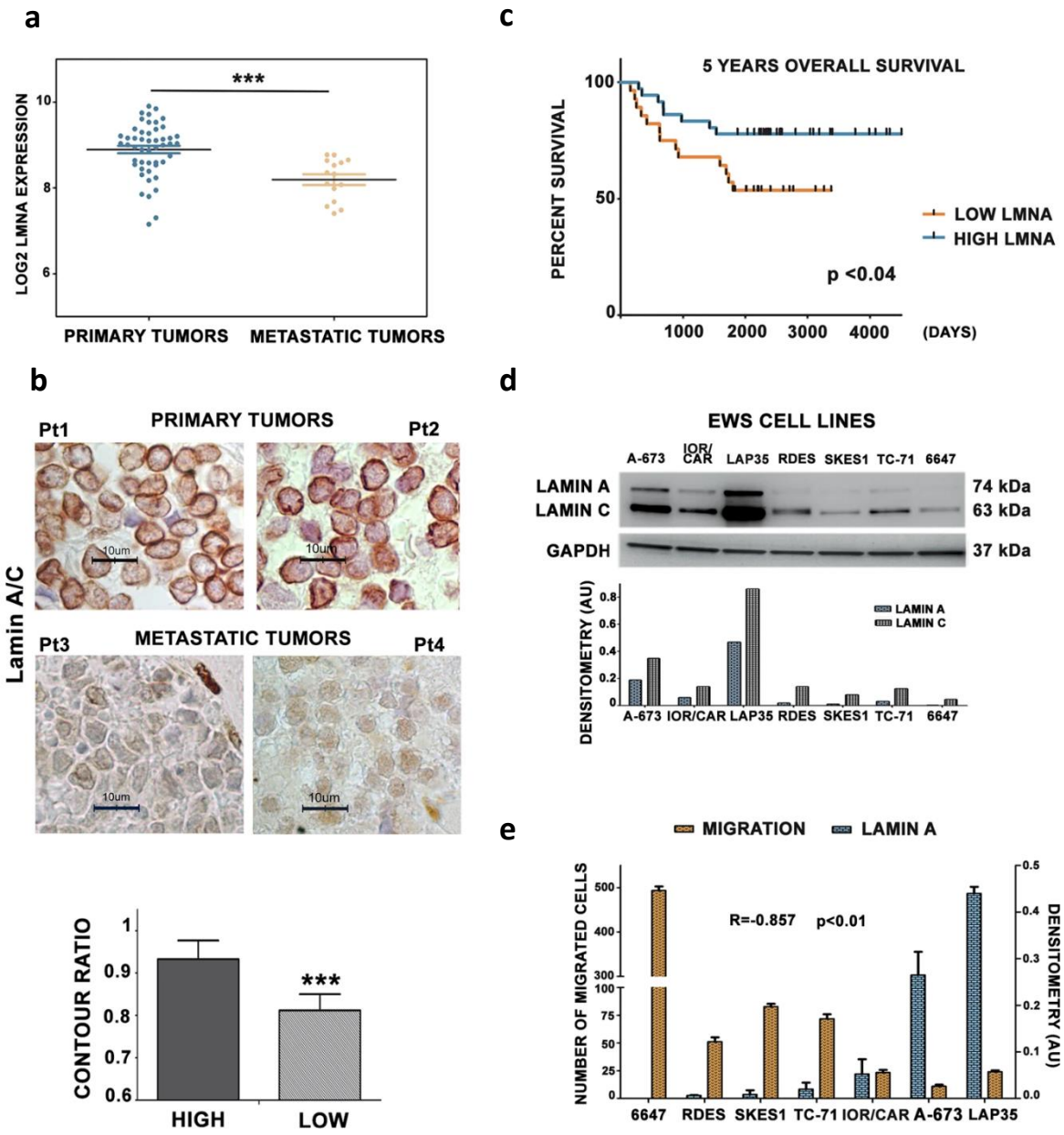

Figure 11: (**a**) *LMNA* gene expression levels (GSE17679) in EWS patients with primary tumors and metastatic tumors; (**b**) Representative images of immunohistochemical staining for lamin A in four EWS patient samples. Magnification 100X, scale bar 10 µm. Contour ratio of nuclei determined in four EWS samples with high and low *LMNA* expression, based on GSE17679 is reported in the graph; (**c**) Comparison between values of *LMNA* gene expression and five-years overall survival shown by Kaplan-Meier curve; (**d**) Western blotting analysis of lamin A/C protein expression in EWS cell lines. Graph shows densitometric analysis as ratio referred to GAPDH, used as loading control; (**e**) Lamin A expression levels and migration ability values are plotted. Spearman's rank correlation test demonstrated a significant inverse correlation among these two characteristics.

Since migration capacity is fundamental to promote metastatic processes, we correlated lamin A/C protein expression with migration abilities of EWS cells, demonstrating a significant inverse

correlation between lamin A expression and cell migration (Spearman's rank correlation r=-0.857; p < 0.01) (Figure 11e).

1.2 Lamin A expression significantly decreases migration and invasion abilities of EWS cells

We assessed the role of lamin A in migration and invasion processes of EWS, performing a gain- or loss-of-function approach to force or silence its expression. We stably expressed lamin A in TC-71 cell line (Supplementary Figure 1a, 1b), while transient overexpression was obtained in the IOR/CAR cell line (Supplementary Figure 1c). We demonstrated that lamin A-overexpressing cells were less able to migrate compared to Empty-GFP cells in wound healing and migration assays (Figure 12a, 12b; Supplementary Figure 1d).

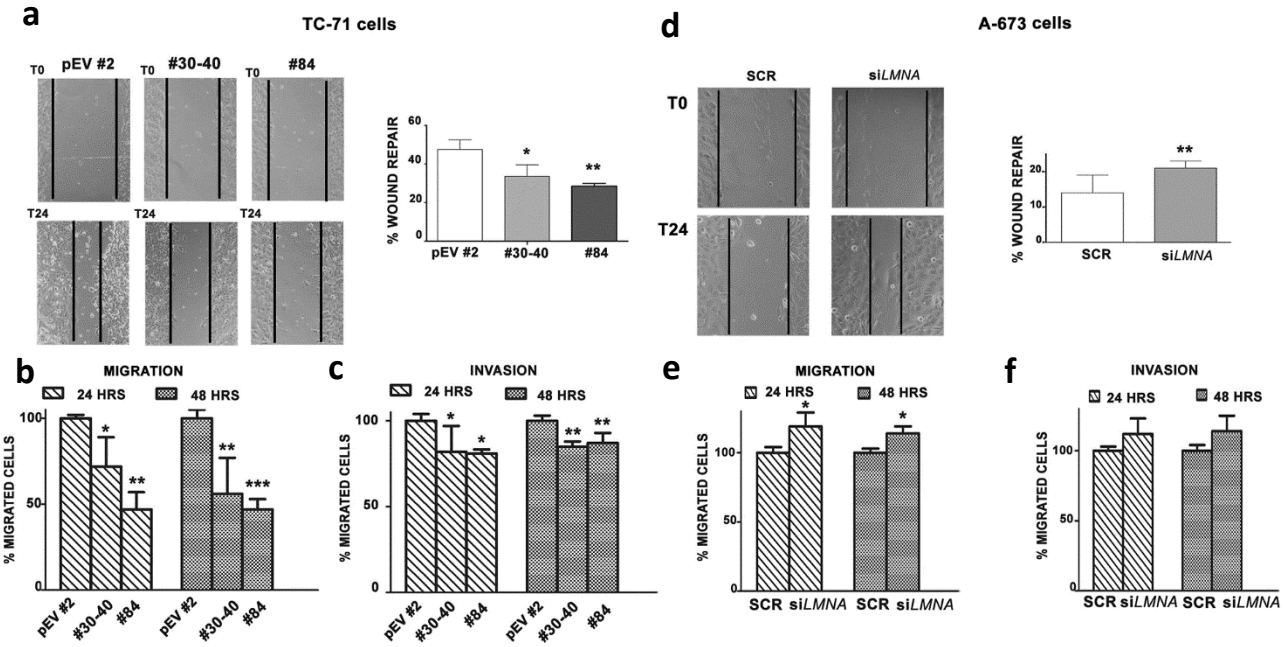

Figure 12: (**a**) Wound healing assay of Empty-GFP clone (pEV #2), lamin A-GFP #30-40 (#30-40) and lamin A-GFP #84 (#84). Representative pictures were taken at 0 and 24 h after scratching. Magnification 10×. Histograms are plotted as mean ± SD of three independent experiments. Asterisks indicate statistically significant differences with respect to Empty-GFP clone; (**b**) Migration assay of pEV #2, #30-40 and #84 performed at 24 and 48 hours. Histograms show the percentage of migrated cells respect to Empty-GFP clone, which was considered as 100%. Asterisks indicate statistically significant differences with respect to Empty-GFP clone; (**c**) Invasion assay pEV #2, #30-40 and #84 performed at 24 and 48 hours. Histograms show the percentage of migrated cells respect to Empty-GFP clone, which was considered as 100%. Asterisks indicate statistically significant differences with respect to Empty-GFP clone; (**d**) Wound healing assay of siRNA scramble cells (SCR) and si*LMNA* A-673 (si*LMNA*). Representative pictures were taken at 0 and 24 h after scratching. Magnification 10×. Histograms were plotted as mean ± SD of three independent experiments. Asterisks indicate statistically significant differences with respect to siRNA scramble cells; (**e**) Migration assay of SCR and si*LMNA* performed at 24 and 48 hours. Histograms show the percentage of migrated cells respect to siRNA scramble cells, which was considered as 100%. Asterisks indicate statistically significant differences with respect to siRNA scramble cells; (**f**) Invasion assay of SCR and si*LMNA* performed at 24 and 48 hours. Histograms show the percentage of migrated cells respect to siRNA scramble cells, which was considered as 100%.

Invasion assay also showed that TC-71 cells transfected with lamin A had significantly decreased invasion ability compared to controls (Figure 12c).

On the other hand, when *LMNA* was silenced in A-673 (Supplementary Figure 2a) or in LAP-35 cells, this (Supplementary Figure 2b) resulted in a significant increased cell motility and migration versus scramble siRNA-transfected cells (Figure 12d; Supplementary Figure 2c, 2d). Moreover, *LMNA*-silenced A-673 cells were more able to migrate and invade compared to control cells (Figure 12e, 12f).

1.3 Forced lamin A expression significantly decreases liver metastatic load in *in vivo* models

As previously reported, most human sarcomas show high metastatic ability in Rag2-/-; Il2rg-/- mice, which are characterized by the loss of B, T, and NK (natural killer) immune response, resulting in a distinctive pattern of organ affected by metastases.

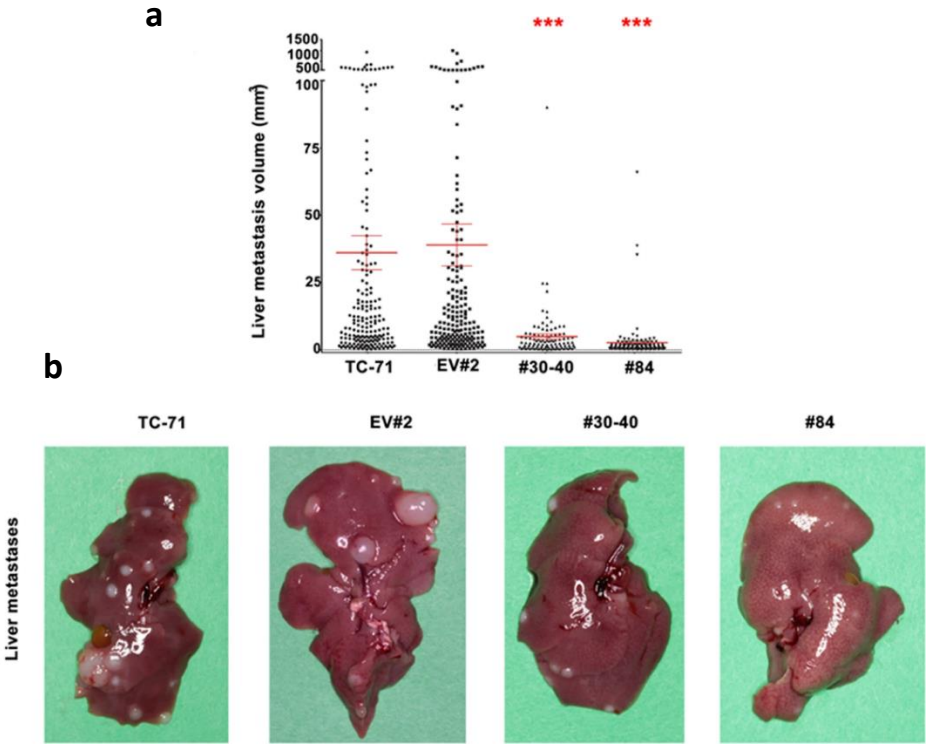

Figure 13: (**a**) Individual liver metastasis volume for TC-71 parental cells (*n* = 190), TC-71 EV#2 (EV#2) (*n* = 199), TC-71 lamin A-GFP #30-40 (#30-40) (*n* = 100) and TC-71 lamin A-GFP #84 (#84) (*n* = 115), red lines represent mean ± SEM for each group. Asterisks indicate statistically significant differences with respect to TC-71 parental cells and Empty-GFP clone; (**b**) Representative images of liver metastases in one mouse of each different group are shown.

The most involved organs are represented by liver, lung and other sites such as lymph nodes, interscapular brown fat pad, kidneys, and adrenal glands (212).

We confirmed this attitude after the intravenous injection of TC-71 cells and their derived stably transfected clones (Empty-GFP vector #2, lamin A-GFP #30-40 and lamin A-GFP #84) in double knockout Rag2-/-;Il2rg-/- mice. Metastases were detected in liver, lungs, lymph nodes, interscapular brown fat, kidneys, and adrenal glands. The growth of liver metastases was significantly reduced in mice after the injection of TC-71 lamin A-GFP #30-40 (#30-40) or TC-71 lamin A-GFP #84 (#84) cells overexpressing lamin A, relative to parental TC-71 or Empty-GFP vector #2 injected animals (Figure 13a, 13b). We also found a global reduction in the total number of metastases in mice that received clones overexpressing lamin A (Supplementary Figure 3a). The number of lung metastases was reduced in mice receiving lamin A-overexpressing clones compared to parental cells but was not reduced compared to Empty-GFP vector #2 (Supplementary Figure 3b).

1.4 LINC complex localization in EWS cells is rescued by lamin A expression

Alteration of nucleo-cytoskeletal dynamics by disruption of the LINC-complex or loss of lamin A can impair cytoskeletal organization resulting in altered cell polarization and migration(209) (213) (214). We observed impaired anchorage of NE proteins in EWS cells. The major constituents of LINC complex, SUN1, SUN2, nesprin 2, and emerin, the main partner protein of lamin A were not only localized at the NE, but were also found in the cytoplasm, although nuclear rim anchorage was partially maintained in TC-71 cells (Figure 14a). We demonstrated that lamin A overexpression was sufficient to recruit SUN1 to the NE (Figure 14a), also determining an overall increase of its protein levels (Figure 14b). The impaired anchorage of LINC complex proteins in fully dependent on lamin A deregulation in EWS cells. Indeed, its forced expression resulted in corrected localization of LINC complex components at the NE, and induced mild increase of SUN2 and nesprin 2 protein levels, compared to parental TC-71 (Figure 14a, 14b).

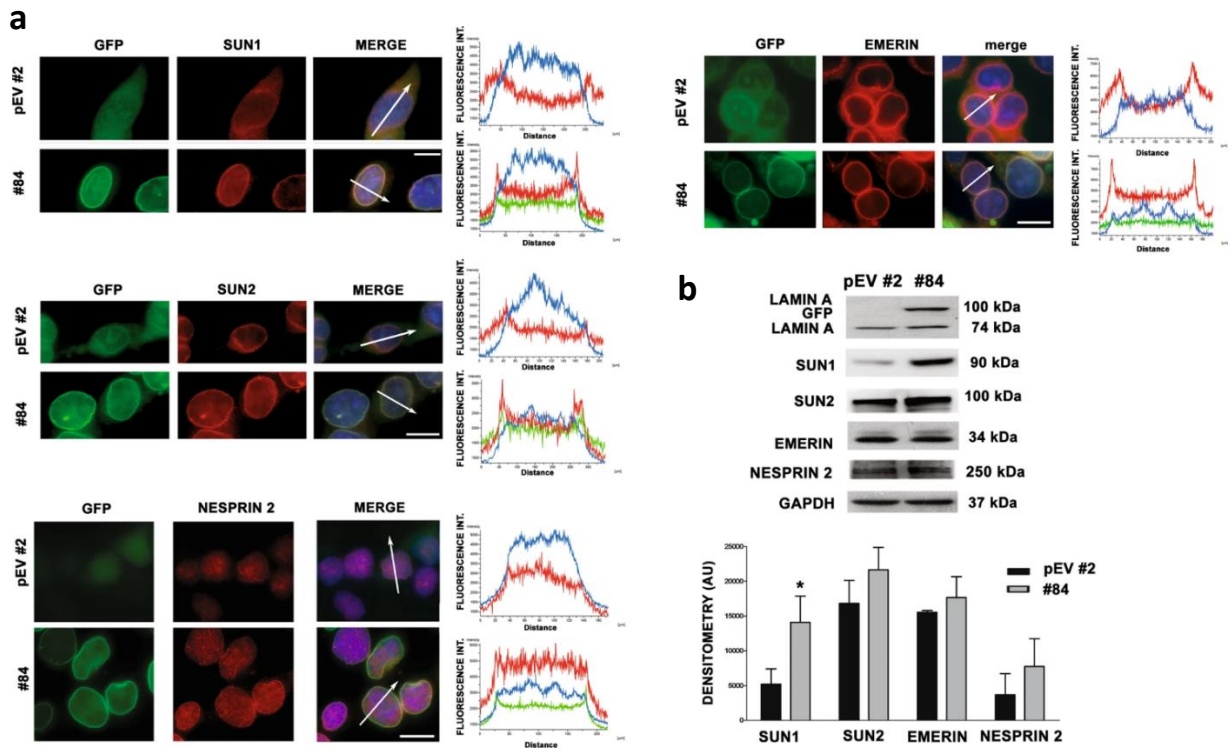

Figure 14: (**a**) Lamin A-GFP (green), SUN1 (red), SUN2 (red), nesprin 2 (red) and emerin (red) localization in TC-71 Empty-GFP clone (pEV #2) and TC-71 lamin A-GFP #84 (#84). DNA was counterstained with 2-(4-amidinophenyl)-1H -indole-6-carboxamidine (DAPI). Merge of fluorescence signals are shown (MERGE). Graphs indicate the fluorescence intensity profile along the white arrows. Representative graphs of at least 30 nuclei analyzed for each sample were shown. Magnification 100x, scale bar 10 µm; (**b**) Western blotting analysis of lamin A, SUN1, SUN2, emerin and nesprin 2 in TC-pEV #2 and #84 clones. GAPDH was used as loading control. Densitometric analysis is shown as mean values ± SD of three different experiments. Asterisks indicate statistically significant differences with respect to TC-71 Empty-GFP clone.

1.5 The expression of lamin A affects YAP and ROCK2 activity and stimulates neural differentiation in EWS cells

Lamin A is known to influence mechano-signaling dynamics through the regulation of nuclear import of transcriptional regulators involved in cytoskeleton remodeling, including YAP/TAZ. Indeed, the influence of lamin A deficiency on YAP/TAZ nuclear import has been recently demonstrated in muscle cells (215, 216). We observed YAP localization to the nucleoplasm in parental TC-71 cells, while lamin A overexpression was able to reduce YAP nuclear retention and increase its phosphorylation (Figure 15a, 15b). We also showed a significant downregulation of MYC protein levels, previously identified as a decisive target of YAP, in EWS cells overexpressing lamin A (Figure 15b).

Besides, we evaluated ROCK2 expression because this kinase is a crucial driver of EWS migration, regulating actin cytoskelatal organization (76). Western blotting analysis showed a significant decrease of ROCK2 protein levels in lamin A overexpressing clones, compared to Empty-GFP cells (Figure 15c). On the contrary, we found a significant upregulation of ROCK2 levels in si*LMNA* A-673

cells (Figure 15d). Moreover, lamin A overxpression pushed EWS cells to more differentiated phenotype as demonstrated by a significant increase of neural markers, including *NEF-H* and *β3-tubulin* in TC-71 clone #84 relative to TC-71 empty vector cells (Figure 15e).

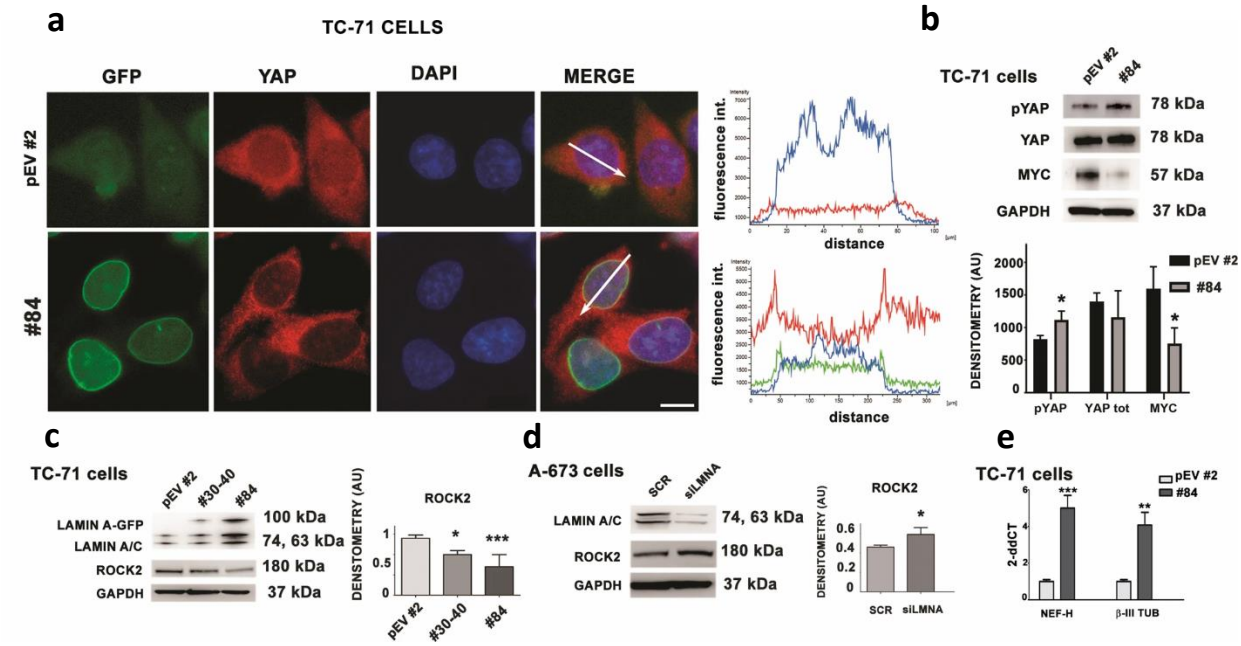

Figure 15: (**a**) Lamin A-GFP (green) and YAP (red) localization in Empty-GFP clone (pEV #2) and lamin A-GFP #84 (#84). DNA was counterstained with DAPI (DAPI). Merge of fluorescence signals are shown (MERGE). Graphs indicate the fluorescence intensity profile along the white arrows. Representative graphs of at least 30 nuclei analyzed for each sample were shown. Magnification 100x, scale bar 10 µm; (**b**) Western blotting analysis of YAP, p(Ser127) YAP and MYC protein expression in pEV #2 and #84 clones. GAPDH was used as loading control. Densitometric analysis is shown as mean values ± SD of three different experiments. Asterisks indicate statistically significant differences with respect to Empty-GFP clone; (**c**) Western blotting analyses of lamin A/C and ROCK2 protein expression in pEV #2, #30-40 and #84 clones. GAPDH was used as loading control. Densitometric analysis is shown as mean values ± SD of three different experiments. Asterisks indicate statistically significant differences with respect to Empty-GFP clone; (**d**) Western blotting analysis of lamin A/C and ROCK2 protein expression in siRNA scramble cells (SCR) and siLMNA A-673 (siLMNA). GAPDH was used as loading control. Densitometric analysis is shown as mean values ± SD of three different experiments. Asterisks indicate statistically significant differences with respect to siRNA scramble cells; (**e**) qRT-PCR analysis of *NEF-H* and *β3-tubulin* in pEV #2 and #84 clones. Data are shown as $2^{-\Delta\Delta Ct}$. GAPDH was used as a housekeeping gene. Asterisks indicate statistically significant differences with respect to Empty-GFP clone.

1.6 Prelamin A accumulation reduces migration and invasion capabilities of EWS cells

Prelamin A, the precursor protein of lamin A, is involved in chromatin organization and in transcriptional regulation. Generally, prelamin A is present at very low levels in normal cells, being rapidly processed, but its moderate accumulation has been observed in senescent cells and it has been linked to the reduction of invasion potential of cancer cells, both in cellular models and laminopathic mice (208) (207). We evaluated if prelamin A accumulation could decrease the invasiveness of EWS cells. To this aim, we expressed a mutated prelamin A sequence, which causes

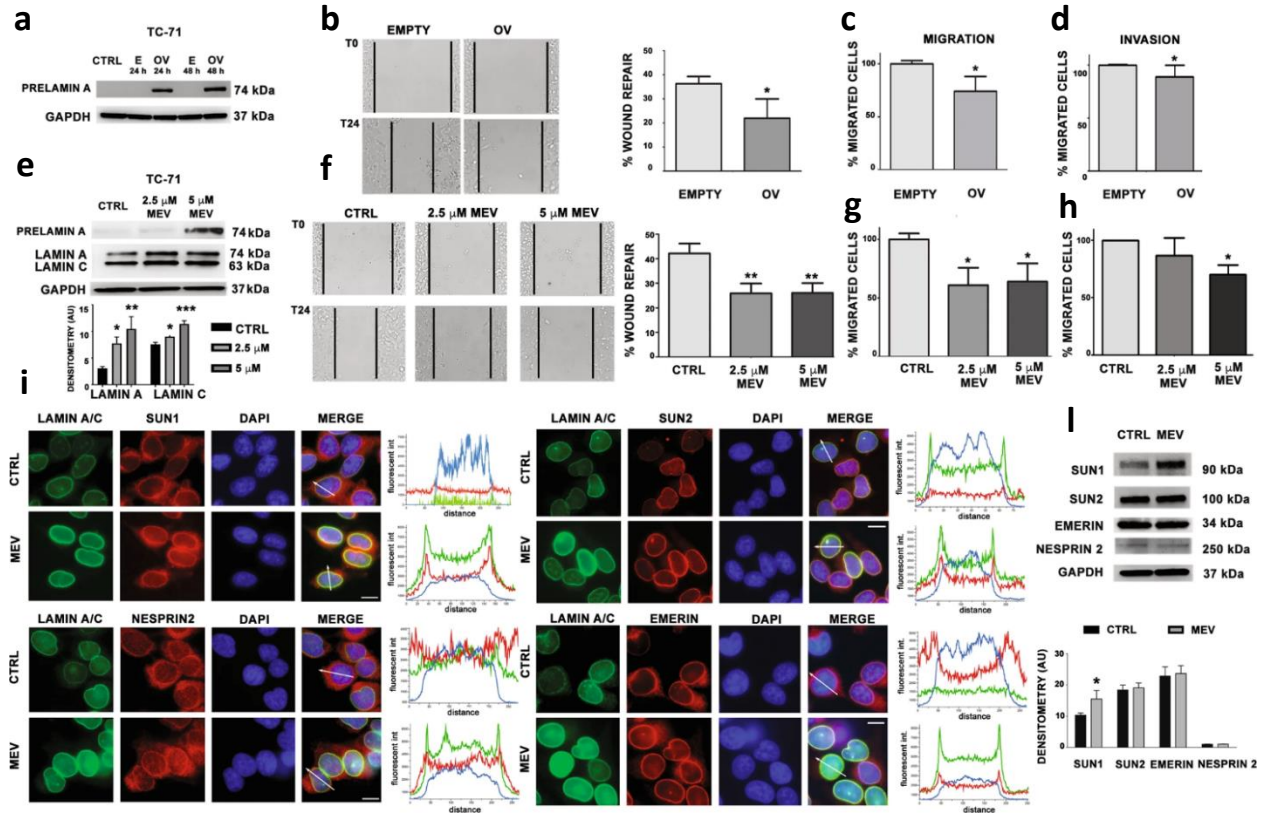

Figure 16: (**a**) Western blotting analysis of prelamin protein expression in parental TC-71 (CTRL), empty vector cells (E) and prelamin transfected TC-71 cells (OV) performed at 24 and 48 hours. GAPDH was used as loading control; (**b**) Wound healing assay of empty vector cells (EMPTY) and prelamin overexpressed TC-71 cells (OV). Representative pictures were taken at 0 and 24 h after scratching. Magnification 10×. Histograms are plotted as mean ± SD of three independent experiments. Asterisks indicate statistically significant differences with respect to empty vector cells; (**c**) Migration assay of EMPTY and prelamin overexpressed TC-71 cells (OV). Histograms show the percentage of migrated cells respect to empty vector cells, which were considered as 100%. Histograms are plotted as mean ± SD of three independent experiments. Asterisks indicate statistically significant differences with respect to empty vector cells; (**d**) Invasion assay of EMPTY and prelamin overexpressed TC-71 cells (OV). Histograms show the percentage of migrated cells respect to empty vector cells, which were considered as 100%. Histograms are plotted as mean ± SD of three independent experiments. Asterisks indicate statistically significant differences with respect to empty vector cells; (**e**) Western blotting analysis of prelamin A and lamin A/C protein expression in non-treated TC-71 cells (CTRL) and in mevinolin treated EWS cells (2.5 μM or 5μM MEV). GAPDH was used as loading control. Densitometric analyses are shown as mean values ± SD of three different experiments. Asterisks indicate statistically significant differences with respect to CTRL cells; (**f**) Wound healing assay of non-treated TC-71 cells (CTRL) and mevinolin treated EWS cells (2.5 μM or 5μM MEV). Representative pictures were taken at 0 and 24 h after scratching. Magnification 10×. Histograms are plotted as mean ± SD of three independent experiments. Asterisks indicate statistically significant differences with respect to non-treated TC-71 cells; (**g**) Migration assay of non-treated TC-71 cells (CTRL) and mevinolin treated EWS cells (2.5 μM or 5μM MEV). Histograms show the percentage of migrated cells respect to non-treated TC-71 cells, which were considered as 100%. Histograms are plotted as mean ± SD of three independent experiments. Asterisks indicate statistically significant differences with respect to non-treated TC-71 cells; (**h**) Invasion assay of non-treated TC-71 cells (CTRL) and mevinolin treated EWS cells (2.5 μM or 5μM MEV). Histograms show the percentage of migrated cells respect to non-treated TC-71 cells, which were considered as 100%. Histograms are plotted as mean ± SD of three independent experiments. Asterisks indicate statistically significant differences with respect to non-treated TC-71 cells; (**i**) Lamin A/C (green), SUN1 (red), SUN2 (red), Nesprin2 (red), and Emerin (red) localization in non-treated TC-71 cells (CTRL) and mevinolin treated (5 μM) EWS cells (MEV). DNA was counterstained with DAPI (DAPI). Merge of fluorescence signals are shown (MERGE). Graphs indicate the fluorescence intensity profile along the white arrows. Magnification 100x, scale bar 10 μm; (**l**) Western blotting analysis of SUN1, SUN2, Emerin, and Nesprin 2 in non-treated TC-71 cells (CTRL) and mevinolin treated (5 μM) EWS cells (MEV). GAPDH was used as loading control. Densitometric analysis is shown as mean values ± SD of three different experiments. Asterisks indicate statistically significant differences with respect to CTRL cells.

the accumulation of non-farnesylated prelamin A (LA-C661M) (194), as demonstrated in western western blot analysis (Figure 16a). Prelamin A overexpression resulted in significant decreased cellular motility, migration and invasion of EWS cells (Figure 16b, 16c, 16d).

We then modulated prelamin A expression by a pharmacological approach, employing mevinolin, which is a statin that inhibits the mevalonate pathway and farnesyl production, fundamental for prelamin A farnesylation and maturation, thus promoting the accumulation of non-farnesylated prelamin A (194, 209). Remarkably, we found that mevinolin treatment caused prelamin A accumulation, as expected, but also induced a significant increase in lamin A/C protein levels (Figure 16e), resulting in significant decrease of cell motility and invasivness of EWS cell (Figure 16f, 16g, 16h). Moreover, tretment with mevinolin caused a rescued localization of LINC complex proteins, accompanied by a significant increase in SUN1 protein levels, as obtained in lamin A overexpressing clones (Figure 16i, 16l).

1.7 Mevinolin induces neural differentiation and rescues YAP and ROCK2 dynamics in EWS cells

As already stated, after mevinolin treatment, we observed an increase in lamin A levels and this modulation is likely to be linked to both differentiation and cytoskeletal remodeling (127, 156) (217). In fact, we found that mevinolin treatment induced neural differentiation in EWS cells, as demontrstaed by the increase of β3-tubulin and neurofilament-H, which are expressed at the early stages of neuronal development (Figure 17a, 17b). qRT-PCR analysis also shown an upregulation of *nestin*, *β3-tubulin* and *NEF-H* genes, associated with a significant increase in *LMNA* gene expression (Figure 17c). To assess the role of lamin A/C during spontaneous neural differentiation of EWS cells, we cultured TC-71 cells in low-serum medium to induce differentiation process (Supplementary Figure 4). We found an increase in lamin A/C protein levels in differentiating TC-71 cells, demonstrating that lamin A/C upregulation is able to push EWS cells in a more differentiated state (Supplementary Figure 4).

Moreover, mevinolin had effects on cytoskeletal components. Indeed, after mevinolin treatment we found downregulation of YAP/TAZ signaling and exclusion of YAP from cell nucleus (Figure 17d). We confirmed the decreased activity of YAP/TAZ signaling evaluating its downstream effectors. qRT-PCR analysis demonstrated a downregulation of *CTGF* and *CYR61*, the main effectors of this pathway (Figure 17e) (218), and we also found a significant increase in phospho-(Ser127)-YAP (inactive form) protein levels (Figure 17f) (219). We then observed a downregulation of MYC (Figure 17f), another

target of YAP/TAZ signaling, as YAP/TAZ is known to activate MYC at transcriptional and post-transcriptional level, promoting tumorigenesis (220). Mevinolin treatment was also able to significantly reduce ROCK2 protein levels in EWS cells (Figure 17f).

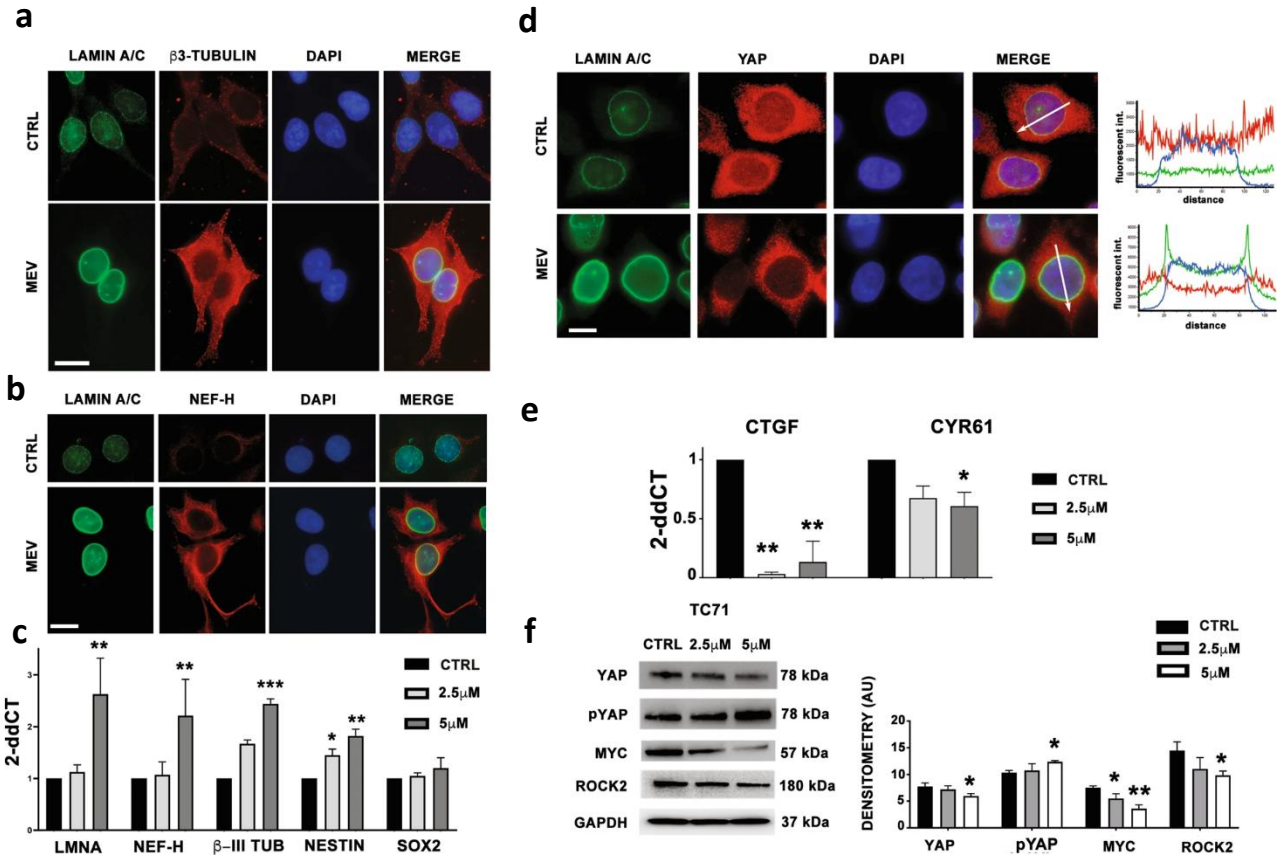

Figure 17: (**a**) Lamin A/C (green) and β3-tubulin (red) localization in non-treated TC-71 cells (CTRL) and in mevinolin treated (5 μM) EWS cells (MEV). DNA was counterstained with DAPI (DAPI). Merge of fluorescence signals are shown (MERGE). Magnification 100x, scale bar 10 μm; (**b**) Lamin A/C (green) and neurofilament-H (NEF-H) (red) localization in non-treated TC-71 cells (CTRL) and in mevinolin treated (5 μM) EWS cells (MEV). DNA was counterstained with DAPI (DAPI). Merge of fluorescence signals are shown (MERGE). Magnification 100x, scale bar 10 μm; (**c**) qRT-PCR analysis of *LMNA*, *NEF-H*, *β3-tubulin*, *nestin* and *SOX2* genes in untreated TC-71 cells (CTRL) and in mevinolin treated EWS cells (2.5 μM or 5μM MEV). Data are shown as $2^{-\Delta\Delta Ct}$. GAPDH was used as a housekeeping gene. Data are shown as mean values ± SD of three different experiments. Asterisks indicate statistically significant differences with respect to CTRL cells; (**d**) Lamin A/C (green) and YAP (red) localization in non-treated TC-71 cells (CTRL) and in mevinolin treated (5 μM) EWS cells (MEV). DNA was counterstained with DAPI (DAPI). Merge of fluorescence signals are shown (MERGE). Graphs indicate the fluorescence intensity profile along the white arrows. Magnification 100x, scale bar 10 μm; (**e**) qRT-PCR analysis of *CTGF* and *CYR61* in non-treated TC-71 cells (CTRL) and in mevinolin treated EWS cells (2.5 μM or 5μM MEV). Data are shown as $2^{-\Delta\Delta Ct}$. GAPDH was used as a housekeeping gene. Data are shown as mean values ± SD of three different experiments. Asterisks indicate statistically significant differences with respect to CTRL cells; (**f**) Western blotting analysis of YAP, p(Ser127) YAP, MYC and ROCK2 protein expression in non-treated TC-71 cells (CTRL) and in mevinolin treated EWS cells (2.5 μM or 5μM MEV). GAPDH was used as loading control. Densitometric analysis is shown as mean values ± SD of three different experiments. Asterisks indicate statistically significant differences with respect to CTRL cells.

As a whole, we demonstrated that mevinolin is able to increase lamin A and prelamin A levels, mediateing LINC complex rescue and modulating soluble mechanosignaling effectors YAP and ROCK2, thus resulting in reduced cell migration abilities of EWS cells. Moreover, mevinolin also pushes EWS cells toward a neural differentiation.

2. Discussion

Due to the high EWS aggressiveness, investigating pathways and mechanisms involved in EWS metastatic process is urgently needed. Indeed, Ewing sarcoma patients with metastases still fare badly, and the therapy carries short-term and long-term toxicities.

Previous studies demonstrated that nuclear stiffness, due to lamin A levels, is crucial to limit nucleus deformability and consequently cellular migration, preventing the passage of the cells through extracellular matrix pores (221). Lamin A has been reported to act as tumor suppressor in several cancers, including endometrial or breast cancer (222) (223).

Here we investigated the role of lamin A in EWS setting. Firstly, we found a significant inverse correlation between lamin A expression and tumor invasiveness in EWS patients. Moreover, we performed *in silico* analysis from EWS patient datasets, showing that *LMNA* gene expression was significantly lower in EWS metastatic lesions compared to primary samples, and higher *LMNA* levels also correlated to a better 5-year EWS patient survival. We also evaluated cell nucleus's shape, observing severe loss of nuclear shape in cell nuclei with very low/absent levels of lamin A protein (metastatic samples). We found that the overexpression of lamin A was able to reduce motility capacity, migration and invasion of EWS cells in *in vitro* experiments and these effects were associated to a significant reduction of metastatic load in mice models, while lamin A silencing induced a more invasive phenotype in EWS cells. In particular, lamin A expression significantly reduced liver metastases' size and count, suggesting that liver-produced growth and motility factors such as insulin-like growth factor (IGF) and hepatocyte growth factor/scatter factor (HGF/SF), which were involved in crucial molecular mechanisms of liver metastasis in sarcomas, may be at least partly implicated in the different behaviors of EWS cells with high or low expression of lamin A (212).

Finally, we demonstrated that also prelamin A accumulation can reduce migration abilities of EWS cells, according to previous results which shown that this protein prevents metastatic potential in several cell and animal models (207). We then wanted to clarify how lamin A expression can influence EWS dynamics, focusing on LINC complex proteins, the main lamin A partners in mechano-signaling transduction, thereby influencing cytoskeleton dynamics and cell migration (214). The

forced expression of lamin A was able to reconstitute the physiological positioning of LINC proteins, SUN1, SUN2, nesprin-2, and emerin confirming previously published data that showed the possible involvement of these proteins in metastatization and cancer progression (98) (181) (220). SUN1 and SUN2 mediate effects on cytoskeletal remodeling and stress fiber formation not only interacting with cytoskeleton components but also modulating RhoA-ROCK2 signaling (224) (211) (225). In particular, SUN1 inhibits RhoA activation and focal adhesion assembly through the inhibition of SUN2 which normally activates RhoA pathway (224). It has been shown that low SUN1 expression increases migration of bone marrow MSCs (211), while the predominant SUN1 splice isoform (SUN1_916) has an inhibitory effect on cellular migration in HeLa cells (225). We demonstrated that the rescue of SUN1 levels and localization resulted in significantly lower levels of ROCK2 and reduced cell motility in both cells overexpressing lamin A or treated with mevinolin. It has been shown that the use of statin reduces migration, proliferation and invasion in gastric cancer cells or in breast cancer cells through the inhibition of YAP signaling pathway (219). The effects of statins on YAP signaling pathway are mediated, at least in part, by Rho-small GTP-ase. When Rho is activated is able to activate YAP-TAZ pathway that supports proliferation, cell plasticity, therapy resistance and metastasis in different type of tumors (226). The use of statin inhibits the geranylgeranyl pyrophosphate production by the mevalonate cascade, required for activation of Rho GTPases (219). It results in cytoplasmic accumulation of YAP, and this leads to inhibition of YAP-target genes transcription and activation. The use of statin was able to induce a downregulation of YAP/TAZ signaling in EWS settings, as demonstrated by the increased levels of p-YAP and by the downregulation of YAP-target genes. Based on the previous mentioned published studies, we propose a similar mechanism in EWS cells. The use of mevinolin, inhibiting the mevalonate pathway, results in inhibition of Rho GTPase and its effector ROCK2. It has been demonstrated that ROCK2 was involved in the maintenance of the nuclear localization of YAP, thus promoting YAP activity (227) (228). A recent work demonstrated that ROCK2 also promoted YAP activity in osteosarcoma cells and the ROCK2 deprivation lead to the inhibition of metastatic potential through the modulation of YAP activity (198). The downregulation of YAP was able to reduce the motility capacity also in EWS cells, confirming the crucial role of this pathway in the metastatic process of cancer cells. Lamin A overexpression further inhibited YAP/TAZ signaling in EWS cells, which might also explain the reduced cell migration, as inhibition of the YAP/TAZ/TEAD complex with verteporfin resulted in reduced cell migration of EWS cells *in vitro* and decreased metastasis formation in EWS xenograft models (97).

Moreover, this signaling pathway was described as a prognostic marker in EWS patients. A study on 55 primary human EWS samples revealed that high YAP/TAZ expression was associated with disease progression and predicted poorer outcome, resulting a negative prognostic factor in EWS (85). Thus, mevinolin could act as an inhibitor of EWS cell migration by increasing prelamin A levels as well as by reducing mevalonate-dependent YAP/TAZ activity.

Upon mevinolin treatment of EWS cells, we also found an unexpected increase in mature lamin A levels, which could be associated to a more differentiated phenotype (127) (202).

Indeed, our results show that mevinolin treatment prompted EWS cells toward a more differentiated phenotype, as demonstrated by significantly increased levels of neural markers, and downregulation of YAP activity, which was associated with neural differentiation (229).

EWS is very undifferentiated tumor due to the presence of *EWS-FLI1* and the overexpression of CD99 protein, which prevent terminal neural differentiation (230) (231). Our study suggests a role for lamin A in addressing cells toward a more differentiated state, as further supported by induction of differentiation markers in EWS clones overexpressing lamin A, despite the presence and activity of either CD99 or *EWS-FLI1*.

As a whole, this study proposes a new lamin A-related mechanisms involved in the metastatization process of EWS cells. In particular, mevinolin treatment induces accumulation of prelamin A and increases lamin A/C levels, favoring the correct rescue of nucleo-cytoskeleton dynamics through LINC complex components, and inhibiting crucial mechano-signaling effectors such as ROCK2 and YAP. Moreover, mevinolin treatment induces a neural differentiation-related cytoskeleton remodeling. The main downstream effect of this rescue mechanism is the reduction of migration ability in mevinolin treated EWS cells.

Importantly, our study identifies a drug already employed in clinical practice, as a tool capable of reducing migration and invasion ability of EWS cells, while triggering neural differentiation, which could be considered as a potential candidate to be fast translated into clinic, especially for those EWS cases with metastatic disease at the diagnosis.

CONCLUSIONS

This PhD project identified a novel strategy to decrease the metastatic potential of bone sarcomas (i.e. osteosarcoma and Ewing sarcoma). In particular, we deciphered how the nuclear protein lamin A can influence the nucleo-cytoskeletal dynamics resulting in less invasive and aggressive bone sarcoma phenotype.

Traditionally, lamin A was considered for its role in genetic diseases called laminopathies (113); however, in recent years, its involvement in cancer progression is emerging (220). Indeed, alterations in lamin A levels are often found in several types of cancer, and are linked to nuclear deformations and increased cellular migration (220). Here, we demonstrated that lamin A protein is able to regulate nuclear envelope stability, rescuing LINC complex proteins localization and reconstituting a functional nucleo-cytoskeletal dynamics which results in reduction of bone sarcoma invasiveness.

Indeed, bone sarcoma cells have low levels of lamin A, and the forced expression of this protein as well as its accumulation with statin treatment, is able to reconstitute a correct nucleo-cytoskeleton dynamics through the regulation of mechano-signaling effectors. The reconstitution of nuclear envelope composition and the modulation of crucial effectors responsible for bone sarcoma migration result in less invasive phenotype, and in the reduction of EWS metastatic load *in vivo*. Moreover, lamin A expression also pushes bone sarcoma cells toward a more differentiated phenotype in both models analyzed.

All in all, these results pave the way to a new possible therapeutic approach that individuate the regulation of nucelo-cytoskeleton interplay, through lamin A modulation, as a strategy that could be exploited to meliorate bone sarcomas' treatment.

To better characterize how lamin A can influence bone sarcoma cells' behavior, the next goal is to decode how lamin A can influence chromatin status and its conformation, through the alteration of lamin associated domains (LADs), thus likely modifying gene expression signatures. Moreover, chromatin conformation status can influence the rigidity of nucleus itself contributing to cellular migration processes (135). Indeed, the spatial organization of chromatin related to nuclear envelope dynamics is linked to its functionality but this biological process and its contribution to cancer progression is a new very interesting field in bone sarcoma and more broadly in cancer.

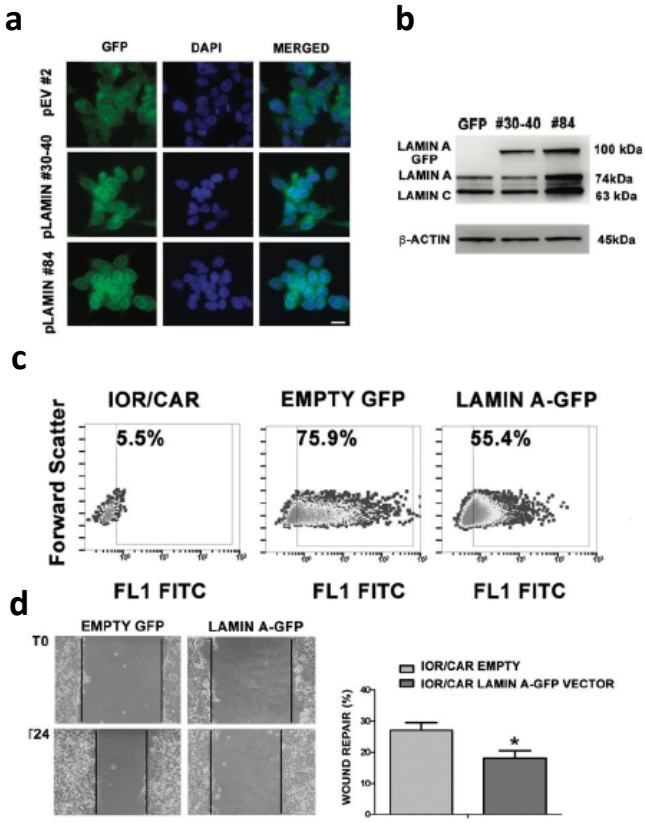

Supplementary Figure 1: **Overexpression of lamin A reduces cell motility in EWS cells**. (**a**) Lamin A (GFP) (green) in Empty-GFP clone (pEV #2), lamin A-GFP #30-40 and lamin A-GFP #84. DNA was counterstained with DAPI (DAPI). Merge of fluorescence signals are shown (MERGE); (**b**) Western blotting analyses of lamin A/C and lamin A/GFP protein expression in Empty-GFP clone (GFP), lamin A-GFP #30-40 (#30-40) and lamin A-GFP #84 (#84). β- actin was used as loading control; (**c**) Flow cytometric analyses of IOR/CAR EWS cells transfected with empty GFP vector or lamin A-GFP vector; (**d**) Wound healing assays of IOR/CAR EWS cells transfected with empty GFP vector or lamin A-GFP vector. Representative pictures were taken at 0 and 24 h after scratching. Magnification 10×. Histograms are plotted as mean ± SD of three independent experiments. Asterisks indicate statistically significant differences with respect to empty GFP transfected cells.

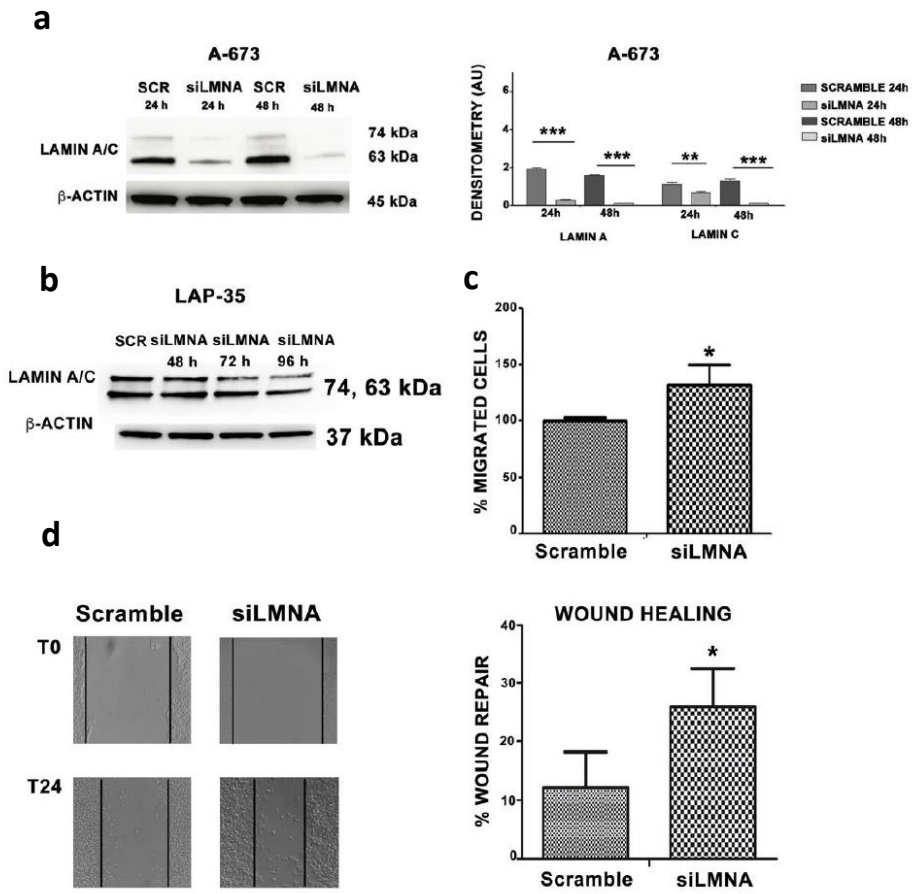

Supplementary Figure 2: **Silencing of lamin A increases cell motility in EWS cells.** (**a**) Western blotting analysis of lamin A/C protein expression A-673 siRNA scramble cells (SCR) and siLMNA A-673 (si*LMNA*) performed at 24 and 48 hours. β-actin was used as loading control. Densitometric analysis is shown as mean values ± SD of three different experiments. Asterisks indicate statistically significant differences with respect to siRNA scramble cells at 24 or 48 hours; (**b**) Western blotting analysis of lamin A/C protein expression in LAP35 siRNA scramble cells (SCR) and si*LMNA* LAP-35 (si*LMNA*) performed at 48, 72, 96 hours. β-actin was used as loading control; (**c**) Migration assay of siRNA scramble cells (SCR) and siLMNA LAP-35 (si*LMNA*) performed at 24 hours. Histograms show the percentage of migrated cells with respect to siRNA scramble cells, which was considered as 100%. Histograms are plotted as mean ± SD of three independent experiments. Asterisks indicate statistically significant differences with respect to siRNA scramble cells; (**d**) Wound healing assay of siRNA scramble cells (SCR) and si*LMNA* LAP-35 (si*LMNA*). Representative pictures were taken at 0 and 24 h after scratching. Magnification 10×. Histograms are plotted as mean ± SD of three independent experiments. Asterisks indicate statistically significant differences with respect to siRNA scramble cells.

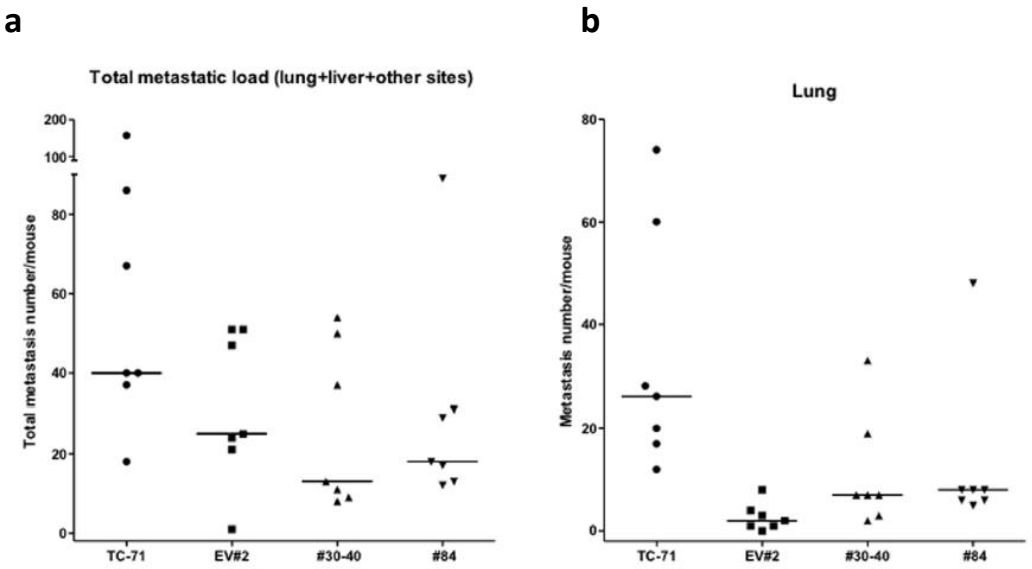

Supplementary Figure 3: Total metastatic load and lung metastatic load in mice injected with TC-71 cells and empty vector or lamin A transfectant clones. (**a**) Total metastatic load in mice receiving i.v. injection of TC71 cells, Empty-GFP clone (pEV #2), lamin A-GFP #30-40 clone (#30-40) and lamin A-GFP #84 clone (#84), expressed as total number of metastasis per mouse including metastasis to the lung, liver and other sites such as lymph nodes, interscapular brown fat, kidneys and adrenal glands. Black lines represent the median number of metastases for each group; (**b**) Number of lung metastasis per mouse receiving i.v. injection of TC-71 cells, Empty-GFP clone (pEV #2), lamin A-GFP #30-40 clone (#30-40) and lamin A-GFP #84 clone (#84). Black lines represent the median number of metastases for each group. All of the transfectant clones were significantly different compared to TC-71 parental cells.

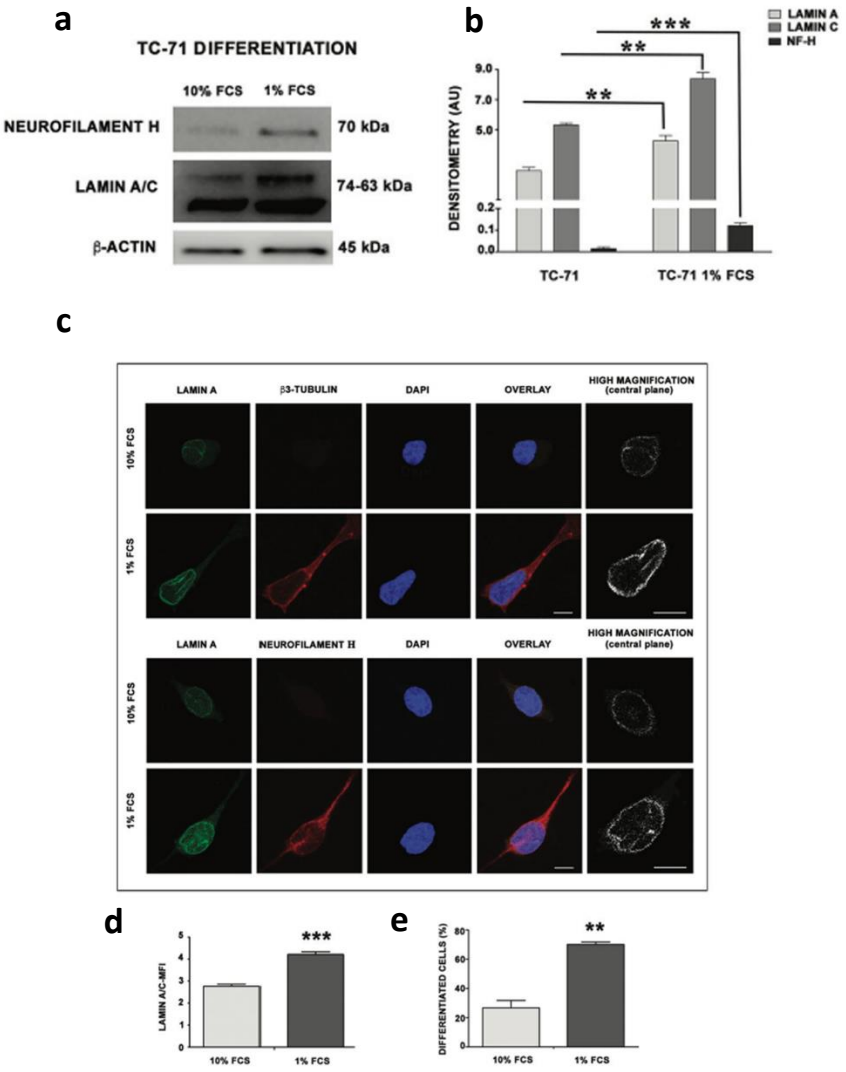

Supplementary Figure 4: Low-serum conditions drive EWS cells toward neural differentiation. (**a**) Western blotting analysis of Neurofilament-H and lamin A/C protein expression in TC-71 cultured in 10% FCS medium or in 1% FCS medium. β-actin was used as loading control; (**b**) Densitometric analysis is shown as mean values ± SD of three different experiments. Asterisks indicate statistically significant differences with respect to TC-71 cultured in 10% FCS medium; (**c**) Confocal microscopy analysis of lamin A (green), β3-tubulin (red) and Neurofilament-H (red) proteins in TC-71 cell lines cultured in 10% FCS medium or in 1% FCS medium. DNA was counterstained with DAPI (DAPI). Merge of fluorescence signals are shown (OVERLAY); (**d**) Mean fluorescence intensity (MFI) of lamin A/C immunoexpression in TC-71 cells cultured in 10% or in 1% FCS medium. Histograms are plotted as mean ± SD of three independent experiments Asterisks indicate statistically significant differences with respect to TC-71 cultured in 10% FCS medium; (**e**) Histograms indicate the percentage of differentiated cells in 1% FCS cultured TC-71 cells. Graphs were plotted as mean ± SD of three independent experiments Asterisks indicate statistically significant differences with respect to 10% FCS cultured TC-71 cells.

REFERENCES

1. Scotlandi K, Hattinger CM, Pellegrini E, Gambarotti M, Serra M. Genomics and Therapeutic Vulnerabilities of Primary Bone Tumors. Cells. 2020;9(4).
2. Group EESNW. Bone sarcomas: ESMO Clinical Practice Guidelines for diagnosis, treatment and follow-up. Ann Oncol. 2012;23 Suppl 7:vii100-9.
3. Brown HK, Schiavone K, Gouin F, Heymann MF, Heymann D. Biology of Bone Sarcomas and New Therapeutic Developments. Calcif Tissue Int. 2018;102(2):174-95.
4. Deschaseaux F, Sensebe L, Heymann D. Mechanisms of bone repair and regeneration. Trends Mol Med. 2009;15(9):417-29.
5. Riggi N, Suva ML, Stamenkovic I. Ewing's Sarcoma. N Engl J Med. 2021;384(2):154-64.
6. Miyagawa Y, Okita H, Nakaijima H, Horiuchi Y, Sato B, Taguchi T, et al. Inducible expression of chimeric EWS/ETS proteins confers Ewing's family tumor-like phenotypes to human mesenchymal progenitor cells. Mol Cell Biol. 2008;28(7):2125-37.
7. Riggi N, Suva ML, Suva D, Cironi L, Provero P, Tercier S, et al. EWS-FLI-1 expression triggers a Ewing's sarcoma initiation program in primary human mesenchymal stem cells. Cancer Res. 2008;68(7):2176-85.
8. von Levetzow C, Jiang X, Gwye Y, von Levetzow G, Hung L, Cooper A, et al. Modeling initiation of Ewing sarcoma in human neural crest cells. PLoS One. 2011;6(4):e19305.
9. Le Douarin NM, Calloni GW, Dupin E. The stem cells of the neural crest. Cell Cycle. 2008;7(8):1013-9.
10. Bousquet M, Noirot C, Accadbled F, Sales de Gauzy J, Castex MP, Brousset P, et al. Whole-exome sequencing in osteosarcoma reveals important heterogeneity of genetic alterations. Ann Oncol. 2016;27(4):738-44.
11. Ekhtiari S, Chiba K, Popovic S, Crowther R, Wohl G, Kin On Wong A, et al. First case of osteosarcoma in a dinosaur: a multimodal diagnosis. Lancet Oncol. 2020;21(8):1021-2.
12. Meltzer PS, Helman LJ. New Horizons in the Treatment of Osteosarcoma. N Engl J Med. 2021;385(22):2066-76.
13. Ottaviani G, Jaffe N. The epidemiology of osteosarcoma. Cancer Treat Res. 2009;152:3-13.
14. Gill J, Gorlick R. Advancing therapy for osteosarcoma. Nat Rev Clin Oncol. 2021;18(10):609-24.
15. Bielack SS, Kempf-Bielack B, Delling G, Exner GU, Flege S, Helmke K, et al. Prognostic factors in high-grade osteosarcoma of the extremities or trunk: an analysis of 1,702 patients treated on neoadjuvant cooperative osteosarcoma study group protocols. J Clin Oncol. 2002;20(3):776-90.
16. Lindsey BA, Markel JE, Kleinerman ES. Osteosarcoma Overview. Rheumatol Ther. 2017;4(1):25-43.
17. Rickel K, Fang F, Tao J. Molecular genetics of osteosarcoma. Bone. 2017;102:69-79.
18. Calvert GT, Randall RL, Jones KB, Cannon-Albright L, Lessnick S, Schiffman JD. At-risk populations for osteosarcoma: the syndromes and beyond. Sarcoma. 2012;2012:152382.
19. Shorokhova M, Nikolsky N, Grinchuk T. Chromothripsis-Explosion in Genetic Science. Cells. 2021;10(5).
20. Stephens PJ, Greenman CD, Fu B, Yang F, Bignell GR, Mudie LJ, et al. Massive genomic rearrangement acquired in a single catastrophic event during cancer development. Cell. 2011;144(1):27-40.
21. Cortes-Ciriano I, Lee JJ, Xi R, Jain D, Jung YL, Yang L, et al. Comprehensive analysis of chromothripsis in 2,658 human cancers using whole-genome sequencing. Nat Genet. 2020;52(3):331-41.
22. D'Antonio M, Tamayo P, Mesirov JP, Frazer KA. Kataegis Expression Signature in Breast Cancer Is Associated with Late Onset, Better Prognosis, and Higher HER2 Levels. Cell Rep. 2016;16(3):672-83.
23. Czarnecka AM, Synoradzki K, Firlej W, Bartnik E, Sobczuk P, Fiedorowicz M, et al. Molecular Biology of Osteosarcoma. Cancers (Basel). 2020;12(8).
24. Hainaut P, Pfeifer GP. Somatic TP53 Mutations in the Era of Genome Sequencing. Cold Spring Harb Perspect Med. 2016;6(11).
25. Murphy KL, Dennis AP, Rosen JM. A gain of function p53 mutant promotes both genomic instability and cell survival in a novel p53-null mammary epithelial cell model. FASEB J. 2000;14(14):2291-302.

26. Walkley CR, Qudsi R, Sankaran VG, Perry JA, Gostissa M, Roth SI, et al. Conditional mouse osteosarcoma, dependent on p53 loss and potentiated by loss of Rb, mimics the human disease. Genes Dev. 2008;22(12):1662-76.
27. Ueda T, Healey JH, Huvos AG, Ladanyi M. Amplification of the MYC Gene in Osteosarcoma Secondary to Paget's Disease of Bone. Sarcoma. 1997;1(3-4):131-4.
28. de Azevedo JWV, de Medeiros Fernandes TAA, Fernandes JV, Jr., de Azevedo JCV, Lanza DCF, Bezerra CM, et al. Biology and pathogenesis of human osteosarcoma. Oncol Lett. 2020;19(2):1099-116.
29. Chen D, Zhao Z, Huang Z, Chen DC, Zhu XX, Wang YZ, et al. Super enhancer inhibitors suppress MYC driven transcriptional amplification and tumor progression in osteosarcoma. Bone Res. 2018;6:11.
30. Zhou Y, Shen JK, Yu Z, Hornicek FJ, Kan Q, Duan Z. Expression and therapeutic implications of cyclin-dependent kinase 4 (CDK4) in osteosarcoma. Biochim Biophys Acta Mol Basis Dis. 2018;1864(5 Pt A):1573-82.
31. Perry JA, Kiezun A, Tonzi P, Van Allen EM, Carter SL, Baca SC, et al. Complementary genomic approaches highlight the PI3K/mTOR pathway as a common vulnerability in osteosarcoma. P Natl Acad Sci USA. 2014;111(51):E5564-E73.
32. Hou P, Ji M, Yang B, Chen Z, Qiu J, Shi X, et al. Quantitative analysis of promoter hypermethylation in multiple genes in osteosarcoma. Cancer. 2006;106(7):1602-9.
33. Gorlick R, Janeway K, Lessnick S, Randall RL, Marina N, Committee COGBT. Children's Oncology Group's 2013 blueprint for research: bone tumors. Pediatr Blood Cancer. 2013;60(6):1009-15.
34. Saraf AJ, Fenger JM, Roberts RD. Osteosarcoma: Accelerating Progress Makes for a Hopeful Future. Front Oncol. 2018;8:4.
35. Allison DC, Carney SC, Ahlmann ER, Hendifar A, Chawla S, Fedenko A, et al. A meta-analysis of osteosarcoma outcomes in the modern medical era. Sarcoma. 2012;2012:704872.
36. Goorin AM, Harris MB, Bernstein M, Ferguson W, Devidas M, Siegal GP, et al. Phase II/III trial of etoposide and high-dose ifosfamide in newly diagnosed metastatic osteosarcoma: a pediatric oncology group trial. J Clin Oncol. 2002;20(2):426-33.
37. Berrak SG, Pearson M, Berberoglu S, Ilhan IE, Jaffe N. High-dose ifosfamide in relapsed pediatric osteosarcoma: therapeutic effects and renal toxicity. Pediatr Blood Cancer. 2005;44(3):215-9.
38. Palmerini E, Jones RL, Marchesi E, Paioli A, Cesari M, Longhi A, et al. Gemcitabine and docetaxel in relapsed and unresectable high-grade osteosarcoma and spindle cell sarcoma of bone. BMC Cancer. 2016;16:280.
39. Chaiyawat P, Settakorn J, Sangsin A, Teeyakasem P, Klangjorhor J, Soongkhaw A, et al. Exploring targeted therapy of osteosarcoma using proteomics data. Onco Targets Ther. 2017;10:565-77.
40. Ribeiro CJ, Rodrigues CM, Moreira R, Santos MM. Chemical Variations on the p53 Reactivation Theme. Pharmaceuticals (Basel). 2016;9(2).
41. Fioramonti M, Fausti V, Pantano F, Iuliani M, Ribelli G, Lotti F, et al. Cabozantinib Affects Osteosarcoma Growth Through A Direct Effect On Tumor Cells and Modifications In Bone Microenvironment. Sci Rep. 2018;8(1):4177.
42. Italiano A, Mir O, Mathoulin-Pelissier S, Penel N, Piperno-Neumann S, Bompas E, et al. Cabozantinib in patients with advanced Ewing sarcoma or osteosarcoma (CABONE): a multicentre, single-arm, phase 2 trial. Lancet Oncol. 2020;21(3):446-55.
43. Bielack SS, Smeland S, Whelan JS, Marina N, Jovic G, Hook JM, et al. Methotrexate, Doxorubicin, and Cisplatin (MAP) Plus Maintenance Pegylated Interferon Alfa-2b Versus MAP Alone in Patients With Resectable High-Grade Osteosarcoma and Good Histologic Response to Preoperative MAP: First Results of the EURAMOS-1 Good Response Randomized Controlled Trial. J Clin Oncol. 2015;33(20):2279-87.
44. Meyers PA, Schwartz CL, Krailo MD, Healey JH, Bernstein ML, Betcher D, et al. Osteosarcoma: the addition of muramyl tripeptide to chemotherapy improves overall survival--a report from the Children's Oncology Group. J Clin Oncol. 2008;26(4):633-8.
45. Ebb D, Meyers P, Grier H, Bernstein M, Gorlick R, Lipshultz SE, et al. Phase II trial of trastuzumab in combination with cytotoxic chemotherapy for treatment of metastatic osteosarcoma with human epidermal growth factor receptor 2 overexpression: a report from the children's oncology group. J Clin Oncol. 2012;30(20):2545-51.

46. Sorenson L, Fu Y, Hood T, Warren S, McEachron TA. Targeted transcriptional profiling of the tumor microenvironment reveals lymphocyte exclusion and vascular dysfunction in metastatic osteosarcoma. Oncoimmunology. 2019;8(9):e1629779.
47. Fujiwara T, Healey J, Ogura K, Yoshida A, Kondo H, Hata T, et al. Role of Tumor-Associated Macrophages in Sarcomas. Cancers (Basel). 2021;13(5).
48. Ewing J. Classics in oncology. Diffuse endothelioma of bone. James Ewing. Proceedings of the New York Pathological Society, 1921. CA Cancer J Clin. 1972;22(2):95-8.
49. Delattre O, Zucman J, Plougastel B, Desmaze C, Melot T, Peter M, et al. Gene fusion with an ETS DNA-binding domain caused by chromosome translocation in human tumours. Nature. 1992;359(6391):162-5.
50. Grunewald TGP, Cidre-Aranaz F, Surdez D, Tomazou EM, de Alava E, Kovar H, et al. Ewing sarcoma. Nat Rev Dis Primers. 2018;4(1):5.
51. Widhe B, Widhe T. Initial symptoms and clinical features in osteosarcoma and Ewing sarcoma. J Bone Joint Surg Am. 2000;82(5):667-74.
52. Pasello M, Manara MC, Scotlandi K. CD99 at the crossroads of physiology and pathology. J Cell Commun Signal. 2018;12(1):55-68.
53. Crompton BD, Stewart C, Taylor-Weiner A, Alexe G, Kurek KC, Calicchio ML, et al. The genomic landscape of pediatric Ewing sarcoma. Cancer Discov. 2014;4(11):1326-41.
54. Brohl AS, Solomon DA, Chang W, Wang J, Song Y, Sindiri S, et al. The genomic landscape of the Ewing Sarcoma family of tumors reveals recurrent STAG2 mutation. PLoS Genet. 2014;10(7):e1004475.
55. Li H, Watford W, Li C, Parmelee A, Bryant MA, Deng C, et al. Ewing sarcoma gene EWS is essential for meiosis and B lymphocyte development. J Clin Invest. 2007;117(5):1314-23.
56. Yoon Y, Park H, Kim S, Nguyen PT, Hyeon SJ, Chung S, et al. Genetic Ablation of EWS RNA Binding Protein 1 (EWSR1) Leads to Neuroanatomical Changes and Motor Dysfunction in Mice. Exp Neurobiol. 2018;27(2):103-11.
57. Li Y, Luo H, Liu T, Zacksenhaus E, Ben-David Y. The ets transcription factor Fli-1 in development, cancer and disease. Oncogene. 2015;34(16):2022-31.
58. Truong AH, Ben-David Y. The role of Fli-1 in normal cell function and malignant transformation. Oncogene. 2000;19(55):6482-9.
59. Riggi N, Cironi L, Suva ML, Stamenkovic I. Sarcomas: genetics, signalling, and cellular origins. Part 1: The fellowship of TET. J Pathol. 2007;213(1):4-20.
60. Shing DC, McMullan DJ, Roberts P, Smith K, Chin SF, Nicholson J, et al. FUS/ERG gene fusions in Ewing's tumors. Cancer Res. 2003;63(15):4568-76.
61. Riggi N, Stamenkovic I. The Biology of Ewing sarcoma. Cancer Lett. 2007;254(1):1-10.
62. Kovar H, Aryee DN, Jug G, Henockl C, Schemper M, Delattre O, et al. EWS/FLI-1 antagonists induce growth inhibition of Ewing tumor cells in vitro. Cell Growth Differ. 1996;7(4):429-37.
63. Tanaka K, Iwakuma T, Harimaya K, Sato H, Iwamoto Y. EWS-Fli1 antisense oligodeoxynucleotide inhibits proliferation of human Ewing's sarcoma and primitive neuroectodermal tumor cells. J Clin Invest. 1997;99(2):239-47.
64. Thompson AD, Teitell MA, Arvand A, Denny CT. Divergent Ewing's sarcoma EWS/ETS fusions confer a common tumorigenic phenotype on NIH3T3 cells. Oncogene. 1999;18(40):5506-13.
65. Riggi N, Knoechel B, Gillespie SM, Rheinbay E, Boulay G, Suva ML, et al. EWS-FLI1 utilizes divergent chromatin remodeling mechanisms to directly activate or repress enhancer elements in Ewing sarcoma. Cancer Cell. 2014;26(5):668-81.
66. Johnson KM, Mahler NR, Saund RS, Theisen ER, Taslim C, Callender NW, et al. Role for the EWS domain of EWS/FLI in binding GGAA-microsatellites required for Ewing sarcoma anchorage independent growth. Proc Natl Acad Sci U S A. 2017;114(37):9870-5.
67. Boulay G, Sandoval GJ, Riggi N, Iyer S, Buisson R, Naigles B, et al. Cancer-Specific Retargeting of BAF Complexes by a Prion-like Domain. Cell. 2017;171(1):163-78 e19.
68. Cotterill SJ, Ahrens S, Paulussen M, Jurgens HF, Voute PA, Gadner H, et al. Prognostic factors in Ewing's tumor of bone: analysis of 975 patients from the European Intergroup Cooperative Ewing's Sarcoma Study Group. J Clin Oncol. 2000;18(17):3108-14.

69. Gaspar N, Hawkins DS, Dirksen U, Lewis IJ, Ferrari S, Le Deley MC, et al. Ewing Sarcoma: Current Management and Future Approaches Through Collaboration. J Clin Oncol. 2015;33(27):3036-46.
70. Ladenstein R, Potschger U, Le Deley MC, Whelan J, Paulussen M, Oberlin O, et al. Primary disseminated multifocal Ewing sarcoma: results of the Euro-EWING 99 trial. J Clin Oncol. 2010;28(20):3284-91.
71. Ban J, Aryee DN, Fourtouna A, van der Ent W, Kauer M, Niedan S, et al. Suppression of deacetylase SIRT1 mediates tumor-suppressive NOTCH response and offers a novel treatment option in metastatic Ewing sarcoma. Cancer Res. 2014;74(22):6578-88.
72. Potratz J, Tillmanns A, Berning P, Korsching E, Schaefer C, Lechtape B, et al. Receptor tyrosine kinase gene expression profiles of Ewing sarcomas reveal ROR1 as a potential therapeutic target in metastatic disease. Mol Oncol. 2016;10(5):677-92.
73. Mendoza-Naranjo A, El-Naggar A, Wai DH, Mistry P, Lazic N, Ayala FR, et al. ERBB4 confers metastatic capacity in Ewing sarcoma. EMBO Mol Med. 2013;5(7):1087-102.
74. Sechler M, Parrish JK, Birks DK, Jedlicka P. The histone demethylase KDM3A, and its downstream target MCAM, promote Ewing Sarcoma cell migration and metastasis. Oncogene. 2017;36(29):4150-60.
75. Karlina I, Schroeder BA, Kirgizov K, Romantsova O, Istranov AL, Nedorubov A, et al. Latest developments in the pathobiology of Ewing sarcoma. J Bone Oncol. 2022;35:100440.
76. Pinca RS, Manara MC, Chiadini V, Picci P, Zucchini C, Scotlandi K. Targeting ROCK2 rather than ROCK1 inhibits Ewing sarcoma malignancy. Oncol Rep. 2017;37(3):1387-93.
77. Grunewald TG, Willier S, Janik D, Unland R, Reiss C, Prazeres da Costa O, et al. The Zyxin-related protein thyroid receptor interacting protein 6 (TRIP6) is overexpressed in Ewing's sarcoma and promotes migration, invasion and cell growth. Biol Cell. 2013;105(11):535-47.
78. Balestra T, Manara MC, Laginestra MA, Pasello M, De Feo A, Bassi C, et al. Targeting CD99 Compromises the Oncogenic Effects of the Chimera EWS-FLI1 by Inducing Reexpression of Zyxin and Inhibition of GLI1 Activity. Mol Cancer Ther. 2022;21(1):58-69.
79. Zhou Z, Stewart KS, Yu L, Kleinerman ES. Bone marrow cells participate in tumor vessel formation that supports the growth of Ewing's sarcoma in the lung. Angiogenesis. 2011;14(2):125-33.
80. Krook MA, Nicholls LA, Scannell CA, Chugh R, Thomas DG, Lawlor ER. Stress-induced CXCR4 promotes migration and invasion of ewing sarcoma. Mol Cancer Res. 2014;12(6):953-64.
81. Chaturvedi A, Hoffman LM, Welm AL, Lessnick SL, Beckerle MC. The EWS/FLI Oncogene Drives Changes in Cellular Morphology, Adhesion, and Migration in Ewing Sarcoma. Genes Cancer. 2012;3(2):102-16.
82. Steinestel K, Trautmann M, Jansen EP, Dirksen U, Rehkamper J, Mikesch JH, et al. Focal adhesion kinase confers pro-migratory and antiapoptotic properties and is a potential therapeutic target in Ewing sarcoma. Mol Oncol. 2020;14(2):248-60.
83. Franzetti GA, Laud-Duval K, van der Ent W, Brisac A, Irondelle M, Aubert S, et al. Cell-to-cell heterogeneity of EWSR1-FLI1 activity determines proliferation/migration choices in Ewing sarcoma cells. Oncogene. 2017;36(25):3505-14.
84. Katschnig AM, Kauer MO, Schwentner R, Tomazou EM, Mutz CN, Linder M, et al. EWS-FLI1 perturbs MRTFB/YAP-1/TEAD target gene regulation inhibiting cytoskeletal autoregulatory feedback in Ewing sarcoma. Oncogene. 2017;36(43):5995-6005.
85. Rodriguez-Nunez P, Romero-Perez L, Amaral AT, Puerto-Camacho P, Jordan C, Marcilla D, et al. Hippo pathway effectors YAP1/TAZ induce an EWS-FLI1-opposing gene signature and associate with disease progression in Ewing sarcoma. J Pathol. 2020;250(4):374-86.
86. Worch J, Ranft A, DuBois SG, Paulussen M, Juergens H, Dirksen U. Age dependency of primary tumor sites and metastases in patients with Ewing sarcoma. Pediatr Blood Cancer. 2018;65(9):e27251.
87. Biswas B, Shukla NK, Deo SV, Agarwala S, Sharma DN, Vishnubhatla S, et al. Evaluation of outcome and prognostic factors in extraosseous Ewing sarcoma. Pediatr Blood Cancer. 2014;61(11):1925-31.
88. Juergens C, Weston C, Lewis I, Whelan J, Paulussen M, Oberlin O, et al. Safety assessment of intensive induction with vincristine, ifosfamide, doxorubicin, and etoposide (VIDE) in the treatment of Ewing tumors in the EURO-E.W.I.N.G. 99 clinical trial. Pediatr Blood Cancer. 2006;47(1):22-9.

89. Luksch R, Tienghi A, Hall KS, Fagioli F, Picci P, Barbieri E, et al. Primary metastatic Ewing's family tumors: results of the Italian Sarcoma Group and Scandinavian Sarcoma Group ISG/SSG IV Study including myeloablative chemotherapy and total-lung irradiation. Ann Oncol. 2012;23(11):2970-6.
90. Womer RB, West DC, Krailo MD, Dickman PS, Pawel BR, Grier HE, et al. Randomized controlled trial of interval-compressed chemotherapy for the treatment of localized Ewing sarcoma: a report from the Children's Oncology Group. J Clin Oncol. 2012;30(33):4148-54.
91. Brennan K, Martin K, FitzGerald SP, O'Sullivan J, Wu Y, Blanco A, et al. A comparison of methods for the isolation and separation of extracellular vesicles from protein and lipid particles in human serum. Sci Rep. 2020;10(1):1039.
92. Erkizan HV, Kong Y, Merchant M, Schlottmann S, Barber-Rotenberg JS, Yuan L, et al. A small molecule blocking oncogenic protein EWS-FLI1 interaction with RNA helicase A inhibits growth of Ewing's sarcoma. Nat Med. 2009;15(7):750-6.
93. Brenner JC, Ateeq B, Li Y, Yocum AK, Cao Q, Asangani IA, et al. Mechanistic rationale for inhibition of poly(ADP-ribose) polymerase in ETS gene fusion-positive prostate cancer. Cancer Cell. 2011;19(5):664-78.
94. Choy E, Butrynski JE, Harmon DC, Morgan JA, George S, Wagner AJ, et al. Phase II study of olaparib in patients with refractory Ewing sarcoma following failure of standard chemotherapy. BMC Cancer. 2014;14:813.
95. Manara MC, Terracciano M, Mancarella C, Sciandra M, Guerzoni C, Pasello M, et al. CD99 triggering induces methuosis of Ewing sarcoma cells through IGF-1R/RAS/Rac1 signaling. Oncotarget. 2016;7(48):79925-42.
96. Celik H, Sciandra M, Flashner B, Gelmez E, Kayraklioglu N, Allegakoen DV, et al. Clofarabine inhibits Ewing sarcoma growth through a novel molecular mechanism involving direct binding to CD99. Oncogene. 2018;37(16):2181-96.
97. Bierbaumer L, Katschnig AM, Radic-Sarikas B, Kauer MO, Petro JA, Hogler S, et al. YAP/TAZ inhibition reduces metastatic potential of Ewing sarcoma cells. Oncogenesis. 2021;10(1):2.
98. Denais C, Lammerding J. Nuclear mechanics in cancer. Adv Exp Med Biol. 2014;773:435-70.
99. Melcer S, Hezroni H, Rand E, Nissim-Rafinia M, Skoultchi A, Stewart CL, et al. Histone modifications and lamin A regulate chromatin protein dynamics in early embryonic stem cell differentiation. Nat Commun. 2012;3:910.
100. Handwerger KE, Gall JG. Subnuclear organelles: new insights into form and function. Trends Cell Biol. 2006;16(1):19-26.
101. Dundr M, Misteli T. Biogenesis of nuclear bodies. Cold Spring Harb Perspect Biol. 2010;2(12):a000711.
102. Carmo-Fonseca M. The contribution of nuclear compartmentalization to gene regulation. Cell. 2002;108(4):513-21.
103. Torbati M, Lele TP, Agrawal A. Ultradonut topology of the nuclear envelope. Proc Natl Acad Sci U S A. 2016;113(40):11094-9.
104. Uhlen M, Bjorling E, Agaton C, Szigyarto CA, Amini B, Andersen E, et al. A human protein atlas for normal and cancer tissues based on antibody proteomics. Mol Cell Proteomics. 2005;4(12):1920-32.
105. de Las Heras JI, Batrakou DG, Schirmer EC. Cancer biology and the nuclear envelope: a convoluted relationship. Semin Cancer Biol. 2013;23(2):125-37.
106. Niethammer P. Components and Mechanisms of Nuclear Mechanotransduction. Annu Rev Cell Dev Biol. 2021;37:233-56.
107. Tapley EC, Starr DA. Connecting the nucleus to the cytoskeleton by SUN-KASH bridges across the nuclear envelope. Curr Opin Cell Biol. 2013;25(1):57-62.
108. Adam SA. The Nucleoskeleton. Cold Spring Harb Perspect Biol. 2017;9(2).
109. Vahabikashi A, Adam SA, Medalia O, Goldman RD. Nuclear lamins: Structure and function in mechanobiology. APL Bioeng. 2022;6(1):011503.
110. Naetar N, Ferraioli S, Foisner R. Lamins in the nuclear interior - life outside the lamina. J Cell Sci. 2017;130(13):2087-96.
111. Jung HJ, Lee JM, Yang SH, Young SG, Fong LG. Nuclear lamins in the brain - new insights into function and regulation. Mol Neurobiol. 2013;47(1):290-301.

112. Herrmann H, Aebi U. Intermediate Filaments: Structure and Assembly. Cold Spring Harb Perspect Biol. 2016;8(11).
113. Worman HJ. Nuclear lamins and laminopathies. J Pathol. 2012;226(2):316-25.
114. Gruenbaum Y, Foisner R. Lamins: nuclear intermediate filament proteins with fundamental functions in nuclear mechanics and genome regulation. Annu Rev Biochem. 2015;84:131-64.
115. de Leeuw R, Gruenbaum Y, Medalia O. Nuclear Lamins: Thin Filaments with Major Functions. Trends Cell Biol. 2018;28(1):34-45.
116. Camozzi D, Capanni C, Cenni V, Mattioli E, Columbaro M, Squarzoni S, et al. Diverse lamin-dependent mechanisms interact to control chromatin dynamics. Focus on laminopathies. Nucleus. 2014;5(5):427-40.
117. Turgay Y, Eibauer M, Goldman AE, Shimi T, Khayat M, Ben-Harush K, et al. The molecular architecture of lamins in somatic cells. Nature. 2017;543(7644):261-4.
118. Kronenberg-Tenga R, Tatli M, Eibauer M, Wu W, Shin JY, Bonne G, et al. A lamin A/C variant causing striated muscle disease provides insights into filament organization. J Cell Sci. 2021;134(6).
119. Murray-Nerger LA, Cristea IM. Lamin post-translational modifications: emerging toggles of nuclear organization and function. Trends Biochem Sci. 2021;46(10):832-47.
120. Towbin BD, Gonzalez-Aguilera C, Sack R, Gaidatzis D, Kalck V, Meister P, et al. Step-wise methylation of histone H3K9 positions heterochromatin at the nuclear periphery. Cell. 2012;150(5):934-47.
121. Guelen L, Pagie L, Brasset E, Meuleman W, Faza MB, Talhout W, et al. Domain organization of human chromosomes revealed by mapping of nuclear lamina interactions. Nature. 2008;453(7197):948-51.
122. Taniura H, Glass C, Gerace L. A chromatin binding site in the tail domain of nuclear lamins that interacts with core histones. J Cell Biol. 1995;131(1):33-44.
123. Bruston F, Delbarre E, Ostlund C, Worman HJ, Buendia B, Duband-Goulet I. Loss of a DNA binding site within the tail of prelamin A contributes to altered heterochromatin anchorage by progerin. FEBS Lett. 2010;584(14):2999-3004.
124. Dittmer TA, Misteli T. The lamin protein family. Genome Biol. 2011;12(5):222.
125. Lund EG, Duband-Goulet I, Oldenburg A, Buendia B, Collas P. Distinct features of lamin A-interacting chromatin domains mapped by ChIP-sequencing from sonicated or micrococcal nuclease-digested chromatin. Nucleus. 2015;6(1):30-9.
126. Solovei I, Wang AS, Thanisch K, Schmidt CS, Krebs S, Zwerger M, et al. LBR and lamin A/C sequentially tether peripheral heterochromatin and inversely regulate differentiation. Cell. 2013;152(3):584-98.
127. Swift J, Ivanovska IL, Buxboim A, Harada T, Dingal PC, Pinter J, et al. Nuclear lamin-A scales with tissue stiffness and enhances matrix-directed differentiation. Science. 2013;341(6149):1240104.
128. Rowat AC, Jaalouk DE, Zwerger M, Ung WL, Eydelnant IA, Olins DE, et al. Nuclear envelope composition determines the ability of neutrophil-type cells to passage through micron-scale constrictions. J Biol Chem. 2013;288(12):8610-8.
129. Harada T, Swift J, Irianto J, Shin JW, Spinler KR, Athirasala A, et al. Nuclear lamin stiffness is a barrier to 3D migration, but softness can limit survival. J Cell Biol. 2014;204(5):669-82.
130. De Vos WH, Houben F, Kamps M, Malhas A, Verheyen F, Cox J, et al. Repetitive disruptions of the nuclear envelope invoke temporary loss of cellular compartmentalization in laminopathies. Hum Mol Genet. 2011;20(21):4175-86.
131. Xie W, Burke B. Lamins. Curr Biol. 2016;26(9):R348-50.
132. Prokocimer M, Davidovich M, Nissim-Rafinia M, Wiesel-Motiuk N, Bar DZ, Barkan R, et al. Nuclear lamins: key regulators of nuclear structure and activities. J Cell Mol Med. 2009;13(6):1059-85.
133. Hutchison CJ. B-type lamins in health and disease. Semin Cell Dev Biol. 2014;29:158-63.
134. Shevelyov YY, Ulianov SV. The Nuclear Lamina as an Organizer of Chromosome Architecture. Cells. 2019;8(2).
135. Schreiner SM, Koo PK, Zhao Y, Mochrie SG, King MC. The tethering of chromatin to the nuclear envelope supports nuclear mechanics. Nat Commun. 2015;6:7159.
136. Booth EA, Spagnol ST, Alcoser TA, Dahl KN. Nuclear stiffening and chromatin softening with progerin expression leads to an attenuated nuclear response to force. Soft Matter. 2015;11(32):6412-8.
137. Kim JK, Louhghalam A, Lee G, Schafer BW, Wirtz D, Kim DH. Nuclear lamin A/C harnesses the perinuclear apical actin cables to protect nuclear morphology. Nat Commun. 2017;8(1):2123.

138. Haque F, Lloyd DJ, Smallwood DT, Dent CL, Shanahan CM, Fry AM, et al. SUN1 interacts with nuclear lamin A and cytoplasmic nesprins to provide a physical connection between the nuclear lamina and the cytoskeleton. Mol Cell Biol. 2006;26(10):3738-51.
139. Jahed Z, Fadavi D, Vu UT, Asgari E, Luxton GWG, Mofrad MRK. Molecular Insights into the Mechanisms of SUN1 Oligomerization in the Nuclear Envelope. Biophys J. 2018;114(5):1190-203.
140. Jahed Z, Domkam N, Ornowski J, Yerima G, Mofrad MRK. Molecular models of LINC complex assembly at the nuclear envelope. J Cell Sci. 2021;134(12).
141. Chang W, Worman HJ, Gundersen GG. Accessorizing and anchoring the LINC complex for multifunctionality. J Cell Biol. 2015;208(1):11-22.
142. Zhang Q, Ragnauth C, Greener MJ, Shanahan CM, Roberts RG. The nesprins are giant actin-binding proteins, orthologous to Drosophila melanogaster muscle protein MSP-300. Genomics. 2002;80(5):473-81.
143. Mellad JA, Warren DT, Shanahan CM. Nesprins LINC the nucleus and cytoskeleton. Curr Opin Cell Biol. 2011;23(1):47-54.
144. Luxton GW, Starr DA. KASHing up with the nucleus: novel functional roles of KASH proteins at the cytoplasmic surface of the nucleus. Curr Opin Cell Biol. 2014;28:69-75.
145. Padmakumar VC, Libotte T, Lu W, Zaim H, Abraham S, Noegel AA, et al. The inner nuclear membrane protein Sun1 mediates the anchorage of Nesprin-2 to the nuclear envelope. J Cell Sci. 2005;118(Pt 15):3419-30.
146. Lee YL, Burke B. LINC complexes and nuclear positioning. Semin Cell Dev Biol. 2018;82:67-76.
147. Arsenovic PT, Ramachandran I, Bathula K, Zhu R, Narang JD, Noll NA, et al. Nesprin-2G, a Component of the Nuclear LINC Complex, Is Subject to Myosin-Dependent Tension. Biophys J. 2016;110(1):34-43.
148. Lei K, Zhu X, Xu R, Shao C, Xu T, Zhuang Y, et al. Inner nuclear envelope proteins SUN1 and SUN2 play a prominent role in the DNA damage response. Curr Biol. 2012;22(17):1609-15.
149. Bouzid T, Kim E, Riehl BD, Esfahani AM, Rosenbohm J, Yang R, et al. The LINC complex, mechanotransduction, and mesenchymal stem cell function and fate. J Biol Eng. 2019;13:68.
150. Wong X, Loo TH, Stewart CL. LINC complex regulation of genome organization and function. Curr Opin Genet Dev. 2021;67:130-41.
151. Espigat-Georger A, Dyachuk V, Chemin C, Emorine L, Merdes A. Nuclear alignment in myotubes requires centrosome proteins recruited by nesprin-1. J Cell Sci. 2016;129(22):4227-37.
152. Khatau SB, Bloom RJ, Bajpai S, Razafsky D, Zang S, Giri A, et al. The distinct roles of the nucleus and nucleus-cytoskeleton connections in three-dimensional cell migration. Sci Rep. 2012;2:488.
153. van Tienen FHJ, Lindsey PJ, Kamps MAF, Krapels IP, Ramaekers FCS, Brunner HG, et al. Assessment of fibroblast nuclear morphology aids interpretation of LMNA variants. Eur J Hum Genet. 2019;27(3):389-99.
154. Chiarini F, Evangelisti C, Cenni V, Fazio A, Paganelli F, Martelli AM, et al. The Cutting Edge: The Role of mTOR Signaling in Laminopathies. Int J Mol Sci. 2019;20(4).
155. Atalaia A, Ben Yaou R, Wahbi K, De Sandre-Giovannoli A, Vigouroux C, Bonne G. Laminopathies' Treatments Systematic Review: A Contribution Towards a 'Treatabolome'. J Neuromuscul Dis. 2021;8(3):419-39.
156. Osmanagic-Myers S, Dechat T, Foisner R. Lamins at the crossroads of mechanosignaling. Genes Dev. 2015;29(3):225-37.
157. Burke B, Stewart CL. The nuclear lamins: flexibility in function. Nat Rev Mol Cell Biol. 2013;14(1):13-24.
158. Zink D, Fischer AH, Nickerson JA. Nuclear structure in cancer cells. Nat Rev Cancer. 2004;4(9):677-87.
159. Ovsiannikova NL, Lavrushkina SV, Ivanova AV, Mazina LM, Zhironkina OA, Kireev, II. Lamin A as a Determinant of Mechanical Properties of the Cell Nucleus in Health and Disease. Biochemistry (Mosc). 2021;86(10):1288-300.
160. Dubik N, Mai S. Lamin A/C: Function in Normal and Tumor Cells. Cancers (Basel). 2020;12(12).
161. Aljada A, Doria J, Saleh AM, Al-Matar SH, AlGabbani S, Shamsa HB, et al. Altered Lamin A/C splice variant expression as a possible diagnostic marker in breast cancer. Cell Oncol (Dordr). 2016;39(2):161-74.
162. Wang J, Kondo T, Nakazawa T, Oishi N, Mochizuki K, Katoh R. Constitutional abnormality of nuclear membrane proteins in small cell lung carcinoma. Virchows Arch. 2019;475(4):407-14.

163. Wang Y, Jiang J, He L, Gong G, Wu X. Effect of lamin-A expression on migration and nuclear stability of ovarian cancer cells. Gynecol Oncol. 2019;152(1):166-76.
164. Kong L, Schafer G, Bu H, Zhang Y, Zhang Y, Klocker H. Lamin A/C protein is overexpressed in tissue-invading prostate cancer and promotes prostate cancer cell growth, migration and invasion through the PI3K/AKT/PTEN pathway. Carcinogenesis. 2012;33(4):751-9.
165. Belt EJ, Fijneman RJ, van den Berg EG, Bril H, Delis-van Diemen PM, Tijssen M, et al. Loss of lamin A/C expression in stage II and III colon cancer is associated with disease recurrence. Eur J Cancer. 2011;47(12):1837-45.
166. Alhudiri IM, Nolan CC, Ellis IO, Elzagheid A, Rakha EA, Green AR, et al. Expression of Lamin A/C in early-stage breast cancer and its prognostic value. Breast Cancer Res Treat. 2019;174(3):661-8.
167. Gatti G, Vilardo L, Musa C, Di Pietro C, Bonaventura F, Scavizzi F, et al. Role of Lamin A/C as Candidate Biomarker of Aggressiveness and Tumorigenicity in Glioblastoma Multiforme. Biomedicines. 2021;9(10).
168. Doerschuk CM, Beyers N, Coxson HO, Wiggs B, Hogg JC. Comparison of neutrophil and capillary diameters and their relation to neutrophil sequestration in the lung. J Appl Physiol (1985). 1993;74(6):3040-5.
169. van Helvert S, Storm C, Friedl P. Mechanoreciprocity in cell migration. Nat Cell Biol. 2018;20(1):8-20.
170. Friedl P, Wolf K, Lammerding J. Nuclear mechanics during cell migration. Curr Opin Cell Biol. 2011;23(1):55-64.
171. Stoitzner P, Pfaller K, Stossel H, Romani N. A close-up view of migrating Langerhans cells in the skin. J Invest Dermatol. 2002;118(1):117-25.
172. Weigelin B, Bakker GJ, Friedl P. Intravital third harmonic generation microscopy of collective melanoma cell invasion: Principles of interface guidance and microvesicle dynamics. Intravital. 2012;1(1):32-43.
173. Zuela-Sopilniak N, Lammerding J. Can't handle the stress? Mechanobiology and disease. Trends Mol Med. 2022;28(9):710-25.
174. Bell ES, Shah P, Zuela-Sopilniak N, Kim D, Varlet AA, Morival JLP, et al. Low lamin A levels enhance confined cell migration and metastatic capacity in breast cancer. Oncogene. 2022;41(36):4211-30.
175. Kaspi E, Frankel D, Guinde J, Perrin S, Laroumagne S, Robaglia-Schlupp A, et al. Low lamin A expression in lung adenocarcinoma cells from pleural effusions is a pejorative factor associated with high number of metastatic sites and poor Performance status. PLoS One. 2017;12(8):e0183136.
176. Urciuoli E, D'Oria V, Petrini S, Peruzzi B. Lamin A/C Mechanosensor Drives Tumor Cell Aggressiveness and Adhesion on Substrates With Tissue-Specific Elasticity. Front Cell Dev Biol. 2021;9:712377.
177. Vahabikashi A, Sivagurunathan S, Nicdao FAS, Han YL, Park CY, Kittisopikul M, et al. Nuclear lamin isoforms differentially contribute to LINC complex-dependent nucleocytoskeletal coupling and whole-cell mechanics. Proc Natl Acad Sci U S A. 2022;119(17):e2121816119.
178. Bell ES, Lammerding J. Causes and consequences of nuclear envelope alterations in tumour progression. Eur J Cell Biol. 2016;95(11):449-64.
179. Matsumoto A, Hieda M, Yokoyama Y, Nishioka Y, Yoshidome K, Tsujimoto M, et al. Global loss of a nuclear lamina component, lamin A/C, and LINC complex components SUN1, SUN2, and nesprin-2 in breast cancer. Cancer Med. 2015;4(10):1547-57.
180. Liddane AG, McNamara CA, Campbell MC, Mercier I, Holaska JM. Defects in Emerin-Nucleoskeleton Binding Disrupt Nuclear Structure and Promote Breast Cancer Cell Motility and Metastasis. Mol Cancer Res. 2021;19(7):1196-207.
181. Reis-Sobreiro M, Chen JF, Novitskaya T, You S, Morley S, Steadman K, et al. Emerin Deregulation Links Nuclear Shape Instability to Metastatic Potential. Cancer Res. 2018;78(21):6086-97.
182. Denais CM, Gilbert RM, Isermann P, McGregor AL, te Lindert M, Weigelin B, et al. Nuclear envelope rupture and repair during cancer cell migration. Science. 2016;352(6283):353-8.
183. Raab M, Gentili M, de Belly H, Thiam HR, Vargas P, Jimenez AJ, et al. ESCRT III repairs nuclear envelope ruptures during cell migration to limit DNA damage and cell death. Science. 2016;352(6283):359-62.
184. Irianto J, Xia Y, Pfeifer CR, Athirasala A, Ji J, Alvey C, et al. DNA Damage Follows Repair Factor Depletion and Portends Genome Variation in Cancer Cells after Pore Migration. Curr Biol. 2017;27(2):210-23.

185. Ward IM, Minn K, van Deursen J, Chen J. p53 Binding protein 53BP1 is required for DNA damage responses and tumor suppression in mice. Mol Cell Biol. 2003;23(7):2556-63.
186. Gibbs-Seymour I, Markiewicz E, Bekker-Jensen S, Mailand N, Hutchison CJ. Lamin A/C-dependent interaction with 53BP1 promotes cellular responses to DNA damage. Aging Cell. 2015;14(2):162-9.
187. Gonzalez-Suarez I, Redwood AB, Perkins SM, Vermolen B, Lichtensztejin D, Grotsky DA, et al. Novel roles for A-type lamins in telomere biology and the DNA damage response pathway. EMBO J. 2009;28(16):2414-27.
188. Patil S, Sengupta K. Role of A- and B-type lamins in nuclear structure-function relationships. Biol Cell. 2021;113(7):295-310.
189. Wolf K, Te Lindert M, Krause M, Alexander S, Te Riet J, Willis AL, et al. Physical limits of cell migration: control by ECM space and nuclear deformation and tuning by proteolysis and traction force. J Cell Biol. 2013;201(7):1069-84.
190. Bagnara GP, Serra M, Giovannini M, Badiali M, Stella M, Montaldi A, et al. Establishment and characterization of a primitive neuroectodermal tumor of bone continuous cell line (LAP-35). Int J Cell Cloning. 1990;8(6):409-24.
191. Savola S, Klami A, Myllykangas S, Manara C, Scotlandi K, Picci P, et al. High Expression of Complement Component 5 (C5) at Tumor Site Associates with Superior Survival in Ewing's Sarcoma Family of Tumour Patients. ISRN Oncol. 2011;2011:168712.
192. Volchenboum SL, Andrade J, Huang L, Barkauskas DA, Krailo M, Womer RB, et al. Gene Expression Profiling of Ewing Sarcoma Tumors Reveals the Prognostic Importance of Tumor-Stromal Interactions: A Report from the Children's Oncology Group. J Pathol Clin Res. 2015;1(2):83-94.
193. Nomura T, Tamaoki N, Takakura A, Suemizu H. Basic concept of development and practical application of animal models for human diseases. Curr Top Microbiol Immunol. 2008;324:1-24.
194. Mattioli E, Andrenacci D, Mai A, Valente S, Robijns J, De Vos WH, et al. Statins and Histone Deacetylase Inhibitors Affect Lamin A/C - Histone Deacetylase 2 Interaction in Human Cells. Front Cell Dev Biol. 2019;7:6.
195. Huang SJ, Fu RH, Shyu WC, Liu SP, Jong GP, Chiu YW, et al. Adipose-derived stem cells: isolation, characterization, and differentiation potential. Cell Transplant. 2013;22(4):701-9.
196. Bikkul MU, Clements CS, Godwin LS, Goldberg MW, Kill IR, Bridger JM. Farnesyltransferase inhibitor and rapamycin correct aberrant genome organisation and decrease DNA damage respectively, in Hutchinson-Gilford progeria syndrome fibroblasts. Biogerontology. 2018;19(6):579-602.
197. Lattanzi G. Prelamin A-mediated nuclear envelope dynamics in normal and laminopathic cells. Biochem Soc Trans. 2011;39(6):1698-704.
198. Zucchini C, Manara MC, Cristalli C, Carrabotta M, Greco S, Pinca RS, et al. ROCK2 deprivation leads to the inhibition of tumor growth and metastatic potential in osteosarcoma cells through the modulation of YAP activity. J Exp Clin Cancer Res. 2019;38(1):503.
199. Konstantinopoulos PA, Karamouzis MV, Papavassiliou AG. Post-translational modifications and regulation of the RAS superfamily of GTPases as anticancer targets. Nat Rev Drug Discov. 2007;6(7):541-55.
200. Luu HH, Kang Q, Park JK, Si W, Luo Q, Jiang W, et al. An orthotopic model of human osteosarcoma growth and spontaneous pulmonary metastasis. Clin Exp Metastasis. 2005;22(4):319-29.
201. Tsukune N, Naito M, Kubota T, Ozawa Y, Nagao M, Ohashi A, et al. Lamin A overexpression promotes osteoblast differentiation and calcification in the MC3T3-E1 preosteoblastic cell line. Biochem Biophys Res Commun. 2017;488(4):664-70.
202. Zhang B, Yang Y, Keyimu R, Hao J, Zhao Z, Ye R. The role of lamin A/C in mesenchymal stem cell differentiation. J Physiol Biochem. 2019;75(1):11-8.
203. Rauner M, Sipos W, Goettsch C, Wutzl A, Foisner R, Pietschmann P, et al. Inhibition of lamin A/C attenuates osteoblast differentiation and enhances RANKL-dependent osteoclastogenesis. J Bone Miner Res. 2009;24(1):78-86.
204. Istvan ES, Deisenhofer J. Structural mechanism for statin inhibition of HMG-CoA reductase. Science. 2001;292(5519):1160-4.
205. Fromigue O, Hamidouche Z, Marie PJ. Blockade of the RhoA-JNK-c-Jun-MMP2 cascade by atorvastatin reduces osteosarcoma cell invasion. J Biol Chem. 2008;283(45):30549-56.

206. Kany S, Woschek M, Kneip N, Sturm R, Kalbitz M, Hanschen M, et al. Simvastatin exerts anticancer effects in osteosarcoma cell lines via geranylgeranylation and c-Jun activation. Int J Oncol. 2018;52(4):1285-94.
207. de la Rosa J, Freije JM, Cabanillas R, Osorio FG, Fraga MF, Fernandez-Garcia MS, et al. Prelamin A causes progeria through cell-extrinsic mechanisms and prevents cancer invasion. Nat Commun. 2013;4:2268.
208. Matralis AN, Xanthopoulos D, Huot G, Lopes-Paciencia S, Cole C, de Vries H, et al. Molecular tools that block maturation of the nuclear lamin A and decelerate cancer cell migration. Bioorg Med Chem. 2018;26(20):5547-54.
209. Mattioli E, Columbaro M, Capanni C, Maraldi NM, Cenni V, Scotlandi K, et al. Prelamin A-mediated recruitment of SUN1 to the nuclear envelope directs nuclear positioning in human muscle. Cell Death Differ. 2011;18(8):1305-15.
210. Haque F, Mazzeo D, Patel JT, Smallwood DT, Ellis JA, Shanahan CM, et al. Mammalian SUN protein interaction networks at the inner nuclear membrane and their role in laminopathy disease processes. J Biol Chem. 2010;285(5):3487-98.
211. Liu L, Luo Q, Sun J, Song G. Cytoskeletal control of nuclear morphology and stiffness are required for OPN-induced bone-marrow-derived mesenchymal stem cell migration. Biochem Cell Biol. 2019;97(4):463-70.
212. Nanni P, Nicoletti G, Landuzzi L, Croci S, Murgo A, Palladini A, et al. High metastatic efficiency of human sarcoma cells in Rag2/gammac double knockout mice provides a powerful test system for antimetastatic targeted therapy. Eur J Cancer. 2010;46(3):659-68.
213. Meinke P, Mattioli E, Haque F, Antoku S, Columbaro M, Straatman KR, et al. Muscular dystrophy-associated SUN1 and SUN2 variants disrupt nuclear-cytoskeletal connections and myonuclear organization. PLoS Genet. 2014;10(9):e1004605.
214. Lombardi ML, Lammerding J. Keeping the LINC: the importance of nucleocytoskeletal coupling in intracellular force transmission and cellular function. Biochem Soc Trans. 2011;39(6):1729-34.
215. Owens DJ, Messeant J, Moog S, Viggars M, Ferry A, Mamchaoui K, et al. Lamin-Related Congenital Muscular Dystrophy Alters Mechanical Signaling and Skeletal Muscle Growth. Int J Mol Sci. 2020;22(1).
216. Owens DJ, Fischer M, Jabre S, Moog S, Mamchaoui K, Butler-Browne G, et al. Lamin Mutations Cause Increased YAP Nuclear Entry in Muscle Stem Cells. Cells. 2020;9(4).
217. Birks S, Uzer G. At the nuclear envelope of bone mechanobiology. Bone. 2021;151:116023.
218. Shome D, von Woedtke T, Riedel K, Masur K. The HIPPO Transducer YAP and Its Targets CTGF and Cyr61 Drive a Paracrine Signalling in Cold Atmospheric Plasma-Mediated Wound Healing. Oxid Med Cell Longev. 2020;2020:4910280.
219. Sorrentino G, Ruggeri N, Specchia V, Cordenonsi M, Mano M, Dupont S, et al. Metabolic control of YAP and TAZ by the mevalonate pathway. Nat Cell Biol. 2014;16(4):357-66.
220. Irianto J, Pfeifer CR, Ivanovska IL, Swift J, Discher DE. Nuclear lamins in cancer. Cell Mol Bioeng. 2016;9(2):258-67.
221. Long JT, Lammerding J. Nuclear Deformation Lets Cells Gauge Their Physical Confinement. Dev Cell. 2021;56(2):156-8.
222. Sakthivel KM, Sehgal P. A Novel Role of Lamins from Genetic Disease to Cancer Biomarkers. Oncol Rev. 2016;10(2):309.
223. Cicchillitti L, Corrado G, Carosi M, Dabrowska ME, Loria R, Falcioni R, et al. Prognostic role of NF-YA splicing isoforms and Lamin A status in low grade endometrial cancer. Oncotarget. 2017;8(5):7935-45.
224. Thakar K, May CK, Rogers A, Carroll CW. Opposing roles for distinct LINC complexes in regulation of the small GTPase RhoA. Mol Biol Cell. 2017;28(1):182-91.
225. Nishioka Y, Imaizumi H, Imada J, Katahira J, Matsuura N, Hieda M. SUN1 splice variants, SUN1_888, SUN1_785, and predominant SUN1_916, variably function in directional cell migration. Nucleus. 2016;7(6):572-84.
226. Zanconato F, Cordenonsi M, Piccolo S. YAP and TAZ: a signalling hub of the tumour microenvironment. Nat Rev Cancer. 2019;19(8):454-64.
227. Dupont S, Morsut L, Aragona M, Enzo E, Giulitti S, Cordenonsi M, et al. Role of YAP/TAZ in mechanotransduction. Nature. 2011;474(7350):179-83.

228. Calvo F, Ege N, Grande-Garcia A, Hooper S, Jenkins RP, Chaudhry SI, et al. Mechanotransduction and YAP-dependent matrix remodelling is required for the generation and maintenance of cancer-associated fibroblasts. Nat Cell Biol. 2013;15(6):637-46.
229. Zhang H, Deo M, Thompson RC, Uhler MD, Turner DL. Negative regulation of Yap during neuronal differentiation. Dev Biol. 2012;361(1):103-15.
230. Rocchi A, Manara MC, Sciandra M, Zambelli D, Nardi F, Nicoletti G, et al. CD99 inhibits neural differentiation of human Ewing sarcoma cells and thereby contributes to oncogenesis. J Clin Invest. 2010;120(3):668-80.
231. Ladanyl M, Heinemann FS, Huvos AG, Rao PH, Chen QG, Jhanwar SC. Neural differentiation in small round cell tumors of bone and soft tissue with the translocation t(11;22)(q24;q12): an immunohistochemical study of 11 cases. Hum Pathol. 1990;21(12):1245-51.